BULETINUL INSTITUTULUI POLITEHNIC DIN IAŞI

F1503/3
FF
8 000000 660152

Editat de
UNIVERSITATEA TEHNICĂ „GH. ASACHI", IAŞI

Tomul XLIV (XLVII)

Fasc. 1 - 2

Secţia III

ELECTROTEHNICĂ
ENERGETICĂ
ELECTRONICĂ

1998

BULETINUL INSTITUTULUI POLITEHNIC DIN IAŞI

Tomul XLIV (XLVIII)
Fasc. 1–2

Secţia III

ELECTROTEHNICĂ. ENERGETICĂ. ELECTRONICĂ

1998

EDITORIAL STAFF

Prof. Dr. Eng. **MIHAI GAFIŢANU** (President)
Prof. Dr. Eng. **VICTOR BULACOVSCHI** (Vice-President)
Prof. Dr. Eng. **LIVIU GROLL** (Vice-President)
Prof. Dr. Eng. **GHEORGHE ZET** (Secretary)
Prof. Dr. Doc. Eng. **ALFRED BRAIER** (Editor)
Prof. Dr. Eng. **HUGO ROSMAN** (Editor)
Prof. Dr. Eng. **MIHAIL VOICU** (Head of the Exchange Service)
Prof. Dr. Eng. **DIMITRIE ALEXA**
Prof. Dr. Eng. **ION BALASANIAN**
Prof. Dr. **AUREL BEJANCU**
Prof. Dr. Eng. **MIRCEA COZMÎNCĂ**
Prof. Dr. Eng. **SPIRIDON CREŢU**
Prof. Dr. Eng. **ION GIURMA**
Prof. Dr. Eng. **AURELIA GRIGORIU**
Prof. Dr. Eng. **CONSTANTIN PREDA**
Prof. Dr. Eng. **PAULICĂ RĂILEANU**

The **Bulletin of the Polytechnic Institute of Jassy** is edited by the **Technical University "Gh.Asachi"** (the former Polytechnic Institute), Jassy.

TEXredaction:
B. Grigoriu, A. Rotaru
Technical University of Jassy

BULETINUL INSTITUTULUI POLITEHNIC DIN IAŞI
BULLETIN OF THE POLYTECHNIC INSTITUTE OF JASSY
Tomul XLIV (XLVIII), Fasc. 1-2 1998

Secţia III

ELECTROTEHNICĂ. ENERGETICĂ. ELECTRONICĂ

INFORMÁCIÓS KÖNYVTÁR BUDAPEST MŰSZAKI EGYETEM

SUMAR

Pag.

I. TULEAŞCĂ, Ecranul plan-paralel inerţial în câmp electromagnetic cvasistaţionar armonic (engl., rez. rom.) 7

HUGO ROSMAN şi DORIN BELAUS, Câteva observaţii referitoare la parametrii unui cuadripol în sens restrâns, primitiv, ataşat unui cuadripol general liniar, neautonom, reciproc, în regim permanent armonic (franc., rez. rom.) 15

DORIN BELAUS şi HUGO ROSMAN, Cuadripoli generali liniari, neautonomi, unidirecţionali, în regim permanent armonic (franc., rez. rom.) 23

ANCA-MIHAELA LAZĂR, O posibilă abordare a calculului puterilor în domeniul timp folosind transformata Hartley (engl., rez. rom.) 29

MARIANA BUZDUGA, Oscilaţii mecanice într-un sistem electromecanic liniar. Studiul semnalelor electrice (franc., rez. rom.) 35

DANIELA TĂRNICERIU şi VALERIU MUNTEANU, Compensarea sistemelor discrete, liniare, variante în timp (engl., rez. rom.) 45

DAMIAN IMBREA, N. COJAN şi CLARISSA GÂTLAN, Asupra colapsării defectelor în circuitele combinaţionale (engl., rez. rom.) 53

C. SĂRMĂŞANU şi M. CREŢU, Performanţele metrologice ale senzorilor de proximitate fuzzy-simbolici (engl., rez. rom.) 59

MARINEL TEMNEANU şi CRISTINA TEMNEANU, Un model de tip Chua al ciclului de histerezis (engl., rez. rom.) 67

VALERIU DAVID, M. ANTONIU şi EMIL VREMERĂ, Un măsurător triaxial de bandă largă al câmpului magnetic cu aplicaţii biomedicale (engl., rez. rom.) 73

I. SUCHAR, Asupra traductoarelor folosite la motoarele de curent continuu cu comutaţie statică (engl., rez. rom.) 79

EMIL-COSTEL TEODORU şi MIRCEA GOGU, Asupra funcţionării maşinii asincrone bifazate alimentate de la un convertor PWM şi o sursă sinusoidală (engl., rez. rom.) 91

ADRIAN MAXIM, DANIELLE ANDREU şi JACQUES BOUCHER, Macromodelarea SPICE analog-comportamentală a transformatoarelor (engl., rez. rom.) 99

Pag.

VIOREL OLARIU, Asupra sintetizoarelor de frecvenţă hibride PLL/DDS (engl., rez. rom.) 105

LAURENŢIU DIMITRIU şi LILIANA VORNICU, Frecvenţmetru cu microprocesor. Aspecte software. Funcţionarea cu măsurarea frecvenţei (engl., rez. rom.) 113

PETRUŢ DUMA, LUMINIŢA SCRIPCARIU şi CLARISSA GÂTLAN, Integrarea funcţiei de recepţionare a informaţiei de selecţie în ton şi puls dintr-o centrală telefonică electronică de capacitate mică (engl., rez. rom.) 117

GH. CÂRŢINĂ şi GH. HAZI, Metodă de programare pătratică succesivă (franc., rez. rom.) 127

EUGEN BÂRLĂDEANU, AL. POEATĂ şi MONICA MUŞAT, Consideraţii privind studiul regimurilor reţelelor electrice utilizând descrierea fuzzy a sarcinilor (engl., rez. rom.) 133

M. GAVRILAŞ, GH. GEORGESCU şi DANIELA RĂDĂŞANU, Selectarea optimală a condensatoarelor pentru compensarea puterii reactive în reţelele de distribuţie utilizând algoritmi genetici (engl., rez. rom.) 139

MIRCEA-SORIN OPRIŞOR 147

RECENZII 149

BULETINUL INSTITUTULUI POLITEHNIC DIN IAŞI
BULLETIN OF THE POLYTECHNIC INSTITUTE OF JASSY
Tome XLIV (XLVIII), Fasc. 1–2 1998

Section III

ELECTROTECHNICS. ENERGETICS. ELECTRONICS

CONTENTS

	p.
I. TULEAŞCĂ, The Plane–Parallel Inertial Shield in Quasistationary Harmonic Electromagnetic Field (English, Romanian summary)	7
HUGO ROSMAN et DORIN BELAUS, Quelques observations concernant les paramètres d'un quadripôle en sens restreint, primitif, attaché à un quadripôle général linéaire, non-autonome, réciproque, en régime permanent harmonique (French, Romanian summary)	15
DORIN BELAUS et HUGO ROSMAN, Quadripôles généraux linéaires, non-autonomes, unidirectionnels, en régime permanent harmonique (French, Romanian summary)	23
ANCA-MIHAELA LAZĂR, Powers Computing in the Time Domain: a Hartley Transform Approach (English, Romanian summary)	29
MARIANA BUZDUGA, Oscillations mécaniques dans un système linéaire électromécanique. Étude des signaux électriques (French, Romanian summary)	35
DANIELA TĂRNICERIU and VALERIU MUNTEANU, Compensation of Discrete, Linear, Time Varying Systems (English, Romanian summary)	45
DAMIAN IMBREA, N. COJAN and CLARISSA GÂTLAN, On the Fault Collapsing in Combinational Circuits (English, Romanian summary)	53
C. SĂRMĂŞANU and M. CREŢU, The Metrological Performance of the Proximity Fuzzy-symbolic Sensor (English, Romanian summary)	59
MARINEL TEMNEANU and CRISTINA TEMNEANU, Chua Type Hysteresis Model (English, Romanian summary)	67
VALERIU DAVID, M. ANTONIU and EMIL VREMERĂ, A Triaxis Broadband Magnetic Field Meter for Biomedical Applications (English, Romanian summary)	73
I. SUCHAR, On the Transducers Used in D.C. Motors with Static Switching (English, Romanian summary)	79
EMIL-COSTEL TEODORU and MIRCEA GOGU, On Two-Phase Squirrel Cage Induction Machine Working, Driven by a Pulse Width Modulated Converter and Sinusoidal Voltage (English, Romanian summary)	91
ADRIAN MAXIM, DANIELLE ANDREU and JACQUES BOUCHER, Analog Behavioural SPICE Macromodeling of Transformers (English, Romanian summary)	99

	Pp.
VIOREL OLARIU, On the Hybrid PLL/DDS Frequency Synthesizer (English, Romanian summary)	105
LAURENŢIU DIMITRIU and LILIANA VORNICU, Frequency-meter with Microprocessor. Software Aspects. Frequency-Measuring Working (English, Romanian summary)	113
PETRUŢ DUMA, LUMINIŢA SCRIPCARIU and CLARISSA GÂTLAN, Integration of the Function of Receiving Pulse and Tone Selection Information in a Low Capacity Electronic Telephone Exchange (English, Romanian summary)	117
GH. CÂRŢINĂ et GH. HAZI, Méthode de programmation quadratique successive (French, Romanian summary)	127
EUGEN BĂRLĂDEANU, AL. POEATĂ and MONICA MUŞAT, Some Aspects regarding the Power Flow Analysis Using a Fuzzy Load Description (English, Romanian summary)	133
M. GAVRILAŞ, GH. GEORGESCU and DANIELA RĂDĂŞANU, Optimal Selection of Capacitors for Reactive Power Compensation in Distribution Systems Using Genetic Algorithms (English, Romanian summary)	139
MIRCEA-SORIN OPRIŞOR	147
BOOK REVIEWS	149

BULETINUL INSTITUTULUI POLITEHNIC DIN IAŞI
Tomul XLIV (XLVIII), Fasc. 1–2, 1998
Secţia III
ELECTROTEHNICĂ. ENERGETICĂ. ELECTRONICĂ

D.C. 621.396.621.551

THE PLANE–PARALLEL INERTIAL SHIELD IN QUASISTATIONARY HARMONIC ELECTROMAGNETIC FIELD

BY

I. TULEAŞCĂ

The paper presents the inertial approach in analysing a plane–parallel shield functioning. There are determined the shield factor, F, and the attenuation, a, after considering the shield walls with inertial behaviour, which implies the field propagation equation to be a Duffing one, solved with the small parameter method.

1. Introduction

A shield represents [1] a metallic enclosure placed between two regions of the space in order to control the propagation of the electric and magnetic field from one region to another.

In practice it can be shielded the perturbation source or the perturbation receiver and, in some cases, both the source and the receiver are shielded. The shielding effect can be evaluated according to the magnetic or electric field minimization caused by the shield. Assuming that $\mathbf{H}_e$ is the field in the absence of the shield (or the field incident to the shield, considered to be far away from the shield), whereas $\mathbf{H}_i$ is the field in the protected space, the shielding effect can be appreciated using a dimensionless quantity, called *shield factor*, F, defined as

$$F = \frac{|\mathbf{H}_i|}{|\mathbf{H}_e|} = \frac{H_i}{H_e}. \tag{1}$$

Considering the electromagnetic field with harmonic variation, due to the phase difference between $\mathbf{H}_e$ and $\mathbf{H}_i$, $\underline{F}$ becomes a complex quantity; according to the definition, $|\underline{F}| \leq 1$.

In far field zone, that is in plane wave field, the shield factor can be calculated using also the relation:

$$F = \frac{|\mathbf{E}_i|}{|\mathbf{E}_e|} = \frac{E_i}{E_e}. \tag{2}$$

In near field the magnetic and electric shielding effects are calculated separately.

In practice, the shielding effect is appreciated in decibels using the quantity called *shield attenuation*, defined as

$$a = 20 \log \frac{1}{|\underline{F}|}, \qquad [\text{db}]. \tag{3}$$

The chosen unit of measure allows to obtain the total attenuation of a structure by adding the attenuations corresponding to its different shields or to its different physical shielding mechanisms.

The shield factor, F, as well as the attenuation, a, depends on the frequency, the shield geometry and material, the place in which the field is measured, the incident field type, direction and polarization.

A shielding problem solving possibility is to elucidate the Helmholtz equation in the exterior, interior and in the shield wall, using adequately the boundary conditions for deducing the shield factor.

Another possibility is to use the inertial approach, [2], [3], for a given medium, which implies to write the diffusion equation in a certain form, obtaining thus a Duffing type equation for describing the penetration of the magnetic field in the shield wall.

Generally speaking, it is desirable to adopt such a field structure so that its constitutive vectors to depend on one space coordinate only, resulting thus a plane wave field, which is a function of time and of a single space coordinate.

The shield functioning can be explained as it follows: the incident field induces in the shield eddy currents, I_F, which produce a magnetic field, $\mathbf{H}_F$, of an opposite direction to the incident field. In the protected space the resulting field is diminished as a vector sum of the two opposite fields, thus obtaining the shielding.

2. The Plane-Parallel Inertial Shield Functioning

Let's consider a shield made in two wide parallel rectangular metallic slabs, of thickness d, conductivity σ and permeability μ, at a distance $2y_0$ one from another. The slabs have great dimensions in comparison with d and $2y_0$. The two slabs are connected together at their edges (Fig.1) with conducting wires or with other slabs ($ADD'A'$ and $BCC'B'$), which have the purpose to allow the eddy currents continuity. Only the slabs $ABB'A'$ and $CDD'C'$ are involved in the shielding process.

The shield is submitted to the action of a homogeneous quasistationary electromagnetic field, whose propagation direction is Oy, perpendicular on the slabs, so that the magnetic field component $\underline{\mathbf{H}}_e$ is parallel with the slabs. Under the action of $\underline{\mathbf{H}}_e$ in the shield are induced eddy currents of intensity I_F, which circulates as in Fig.1, producing a magnetic field $\underline{\mathbf{H}}_F$, opposite to $\underline{\mathbf{H}}_e$. Assuming the slabs to have great dimensions, theoretically infinite ones, the magnetic field $\underline{\mathbf{H}}_F$ is practically zero outside the shield. In the slabs, as well as in the protected space between the slabs, the magnetic field $\underline{\mathbf{H}}_F$ is vectorial added to $\underline{\mathbf{H}}_e$, the resulting magnetic field, $\underline{\mathbf{H}}_i$, being less than the incident one.

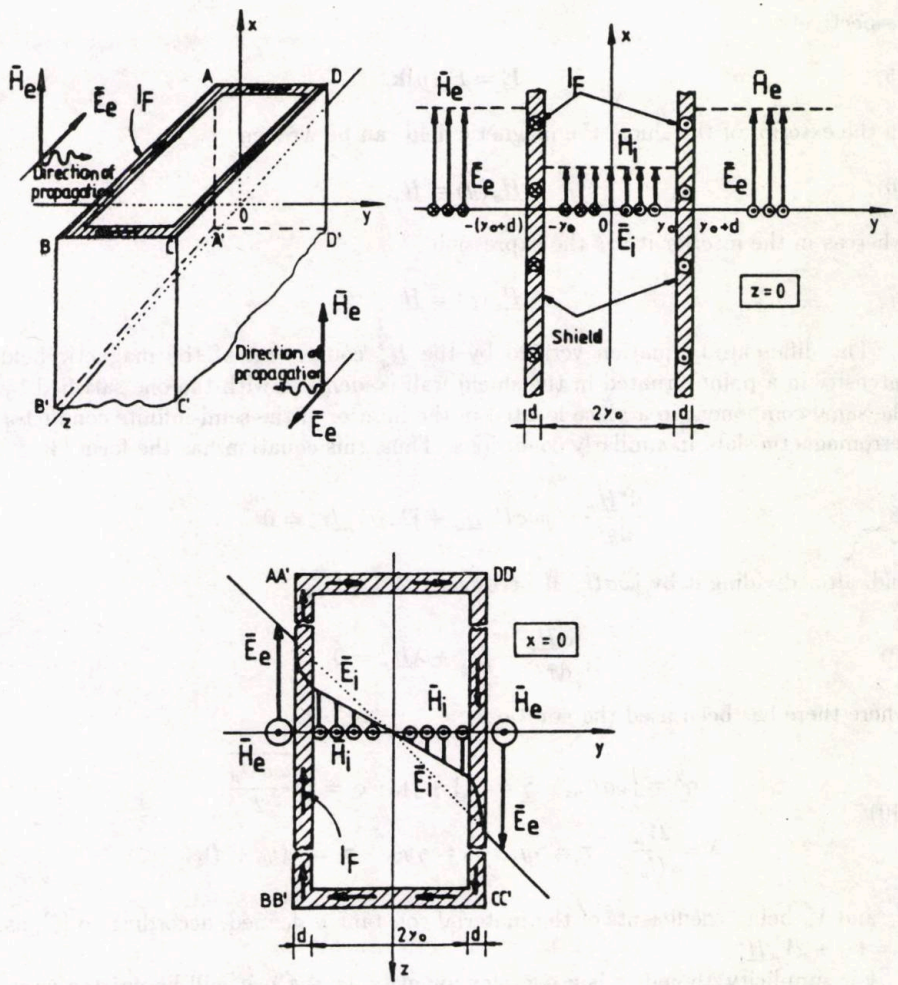

Fig. 1.– Plane-parallel inertial shield.

In order to calculate both the shield factor $\underline{F}$ and the attenuation a there are considered the shield characteristics. Thus, due to the huge, quasi-infinite dimensions in the directions x and z, there is no end effect so that in the protected space between the slabs the magnetic field $\underline{\mathbf{H}}_i$ is constant everywhere. Taking into consideration both the medium infinite extension and the incident magnetic field uniformity, as well as the tangential components continuity at the surface of the conductor, the magnetic field, oriented (according to Fig.1) in the Ox direction, depends only on y and t, similarly with $\underline{\mathbf{E}}$ and $\underline{\mathbf{J}}$. Thus, the magnetic and electric field intensity have the complex images

$$\underline{\mathbf{H}} = \underline{H}_x(y)\mathbf{i}, \tag{4}$$

respectively

$$\underline{\mathbf{E}} = \underline{E}_z(y)\mathbf{k}. \tag{5}$$

In the exterior of the shield the magnetic field can be written

$$\underline{H}_x(y) = \underline{H}_e, \tag{6}$$

whereas in the interior it has the expression

$$\underline{H}_x(y) = \underline{H}_i. \tag{7}$$

The differential equation verified by the $\underline{H}_x$ component of the magnetic field intensity in a point situated in the shield wall is identical with the one satisfied by the same component in a place located in the interior of the semi-infinite conductor ferromagnetic slab, in similarly conditions. Thus, this equation has the form [3]:

$$\frac{\mathrm{d}^2\underline{H}_x}{\mathrm{d}y^2} - \mathrm{j}\omega\sigma U_\mu \underline{H}_x + \mathrm{j}2\omega\sigma V_\mu \underline{H}_x^3 = 0 \tag{8}$$

and, after dividing it by $\mathrm{j}\omega\sigma U_\mu$, it becomes

$$\frac{\mathrm{d}^2\underline{H}_x}{\mathrm{d}\tau^2} - \underline{H}_x + \lambda \underline{H}_x^3 = 0, \tag{9}$$

where there has been used the notations

$$\begin{gathered} \underline{\gamma}^2 = \mathrm{j}\omega\sigma U_\mu, \quad \underline{\gamma} = \alpha(1+\mathrm{j}), \quad \alpha = \sqrt{\frac{\omega\sigma U_\mu}{2}}, \\ \lambda = \frac{2V_\mu}{U_\mu}, \quad \tau = \underline{\gamma} y, \quad \tau_0 = \gamma y_0, \quad \tau_1 = \underline{\gamma}(y_0 + d), \end{gathered} \tag{10}$$

U_μ and V_μ being coefficients of the material constant μ defined, according to [6], as $\mu = U_\mu + 2V_\mu \underline{H}_x^2$.

For simplicity, though τ is a complex quantity, ($\tau \in \mathbb{C}$), it will be written as in (10), without the usual underline. In addition, there is taken into account that, in the case of this type of shield, the boundary conditions for determining the integration constants in the expressions of $\underline{H}_{x0}$, $\underline{H}_{x1}$ and $\underline{H}_{x2}$ are

$$\begin{gathered} \underline{H}_{x0}(y_0) = \underline{H}_i, \quad \underline{H}_{x0}(y_0 + d) = \underline{H}_e, \\ \underline{H}_{x1}(y_0) = \underline{H}_{x1}(y_0 + d) = \underline{H}_{x2}(y_0) = \underline{H}_{x2}(y_0 + d) = 0. \end{gathered} \tag{11}$$

The demonstration that $\lambda \ll 1$ having been already done [3], the equation (9) can be solved using the perturbation (small parameter) method (s. Appendix).

The magnetic field in the wall may be calculated with the relation (s. (A.10)):

$$\underline{H}_x = a\mathrm{e}^{-\underline{\gamma}y} + b\mathrm{e}^{\underline{\gamma}y} + \lambda(a\mathrm{e}^{-\underline{\gamma}y} + b\mathrm{e}^{\underline{\gamma}y})^3(1 - c\mathrm{e}^{-\underline{\gamma}y} - d\mathrm{e}^{\underline{\gamma}y}). \tag{12}$$

3. The Shield Factor $\underline{F}$ and Attenuation a Calculus

In order to determine the shield factor, $\underline{F}$ and the attenuation, a, it is taken into account that for the electric field $\underline{\mathbf{E}} = \underline{E}_z(y)\mathbf{k}$ it can be written

$$\text{rot}\,\underline{\mathbf{E}} = \begin{vmatrix} \mathbf{i} & \mathbf{j} & \mathbf{k} \\ \dfrac{\partial}{\partial x} & \dfrac{\partial}{\partial y} & \dfrac{\partial}{\partial z} \\ 0 & 0 & \underline{E}_z(y) \end{vmatrix}. \tag{13}$$

On the other hand, it is known that

$$\text{rot}\,\underline{\mathbf{E}} = -\mathrm{j}\omega\mu\underline{\mathbf{H}} = -\mathrm{j}\omega\mu\underline{H}_x(y)\mathbf{i}. \tag{14}$$

After simple calculus, by identification, it results

$$\frac{\partial \underline{E}_z(y)}{\partial y} = -\mathrm{j}\omega\mu\underline{H}_x(y). \tag{15}$$

Consequently, the differential equation

$$\mathrm{d}\underline{E}_z(y) = -\mathrm{j}\omega\mu\underline{H}_x(y)\,\mathrm{d}y, \tag{16}$$

obtained from (15), for the interior space, must be integrated, resulting

$$\underline{E}_z(y) = -\mathrm{j}\omega\mu_0\underline{H}_i y_0. \tag{17}$$

In order to find another connecting relation between the electric and the magnetic field and to particularize it for the shield wall, it is calculated

$$\text{rot}\,\underline{\mathbf{H}} = \begin{vmatrix} \mathbf{i} & \mathbf{j} & \mathbf{k} \\ \dfrac{\partial}{\partial x} & \dfrac{\partial}{\partial y} & \dfrac{\partial}{\partial z} \\ \underline{H}_x(y) & 0 & 0 \end{vmatrix}. \tag{18}$$

Having in view that

$$\text{rot}\,\underline{\mathbf{H}} = \sigma\underline{\mathbf{E}} = \sigma\underline{E}_z(y)\mathbf{k} \tag{19}$$

and identifying the terms multiplyed by $\mathbf{k}$ it results:

$$-\frac{\mathrm{d}\underline{H}_x(y)}{\mathrm{d}y} = \sigma\underline{E}_z(y). \tag{20}$$

Knowing the expression (12) of $\underline{H}_x(y)$, the relation

$$\frac{\mathrm{d}\underline{H}_x(y)}{\mathrm{d}y} = \frac{\underline{\gamma}}{\mathrm{e}^{2\underline{\gamma}d} - 1}[\underline{H}_i(\mathrm{e}^{2\underline{\gamma}d} + 1)(\lambda - 1) + 2\mathrm{e}^{\underline{\gamma}d}\underline{H}_e] \tag{21}$$

may be obtained and consequently

$$\underline{E}_z(y) = -\frac{1}{\sigma}\cdot\frac{\mathrm{d}\underline{H}_x(y)}{\mathrm{d}y} = -\frac{\underline{\gamma}}{\sigma(\mathrm{e}^{2\underline{\gamma}d}-1)}[\underline{H}_i(\mathrm{e}^{2\underline{\gamma}d}+1)(\lambda-1)+2\mathrm{e}^{\underline{\gamma}d}\underline{H}_e]. \tag{22}$$

The boundary condition is

$$\underline{E}_t(y_0)_- = \underline{E}_t(y_0)_+ \tag{23}$$

and, after substitution of the appropriate expressions for the left (s. (17)), respectively for the right (s. (22)) term, it is obtained

$$\begin{aligned}\underline{H}_i &= \frac{2\underline{\gamma}\mathrm{e}^{\underline{\gamma}d}\underline{H}_e}{\mathrm{j}\omega\sigma\mu_0 y_0(\mathrm{e}^{2\underline{\gamma}d}-1)-\underline{\gamma}(\mathrm{e}^{2\underline{\gamma}d}+1)(\lambda-1)} = \\ &= \frac{2\mathrm{e}^{\underline{\gamma}d}\underline{H}_e}{\underline{\gamma}\frac{\mu_0}{U_\mu}y_0(\mathrm{e}^{2\underline{\gamma}d}-1)-(\mathrm{e}^{2\underline{\gamma}d}+1)(\lambda-1)}.\end{aligned} \tag{24}$$

Using the notation

$$\underline{K} = \underline{\gamma}\frac{\mu_0}{U_\mu}y_0 \tag{25}$$

and dividing by $2\mathrm{e}^{\underline{\gamma}d}$ it results

$$\underline{H}_i = \frac{\underline{H}_e}{\underline{K}\dfrac{\mathrm{e}^{2\underline{\gamma}d}-1}{2\mathrm{e}^{\underline{\gamma}d}}-\dfrac{\mathrm{e}^{2\underline{\gamma}d}+1}{2\mathrm{e}^{\underline{\gamma}d}}(\lambda-1)} = \frac{\underline{H}_e}{\underline{K}\sinh\underline{\gamma}d+(1-\lambda)\cosh\underline{\gamma}d}, \tag{26}$$

from where may be obtained the expression of the shield factor:

$$\underline{F} = \frac{\underline{H}_i}{\underline{H}_e} = \frac{1}{\underline{K}\sinh\underline{\gamma}d+(1-\lambda)\cosh\underline{\gamma}d}, \tag{27}$$

identical, for $\lambda = 0$, with the one given in [1].

Using the same calculus procedure as in [1] the attenuation may be obtained namely:

$$\begin{aligned}a &= 20\log\frac{1}{|\underline{F}|} = 20\log\sqrt{\Re e^2\left(\frac{1}{\underline{F}}\right)+\Im m^2\left(\frac{1}{\underline{F}}\right)} = \\ &= 10\log\left[\frac{1}{2}(\cosh 2\alpha d+\cos 2\alpha d)(1-\lambda)^2+\right. \\ &\left.+\frac{\alpha\mu_0 y_0}{U_\mu}(\sinh 2\alpha d-\sin 2\alpha d)(1-\lambda)+\left(\frac{\alpha\mu_0 y_0}{U_\mu}\right)^2(\cosh 2\alpha d-\cos 2\alpha d)\right],\end{aligned} \tag{28}$$

where there have been used the notations (10).

The deduced relations can be used either to calculate the attenuation obtained for a given thickness of the shield, or to calculate the necessary thickness in order to obtain an imposed attenuation.

4. Conclusions

It is taken into consideration the possibility of studying a plane–parallel shield with inertial behaviour. This leads to a Duffing type differential equation (9) to describe the magnetic field penetration in the shield walls. The solution (A.10) is obtained using the small parameter method.

Using both connecting relations between the magnetic and the electric field, (17), (22), as well as the boundary condition (23), there is calculated the expression (25) of the interior magnetic field, $\underline{H}_i$.

At the same time it is obtained the shield factor, $\underline{F}$ (s. (27)), and the attenuation, a (s. (28)), resulting relations characteristic for the plane–parallel shield with the walls made in non-linear inertial media. These expressions are different from those calculated for linear media by the term $1 - \lambda, U_\mu$ and α being different as well.

Furthermore, using OLC 35 of 3 mm thickness as shield material, after calculating both the inertial attenuation with the formula (28) and the linear one, for $\mu_r = 1,000$, according to [1], it can be noticed [6] that for a wide range of frequencies ($f \in [10, 10^6]$ Hz) the percentual difference $\left(\Delta a = \dfrac{a - a_{ct}}{a} \cdot 100\%\right)$ is very small ($\Delta a \in [2, 10]\%$).

Appendix

It is admitted [4] as solution of the equation (9) the series

$$\underline{H}_r = \underline{H}_{r0} + \lambda \underline{H}_{r1} + \lambda^2 \underline{H}_{r2} + \cdots. \tag{A.1}$$

from which, if it converges fast enough, there can be retained, with a satisfactory approximation, only the first three terms. It is imposed that this solution satisfies the equation (9); therefore it will be obtained

$$\frac{\mathrm{d}^2 \underline{H}_{r0}}{\mathrm{d}\tau^2} + \lambda \frac{\mathrm{d}^2 \underline{H}_{r1}}{\mathrm{d}\tau^2} + \lambda^2 \frac{\mathrm{d}^2 \underline{H}_{r2}}{\mathrm{d}\tau^2} - (\underline{H}_{ro} + \lambda \underline{H}_{r1} + \lambda^2 \underline{H}_{r2}) + \lambda (\underline{H}_{ro} + \lambda \underline{H}_{r1} + \lambda^2 \underline{H}_{r2})^3 = 0. \tag{A.2}$$

Identifying the terms in λ, λ^1 and λ^2 there are obtained linear differential equations. After their integration it is determined the generating solution and the correction terms. Thus,

a) the generating equation, which is a differential, linear, homogeneous one, with constant coefficients, specific for the linear media, is

$$\frac{\mathrm{d}^2 \underline{H}_{r0}}{\mathrm{d}\tau^2} - \underline{H}_{r0} = 0, \tag{A.3}$$

with the solution

$$\underline{H}_{r0} = \mathrm{e}^{\tau_1 + \tau_0} \frac{\underline{H}_i \mathrm{e}^{\tau_1} - \underline{H}_e \mathrm{e}^{\tau_0}}{\mathrm{e}^{2\tau_1} - \mathrm{e}^{2\tau_0}} \mathrm{e}^{-\tau} + \frac{\underline{H}_e \mathrm{e}^{\tau_1} - \underline{H}_i \mathrm{e}^{\tau_0}}{\mathrm{e}^{2\tau_1} - \mathrm{e}^{2\tau_0}} \mathrm{e}^{\tau} = a\mathrm{e}^{-\tau} + b\mathrm{e}^{\tau}; \tag{A.4}$$

b) the equation of the first approximation

$$\frac{\mathrm{d}^2 \underline{H}_{r1}}{\mathrm{d}\tau^2} - \underline{H}_{r1} + \underline{H}_{r0}^3 = 0 \tag{A.5}$$

has the solution

$$\underline{H}_{x1} = \underline{H}_{x0}^3 \left(1 - \frac{e^{\tau_1+\tau_0}}{e^{\tau_0}+e^{\tau_1}} e^{-\tau} - \frac{1}{e^{\tau_0}+e^{\tau_1}} e^{\tau}\right) = (ae^{-\tau} + be^{\tau})^3(1 - ce^{-\tau} - de^{\tau}), \tag{A.6}$$

which is obtained utilizing the method of variation of parameters [5];

c) the equation of the second approximation

$$\frac{d^2\underline{H}_{x2}}{d\tau^2} - \underline{H}_{x2} + 3\underline{H}_{x0}^2\underline{H}_{x1} = 0, \tag{A.7}$$

admits the solution

$$\underline{H}_{x2} = 3\underline{H}_{x0}^3\underline{H}_{x1}\left(1 - \frac{e^{\tau_1+\tau_0}}{e^{\tau_0}+e^{\tau_1}} e^{-\tau} - \frac{1}{e^{\tau_0}+e^{\tau_1}} e^{\tau}\right) = 3(ae^{-\tau} + be^{\tau})^5(1 - ce^{-\tau} - de^{\tau})^2, \tag{A.8}$$

obtained using the same method.

Consequently, the general solution, with the shape (A.1), is

$$\begin{aligned}\underline{H}_x = {} & ae^{-\underline{\gamma}y} + be^{\underline{\gamma}y} + \lambda(ae^{-\underline{\gamma}y} + be^{\underline{\gamma}y})^3(1 - ce^{-\underline{\gamma}y} - de^{\underline{\gamma}y}) + \\ & + 3\lambda^2(ae^{-\underline{\gamma}y} + be^{\underline{\gamma}y})^5(1 - ce^{-\underline{\gamma}y} - de^{\underline{\gamma}y})^2.\end{aligned} \tag{A.9}$$

In this expression, with a satisfactory approximation, there are kept only the first two terms. Thus, for subsequent calculus, the field in the wall is considered:

$$\underline{H}_x = ae^{-\underline{\gamma}y} + be^{\underline{\gamma}y} + \lambda(ae^{-\underline{\gamma}y} + be^{\underline{\gamma}y})^3(1 - ce^{-\underline{\gamma}y} - de^{\underline{\gamma}y}). \tag{A.10}$$

Received, September 18, 1997

Technical University "Gh.Asachi", Jassy,
Department of General Electrotechnics
and Electrical Machines

REFERENCES

1. R a d u S., *Compatibilitate electromagnetică.* Vol.1, Rotaprint, Univ. Tehnică „Gh.Asachi", Iaşi, 1995.
2. R o s m a n H., *Constantele de material ale mediilor electromagnetice cu neliniaritate slabă, inerţiale, în regim cvasistaţionar armonic.* Mem. secţ. şt., Acad. Rom., s.IV, **II**, 189-194 (1979).
3. T u l e a ş c ă I., *About Electromagnetic Waves Scattering in Nonlinear Inertial Media.* Bul. Inst. polit., Iaşi, **XLI (XLV)**, *3-4*, s. III, 7-18 (1995).
4. S a v i n Gh., R o s m a n H., *Circuite electrice neliniare şi parametrice.* Ed. Tehnică, Bucureşti, 1973.
5. D e m i d o v i c h B., *Problems in Mathematical Analysis.* Mir Publ., Moscow, 1976.
6. T u l e a ş c ă I., *Contribuţii la studiul propagării undelor electromagnetice în medii cu neliniaritate slabă.* Ph.D. Diss., Techn. Univ. "Gh.Asachi", Jassy, 1997.

ECRANUL PLAN-PARALEL INERŢIAL ÎN CÂMP ELECTROMAGNETIC CVASISTAŢIONAR ARMONIC

(Rezumat)

Se pune în evidenţă posibilitatea de a folosi metoda inerţializării mediului în studiul ecranelor electromagnetice, în speţă ecranul plan-paralel. Pentru descrierea pătrunderii câmpului electromagnetic în peretele ecranului se obţine o ecuaţie de tip Duffing care se integrează prin metoda parametrului mic. După obţinerea expresiei intensităţii câmpului magnetic în perete se calculează factorul de ecranare $\underline{F}$ şi atenuarea a a ecranului feromagnetic cu neliniaritate slabă.

BULETINUL INSTITUTULUI POLITEHNIC DIN IAŞI
Tomul XLIV (XLVIII), Fasc. 1–2, 1998
Secţia III
ELECTROTEHNICĂ. ENERGETICĂ. ELECTRONICĂ

C.D. 621.392.5

QUELQUES OBSERVATIONS CONCERNANT LES PARAMÈTRES D'UN QUADRIPÔLE EN SENS RESTREINT, PRIMITIF, ATTACHÉ À UN QUADRIPÔLE GÉNÉRAL LINÉAIRE, NON-AUTONOME, RÉCIPROQUE, EN RÉGIME PERMANENT HARMONIQUE

PAR

HUGO ROSMAN et DORIN BELAUS

On détermine les paramètres $\underline{A}'_{ij}, \underline{Y}'_{ij}, \underline{Z}'_{ij}, \underline{H}'_{ij}, \underline{F}'_{ij}$, $(i, j=1, 2)$, d'un quadripôle en sens restreint, primitif, attaché à un quadripôle général linéaire, non-autonome, réciproque, en régime permanent harmonique. Ceux-ci sont des fonctions des paramètres $\underline{A}_{ij}$, $(i, j = 1.2.3)$, du quadripôle général et de l'impédance $\underline{Z}_3$ de la branche de couplage entre les portes d'accès de celui-ci.

Les paramètres d'un quadripôle primitif ont des valeurs (complexes) situées à l'intérieur et sur les frontières de certains domaines d'existence délimités par des cercles.

On établit les relations de calcul des impédances de transfert à vide, des admittances de transfert en court-circuit, des coefficients de transmission de la tension à vide et des coefficients de transmission du courant en court-circuit d'un quadripôle primitif attaché à un quadripôle général.

1. Introduction

Dans une Note antérieure [1] l'un des auteurs (H.R.) a prouvé qu'il y a la possibilité d'attacher d'une manière univoque, à un quadripôle général linéaire, non-autonome, caractérisé par la matrice des paramètres fondamentaux:

$$[\underline{A}] = \begin{bmatrix} \underline{A}_{11} & \underline{A}_{12} & \underline{A}_{13} \\ \underline{A}_{21} & \underline{A}_{22} & \underline{A}_{23} \\ \underline{A}_{31} & \underline{A}_{32} & \underline{A}_{33} \end{bmatrix}, \tag{1}$$

un quadripôle en sens restreint, de même linéaire et non-autonome, que l'on a dénommé primitif, ayant la matrice des paramètres fondamentaux:

$$[\underline{A}'] = \begin{bmatrix} \underline{A}'_{11} & \underline{A}'_{12} \\ \underline{A}'_{21} & \underline{A}'_{22} \end{bmatrix}. \tag{2}$$

L'équivalence des deux quadripôles (général et primitif) est assurée par les relations

[1]:

$$\underline{A}'_{11} = \underline{A}_{11} + \frac{\underline{A}_{13}\underline{A}_{31}}{\underline{Z}_3 - \underline{A}_{33}}, \quad \underline{A}'_{12} = \underline{A}_{12} + \frac{\underline{A}_{12}\underline{A}_{32}}{\underline{Z}_3 - \underline{A}_{33}},$$

(3)

$$\underline{A}'_{21} = \underline{A}_{21} + \frac{\underline{A}_{23}\underline{A}_{31}}{\underline{Z}_3 - \underline{A}_{33}}, \quad \underline{A}'_{22} = \underline{A}_{22} + \frac{\underline{A}_{23}\underline{A}_{32}}{\underline{Z}_3 - \underline{A}_{33}},$$

où $\underline{Z}_3$ est l'impédance de la branche de **couplage** entre les portes d'accès du quadripôle général (Fig.1 *a*).

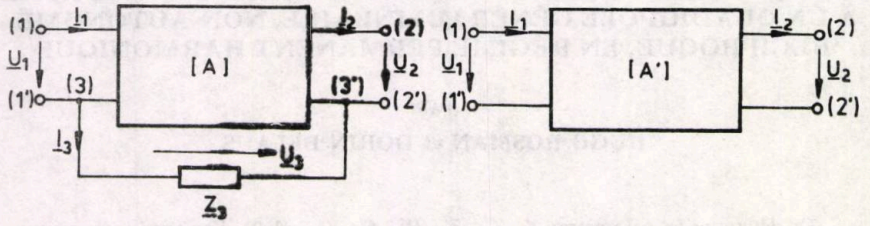

a *b*

Fig. 1

Compte **tenu** des relations (3) on peut écrire la matrice $[\underline{A}']$ (v.(2)) sous la forme équivalente:

$$(4) \quad [\underline{A}'] = \frac{1}{\underline{Z}_3 - \underline{A}_{33}} \begin{bmatrix} \underline{A}_{11}\underline{Z}_3 + \underline{A}_{13}\underline{A}_{31} - \underline{A}_{11}\underline{A}_{33} & \underline{A}_{12}\underline{Z}_3 + \underline{A}_{13}\underline{A}_{32} - \underline{A}_{12}\underline{A}_{33} \\ \underline{A}_{21}\underline{Z}_3 + \underline{A}_{23}\underline{A}_{31} - \underline{A}_{21}\underline{A}_{33} & \underline{A}_{22}\underline{Z}_3 + \underline{A}_{23}\underline{A}_{32} - \underline{A}_{22}\underline{A}_{33} \end{bmatrix}.$$

L'avantage conféré par l'association d'un quadripôle primitif (Fig.1 *b*) à un **quadripôle général** est évident. En effet, à l'aide des relations (3) (ou (4)) on peut assurer la conversion rapide des relations bien connues qui caractérisent un quadripôle en sens restreint, en celles qui correspondent à un quadripôle général, rarement rencontrées dans la littérature de spécialité et, en tout cas, assez difficile d'établir par voie directe.

2. Paramètres du quadripôle primitif

Une fois connue la matrice $[\underline{A}']$ il est possible à déterminer les autres matrices d'un quadripôle primitif ($[\underline{Z}']$, $[\underline{Y}']$, $[\underline{H}']$, $[\underline{F}']$) en fonction des paramètres fondamentaux $\underline{A}_{ij}$, $(i,j=1,2,3)$, du quadripôle général auquel est attaché le quadripôle primitif et de l'impédance $\underline{Z}_3$. Si on poursuit à déterminer ces matrices on utilise les relations de liaison entre $[\underline{A}']$, d'une part et $[\underline{Z}']$, $[\underline{Y}']$, $[\underline{H}']$, $[\underline{F}']$, d'autre part (par ex. [2]). En considérant seulement le cas plus simple des quadripôles réciproques, on obtient, tous calculs effectués, les relations:

$$[\underline{Y}'] = \frac{1}{\underline{A}_{12}\underline{Z}_3 + \underline{A}_{13}\underline{A}_{32} - \underline{A}_{12}\underline{A}_{33}} \times$$

(5)

$$\times \begin{bmatrix} \underline{A}_{22}\underline{Z}_3 + \underline{A}_{23}\underline{A}_{32} - \underline{A}_{22}\underline{A}_{33} & -\underline{A}_{12}\underline{Z}_3 - \underline{A}_{13}\underline{A}_{32} + \underline{A}_{12}\underline{A}_{33} \\ \underline{A}_{12}\underline{Z}_3 + \underline{A}_{13}\underline{A}_{32} - \underline{A}_{12}\underline{A}_{33} & -\underline{A}_{11}\underline{Z}_3 + \underline{A}_{11}\underline{A}_{33} - \underline{A}_{13}\underline{A}_{31} \end{bmatrix},$$

$$[\underline{Z}'] = \frac{1}{\underline{A}_{21}\underline{Z}_3 + \underline{A}_{23}\underline{A}_{31} - \underline{A}_{21}\underline{A}_{33}} \times$$

(6)

$$\times \begin{bmatrix} \underline{A}_{11}\underline{Z}_3 + \underline{A}_{13}\underline{A}_{31} - \underline{A}_{11}\underline{A}_{33} & -\underline{A}_{21}\underline{Z}_3 - \underline{A}_{23}\underline{A}_{31} + \underline{A}_{21}\underline{A}_{33} \\ \underline{A}_{21}\underline{Z}_3 + \underline{A}_{23}\underline{A}_{31} - \underline{A}_{21}\underline{A}_{33} & -\underline{A}_{22}\underline{Z}_3 + \underline{A}_{22}\underline{A}_{23} - \underline{A}_{23}\underline{A}_{32} \end{bmatrix},$$

$$[\underline{H}'] = \frac{1}{\underline{A}_{22}\underline{Z}_3 + \underline{A}_{23}\underline{A}_{32} - \underline{A}_{22}\underline{A}_{33}} \times$$

(7)

$$\times \begin{bmatrix} \underline{A}_{12}\underline{Z}_3 + \underline{A}_{13}\underline{A}_{32} - \underline{A}_{12}\underline{A}_{33} & \underline{A}_{22}\underline{Z}_3 + \underline{A}_{23}\underline{A}_{32} - \underline{A}_{22}\underline{A}_{33} \\ \underline{A}_{22}\underline{Z}_3 + \underline{A}_{23}\underline{A}_{32} - \underline{A}_{22}\underline{A}_{33} & -\underline{A}_{21}\underline{Z}_3 + \underline{A}_{22}\underline{A}_{33} - \underline{A}_{23}\underline{A}_{31} \end{bmatrix},$$

$$[\underline{F}'] = \frac{1}{\underline{A}_{11}\underline{Z}_3 + \underline{A}_{13}\underline{A}_{31} - \underline{A}_{11}\underline{A}_{33}} \times$$

(8)

$$\times \begin{bmatrix} \underline{A}_{21}\underline{Z}_3 + \underline{A}_{23}\underline{A}_{31} - \underline{A}_{21}\underline{A}_{33} & \underline{A}_{11}\underline{Z}_3 + \underline{A}_{13}\underline{A}_{31} - \underline{A}_{11}\underline{A}_{33} \\ \underline{A}_{11}\underline{Z}_3 + \underline{A}_{13}\underline{A}_{31} - \underline{A}_{11}\underline{A}_{33} & -\underline{A}_{12}\underline{Z}_3 + \underline{A}_{12}\underline{A}_{33} - \underline{A}_{13}\underline{A}_{32} \end{bmatrix}.$$

Evidemment on peut calculer d'une façon analogue les paramètres du quadripôle primitif alimenté simultanément aux deux portes d'accès. Dans ce but on tient compte que [3]:

$$(\underline{Y}'_1)_1 = \underline{Y}'_{11} + \underline{Y}'_{12}, \quad (\underline{Y}'_2)_1 = -\underline{Y}'_{22} + \underline{Y}'_{21},$$

(9)

$$(\underline{Y}'_1)_{-1} = \underline{Y}'_{11} - \underline{Y}'_{12}, \quad (\underline{Y}'_2)_{-1} = -\underline{Y}'_{22} + \underline{Y}'_{21}.$$

Eu égard les expressions (5) des paramètres $\underline{Y}_{ij}$, $(i,j=1,2,3)$, on obtient:

$$(\underline{Y}'_1)_1 = \frac{1}{\underline{A}_{12}\underline{Z}_3 + \underline{A}_{13}\underline{A}_{32} - \underline{A}_{12}\underline{A}_{33}} \times$$

$$\times[(-\underline{A}_{12} + \underline{A}_{22})\underline{Z}_3 + (\underline{A}_{23} - \underline{A}_{13})\underline{A}_{32} + (\underline{A}_{12} - \underline{A}_{22})\underline{A}_{33}],$$

$$(\underline{Y}'_2)_1 = \frac{1}{\underline{A}_{12}\underline{Z}_3 + \underline{A}_{13}\underline{A}_{32} - \underline{A}_{12}\underline{A}_{33}} \times$$

$$\times[(\underline{A}_{11} - \underline{A}_{12})\underline{Z}_3 + (\underline{A}_{12} - \underline{A}_{11})\underline{A}_{33} + (\underline{A}_{31} - \underline{A}_{32})\underline{A}_{13}],$$

(10)

$$(\underline{Y}'_1)_{-1} = \frac{1}{\underline{A}_{12}\underline{Z}_3 + \underline{A}_{13}\underline{A}_{32} - \underline{A}_{12}\underline{A}_{33}} \times$$

$$\times[(\underline{A}_{12} + \underline{A}_{22})\underline{Z}_3 + (\underline{A}_{13} + \underline{A}_{23})\underline{A}_{32} - (\underline{A}_{12} + \underline{A}_{22})\underline{A}_{33}],$$

$$(\underline{Y}'_2)_{-1} = \frac{1}{\underline{A}_{12}\underline{Z}_3 + \underline{A}_{13}\underline{A}_{32} - \underline{A}_{12}\underline{A}_{33}} \times$$

$$\times[(\underline{A}_{11} + \underline{A}_{12})\underline{Z}_3 - (\underline{A}_{11} + \underline{A}_{12})\underline{A}_{33} + (\underline{A}_{31} + \underline{A}_{32})\underline{A}_{31}].$$

Un cas particulier intéressant c'est celui des quadripôles généraux linéaires, non-autonomes, ayant la branche de couplage entre les deux portes d'accés en court-circuit ($\underline{Z}_3=0$), en résultant des expressions spécifiques, particulières à leur tour, pour les matrices des paramètres du quadripôle primitif. Par exemple la matrice des paramètres fondamentaux est dans ce cas:

$$[\underline{A}'] = \begin{bmatrix} \underline{A}_{11} - \dfrac{\underline{A}_{13}\underline{A}_{31}}{\underline{A}_{33}} & \underline{A}_{12} - \dfrac{\underline{A}_{13}\underline{A}_{32}}{\underline{A}_{33}} \\ \underline{A}_{21} - \dfrac{\underline{A}_{23}\underline{A}_{31}}{\underline{A}_{33}} & \underline{A}_{22} - \dfrac{\underline{A}_{23}\underline{A}_{32}}{\underline{A}_{33}} \end{bmatrix}. \tag{11}$$

Par une voie analogue on peut obtenir, dans ce cas particulier, les expressions des matrices $[\underline{Y}']$, $[\underline{Z}']$, $[\underline{H}']$, $[\underline{F}']$ et celles des paramètres $(\underline{Y}'_1)_1$, $(\underline{Y}'_2)_1$, $(\underline{Y}'_1)_{-1}$, $(\underline{Y}'_2)_{-1}$.

Malgré qu'ils ne constituent pas, proprement dit, des paramètres du quadripôle (primitif), on peut étudier, dans le sens suivi dans cette Note, autant le coefficient de réciprocité que le facteur de symétrie:

$$\underline{m} = \sqrt{\underline{A}'_{11}\underline{A}'_{22} - \underline{A}'_{12}\underline{A}'_{21}}, \quad \text{respectivement} \quad \underline{n} = \sqrt{\frac{\underline{A}'_{22}}{\underline{A}'_{11}}}. \tag{12}$$

Si on tient compte des relations (3) on peut écrire l'expression (12) du coefficient de réciprocité en fonction des paramètres fondamentaux $\underline{A}_{ij}$, $(i,j=1,2,3)$, du quadripôle général et de l'impédance $\underline{Z}_3$:

(13)

$$\underline{m} = \frac{1}{\underline{Z}_3 - \underline{A}_{33}}\sqrt{(\underline{A}_{11}\underline{A}_{22} - \underline{A}_{12}\underline{A}_{21})\underline{Z}_3^2 - [\underline{A}_{33}(\underline{A}_{11}\underline{A}_{22} - \underline{A}_{12}\underline{A}_{21}) + |\underline{A}|]\underline{Z}_3 + \underline{A}_{33}|A|},$$

ou

$$|\underline{A}| = \det[\underline{A}_{ij}], \ (i,j = 1,2,3). \tag{14}$$

Dans les mêmes conditions le facteur de symétrie est

$$\underline{n} = \sqrt{\frac{\underline{A}_{22}\underline{Z}_3 + \underline{A}_{23}\underline{A}_{32} - \underline{A}_{22}\underline{A}_{33}}{\underline{A}_{11}\underline{Z}_3 + \underline{A}_{13}\underline{A}_{31} - \underline{A}_{11}\underline{A}_{33}}}. \tag{15}$$

Si la branche du couplage entre les portes d'accès du quadripôle général est en court-circuit ($\underline{Z}_3 = 0$), les relations (13) et (15) deviennent:

$$\underline{m} = \sqrt{\frac{|\underline{A}|}{\underline{A}_{33}}}, \quad \text{respectivement} \quad \underline{n} = \sqrt{\frac{\underline{A}_{23}\underline{A}_{32} - \underline{A}_{22}\underline{A}_{33}}{\underline{A}_{13}\underline{A}_{31} - \underline{A}_{11}\underline{A}_{33}}}. \tag{16}$$

3. Domaines d'existence des paramètres d'un quadripôle primitif

Si on analyse les relations (5),...,(9) on arrive rapidement à la conclusion que les paramètres d'un quadripôle (en sens restreint) primitif sont de la forme:

$$\underline{T} = \frac{\underline{\alpha} + \underline{\beta} \underline{Z}_3}{\underline{\gamma} + \underline{\delta} \underline{Z}_3}, \tag{17}$$

où $\underline{\alpha}, \underline{\beta}, \underline{\gamma}, \underline{\delta}$ sont des fonctions complexes, seulement des paramètres $\underline{A}_{ij}, (i, j = 1, 2, 3)$, du quadripôle général étudié. Compte tenu que celui-ci est linéaire il résulte que

$$\Re e(\underline{Z}_3) \geq 0, \tag{18}$$

de sorte que les paramètres du quadripôle primitif ont des valeurs (complexes) situées seulement à l'intérieur et sur la frontière de certaines domaines denommés d'existence. La relation (17) représente une *transformation linéaire* [4] qui réalise la transformation conforme du demi-plan $\Re e(\underline{Z}_3) \geq 0$ en cercles situés dans les plans complexes des paramètres du quadripôle primitif.

A titre d'exemple on détermine, dans l'Annexe, l'équation du cercle qui délimite le domaine d'existence du paramètre fondamental $\underline{A}'_{11}$.

Il faut souligner le fait que si dans le cas d'un quadripôle en sens restreint, réciproque, trois de chaque set de quatre paramètres de celui-ci peuvent prendre des valeurs (complexes) arbitraires, le quatrième en étant imposé par la condition de réciprocité, pour n'importe quel quadripôle primitif, attaché à un quadripôle général, chacun des quatre paramètres appartenant à un certain set prend obligatoirement des valeurs situées seulement à l'intérieur et sur la frontière du domaine d'existence respectif; en outre, si nécessaire, les paramètres du quadripôle satisfont aussi à la condition de réciprocité.

Non seulement les paramètres $\underline{A}'_{ij}$, $\underline{Y}'_{ij}$, $\underline{Z}'_{ij}$,...,$(i, j=1,2)$, d'un quadripôle (en sens restreint) primitif prennent des valeurs situées à l'intérieur et sur la frontière de certaines domaines, bien définis, mais aussi: a) les impédances de transfert à vide et les admittances de transfert en court-circuit; b) les rapports de transformation des tensions à vide et des courants en court-circuit. On tient compte dans ces cas que [2]:

$$\begin{gathered}
\underline{Z}'_{m10} = \frac{1}{\underline{A}'_{11}},\ \underline{Z}'_{m20} = \frac{1}{\underline{A}'_{21}},\ \underline{Z}'_{m1cc} = 0,\ \underline{Z}'_{m2cc} = 0; \\
\underline{Y}'_{m10} = 0,\ \underline{Y}'_{m20} = 0,\ \underline{Y}'_{m1cc} = \frac{1}{\underline{A}'_{12}},\ \underline{Y}'_{m2cc} = \frac{1}{\underline{A}'_{22}}; \\
\underline{k}'_{u10} = \frac{1}{\underline{A}'_{11}},\ \underline{k}'_{u20} = \frac{1}{\underline{A}'_{22}},\ \underline{k}'_{u1cc} = 0,\ \underline{k}'_{u2cc} = 0; \\
\underline{k}'_{i10} = 0,\ \underline{k}'_{i20} = 0,\ \underline{k}'_{i1cc} = \frac{1}{\underline{A}'_{22}},\ \underline{k}'_{i2cc} = \frac{1}{\underline{A}'_{11}},
\end{gathered} \tag{19}$$

en considérant le cas, plus simple, lorsque le quadripôle primitif est réciproque. Vu que les paramètres fondamentaux, $\underline{A}'_{ij}$, $(i, j=1,2)$, d'un quadripôle primitif ont des valeurs situées seulement à l'intérieur et sur la frontière de certains domaines il résulte, évidemment, que $\underline{Z}'_{m10}$, $\underline{Z}'_{m20}$, $\underline{Y}'_{m1cc}$, $\underline{Y}'_{m2cc}$, $\underline{k}'_{u10}$, $\underline{k}'_{u20}$, $\underline{k}'_{i1cc}$, $\underline{k}'_{rcc}$ satisfont à

des restrictions similaires. Il est facile à constater que les domaines d'existence de ces derniers paramètres sont délimités, aussi, par des cercles, en général, en pouvant dégénerer, dans certains cas, en (demi)droites.

Un raisonnement tout à fait similaire à celui utilisé ci-dessus permet à aboutir à la conclusion que même le coefficient de réciprocité, $\underline{m}$, et le facteur de nonsymétrie, $\underline{n}$, ont des valeurs situées à l'intérieur et sur la frontière de certains domaines délimités par des courbes fermées, dont les équations, de degré >2, peuvent être déterminées avec des moyens semblables.

4. Conclusions

1° On établit les relations qui permettent à calculer les matrices $[\underline{A}']$, $[\underline{Y}']$, $[\underline{Z}']$, $[\underline{H}']$, $[\underline{F}']$ d'un quadripôle en sens restreint, primitif, attaché à un quadripôle général linéaire, non-autonome, réciproque, en régime permanent harmonique; les éléments de ces matrices sont fonctions des paramètres fondamentaux $\underline{A}'_{ij}$, $(i,j=1,2,3)$, du quadripôle général et de l'impédance $\underline{Z}_3$ de la branche de couplage entre les portes d'accès du quadripôle.

2° On prouve que les paramètres $\underline{A}'_{ij}$, $\underline{Y}'_{ij}$, $\underline{Z}'_{ij}$, $\underline{H}'_{ij}$, $\underline{F}'_{ij}$, $(i,j=1,2)$, d'un quadripôle primitif réciproque ont des valeurs situées seulement dans certains domaines (d'existence) qui sont des cercles et leurs frontières.

3° Outre ces paramètres on met en évidence encore une propriété spécifique aux quadripôles primitifs à savoir les impédances de transfert à vide, les admittances de transfert en court-circuit, les rapports de transformation des tensions à vide et les rapports de transformation des courants en court-circuit ont des valeurs situées seulement à l'intérieur de certains domaines, y compris sur leurs frontières. Les équations des courbes qui délimitent ces domaines sont fonctions seulement des paramètres fondamentaux du quadripôle général auquel est attaché le quadripôle primitif.

4° On établit les relations de calcul du coefficient de réciprocité et du facteur de nonsymétrie d'un quadripôle primitif, en prouvant que même ces grandeurs dépendent seulement des paramètres fondamentaux du quadripôle général auquel est attaché le quadripôle primitif et de l'impédance $\underline{Z}_3$ de la branche de couplage entre les portes d'accès. Tant le coefficient de réciprocité que le facteur de nonsymétrie ont des valeurs, dans le cas considéré d'un quadripôle primitif, situées à l'intérieur de certains domaines qu'on peut déterminer, y compris sur leurs frontières.

Annexe

Domaine d'existence du paramètre $\underline{A}'_{11}$

Pour déterminer l'équation de la courbe qui délimite le domaine d'existence de $\underline{A}_{11}$ on détermine, tout d'abord, l'impédance $\underline{Z}_3$ de l'équation (31) et on impose la condition $\Re e(\underline{Z}_3) = 0$. On obtient l'expression:

$$\begin{aligned}(A.1)\quad &\Re e(\underline{A}_{33})\{[\Re e(\underline{A}'_{11})]^2 + [\Im m(\underline{A}'_{11})]^2\} - [2\Re e(\underline{A}_{11})\Re e(\underline{A}_{33}) - \Re e(\underline{A}_{13}\underline{A}_{31})]\Re e(\underline{A}'_{11}) + \\ &+[2\Re e(\underline{A}_{11})\Im m(\underline{A}_{33}) + \Im m(\underline{A}_{13}\underline{A}_{31})]\Im m(\underline{A}'_{11}) + \Re e[\underline{A}^*_{11}(\underline{A}_{11}\underline{A}_{33} - \underline{A}_{13}\underline{A}_{31})] = 0.\end{aligned}$$

On peut distinguer deux cas: a) $\Re e(\underline{A}_{33}) \neq 0$; b) $\Re e(\underline{A}_{33}) = 0$. Dans le premier cas l'expression (A.1) conduit à

$$[\Re e(\underline{A}'_{11})]^2 + [\Im m(\underline{A}'_{11})]^2 - \frac{2\Re e(\underline{A}_{11})\Re e(\underline{A}_{33}) - \Re e(\underline{A}_{13}\underline{A}_{31})}{\Re e(\underline{A}_{33})}\Re e(\underline{A}'_{11}) +$$

$$+\frac{2\Re e(\underline{A}_{11})\Im m(\underline{A}_{33}) + \Im m(\underline{A}_{13}\underline{A}_{31})}{\Re e(\underline{A}_{33})}\Im m(\underline{A}'_{11}) + \frac{\Re e[\underline{A}^*_{11}(\underline{A}_{11}\underline{A}_{33} - \underline{A}_{13}\underline{A}_{31})]}{\Re e(\underline{A}_{33})} = 0, \tag{A.2}$$

qui représente l'équation d'un cercle ayant le centre dans le point de coordonnées:

$$\frac{2\Re e(\underline{A}_{11})\Re e(\underline{A}_{33}) - \Re e(\underline{A}_{13}\underline{A}_{31})}{2\Re e(\underline{A}_{33})}, \quad -\frac{2\Re e(\underline{A}_{11})\Im m(\underline{A}_{33}) + \Im m(\underline{A}_{13}\underline{A}_{31})}{2\Re e(\underline{A}_{33})} \tag{A.3}$$

et le rayon

(A.4)

$$r_{\underline{A}'_{11}} = \frac{\sqrt{4[\Re e(\underline{A}_{33})]^2 A_{11}^2 + |\underline{A}_{13}\underline{A}_{31}|^2 - 4\Re e(\underline{A}_{33})\Re e(\underline{A}_{11}\underline{A}_{13}\underline{A}_{31}) + \Re e[\underline{A}^*_{11}(\underline{A}_{11}\underline{A}_{33} - \underline{A}_{13}\underline{A}_{31})]}}{2\Re e(\underline{A}_{33})}.$$

Evidemment les paramètres fondamentaux $\underline{A}_{ij}, (i, j = 1, 2, 3)$, du quadripole général, doivent satisfaire l'inégalité:

$$4[\Re e(\underline{A}_{33})]^2 A_{11}^2 + |\underline{A}_{13}\underline{A}_{31}|^2 - 4\Re e(\underline{A}_{33})\Re e(\underline{A}_{11}\underline{A}_{13}\underline{A}_{31}) + \Re e[\underline{A}^*_{11}(\underline{A}_{11}\underline{A}_{33} - \underline{A}_{13}\underline{A}_{31})] \geq 0. \tag{A.5}$$

Dans le deuxième cas l'équation (A.1) se réduit à

$$-\Re e(\underline{A}_{13}\underline{A}_{31})\Re e(\underline{A}'_{11}) + [2\Re e(\underline{A}_{11})\Im m(\underline{A}_{33}) + \Im m(\underline{A}_{13}\underline{A}_{31})]\Im m(\underline{A}'_{11}) = 0, \tag{A.6}$$

qui est celle d'une droite.

D'une façon analogue on peut déterminer les équations des courbes (ce sont des cercles) qui délimitent les domaines d'existence des autres paramètres du quadripôle primitif.

Reçue le 31 mai 1997

Université Technique „Gh. Asachi", Jassy,
Chaire d'Electrotechnique
et
Chaire d'Electrotechnique
générale et Machines électriques

BIBLIOGRAPHIE

1. R o s m a n H., *Sur les conditions de réciprocité et de symétrie d'un biporte général linéaire, non-autonome, en régime permanent harmonique.* Bul. Inst. polit., Iaşi, **XL (XLIV)**, *1-4*, s. III, 23-30 (1994).
2. Ş o r a C., *Cuadripolul electric.* Ed. Tehnică, Bucureşti, 1964.
3. S t o i l o v S., *Teoria funcţiilor de o variabilă complexă.* Ed. Acad., Bucureşti, 1964.
4. Ş o r a C., *Admitanţele echivalente ale cuadripolilor alimentaţi pe la ambele capete.* Thèse de doctorat, Inst. polit. „Traian Vuia", Timişoara, 1961.

CÂTEVA OBSERVAŢII REFERITOARE LA PARAMETRII UNUI CUADRIPOL IN SENS RESTRÂNS, PRIMITIV, ATAŞAT UNUI CUADRIPOL GENERAL LINIAR, NEAUTONOM, RECIPROC, ÎN REGIM PERMANENT ARMONIC

(Rezumat)

Se determină parametrii $\underline{A}'_{ij}, \underline{Y}'_{ij}, \underline{Z}'_{ij}, \underline{H}'_{ij}, \underline{F}'_{ij}, (i, j = 1, 2)$, ai unui cuadripol în sens restrâns, primitiv, ataşat unui cuadripol general liniar neautonom, reciproc, în regim permanent armonic.

Aceştia sunt funcţii de parametrii $\underline{A}_{ij}, (i,j = 1,2,3)$, ai cuadripolului general şi de impedanţa $\underline{Z}_3$ a laturii de cuplaj dintre porţile de acces ale sale.

Parametrii unui cuadripol primitiv pot lua valori numai în interiorul şi pe frontierele unor domenii de existenţă delimitate de cercuri.

Se stabilesc formulele de calcul ale impedanţelor de transfer la gol, admitanţelor de transfer în scurtcircuit, coeficienţilor de transmisie a tensiunilor la gol şi a curenţilor în scurtcircuit, în acelaşi caz al unui cuadripol primitiv ataşat unui cuadripol general având aceleaşi caracteristici. Totodată se stabilesc domeniile de existenţă ale acestor mărimi, ecuaţiile curbelor care le delimitează fiind funcţii numai de parametrii fundamentali $\underline{A}_{ij}, (i,j = 1,2,3)$, ai cuadripolului general considerat.

Se determină expresiile coeficientului de reciprocitate şi factorului de nesimetrie ale unui cuadripol primitiv, în aceleaşi condiţii şi se stabilesc domeniile lor de existenţă.

BULETINUL INSTITUTULUI POLITEHNIC DIN IAŞI
Tomul XLIV (XLVIII), Fasc. 1-2, 1998
Secţia III
ELECTROTEHNICĂ. ENERGETICĂ. ELECTRONICĂ

C.D. 621.392.5

QUADRIPÔLES GÉNÉRAUX LINÉAIRES, NON-AUTONOMES, UNIDIRECTIONNELS, EN RÉGIME PERMANENT HARMONIQUE

PAR

DORIN BELAUS et HUGO ROSMAN

On prouve que tout comme les quadripôles en sens restreint, les quadripôles généraux linéaires, non-autonomes, sont capables d'avoir des propiétés unidirectionnelles. Il est question des quadripoles généraux à forte unidirectionnalité, qui sont obligatoirement non-réciproques et des quadripoles généraux à faible unidirectionnalité, qui sont soit non-réciproques, soit réciproques.

1. Introduction

Selon les données de la littérature (par ex. [1]) tout quadripôle en sens restreint peut avoir des propriétés unidirectionnelles si ses paramètres fondamentaux $\underline{A}_{ij}$, $(i,j=1,2)$, satisfont la relation

$$\underline{A}_{11}\underline{A}_{22} - \underline{A}_{12}\underline{A}_{21} = 0. \tag{1}$$

Dans le cas de tels quadripôles l'impédance équivalente $\underline{Z}_{e1}$ à la porte d'entrée est indépendante de l'impédance $\underline{Z}_2$ du récepteur si

$$\underline{Z}_{e10} = \underline{Z}_{e1cc}, \tag{2}$$

c'est-à-dire si les impédances équivalentes à vide et en court-circuit à la porte (1), $(1')$, d'entrée, sont égales. Dans cette situation on réalise le transfert de l'énergie électromagnétique seulement dans un seul sens, à savoir de la porte d'entrée (1), $(1')$ vers celle de sortie (2), $(2')$ (Fig.1 *a*).

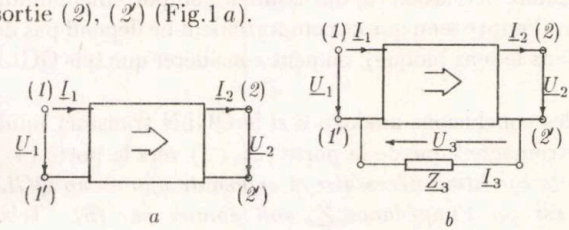

Fig. 1

Le but de cette Note est d'étudier la possibilité qu'un quadripôle général linéaire, non-autonome (dans le sens défini par S i g o r s k y [2]), ait des propriétés unidirectionnelles, en assurant le transfert de l'énergie électromagnétique à partir de la porte d'entrée vers celle de sortie (Fig.1 *b*), le sens opposé étant bloqué.

2. Quadripôles généraux linéaires, nonautonomes, à forte unidirectionnalité

Dans une Note antérieure [3] l'un des auteurs (D.B.) a prouvé que dans le cas d'un quadripôle général linéaire, nonautonome (QGLN), ayant les équations:

$$\begin{bmatrix} \underline{U}_1 \\ \underline{I}_1 \\ \underline{U}_3 \end{bmatrix} = \begin{bmatrix} \underline{A}_{11} & \underline{A}_{12} & \underline{A}_{13} \\ \underline{A}_{21} & \underline{A}_{22} & \underline{A}_{23} \\ \underline{A}_{31} & \underline{A}_{32} & \underline{A}_{33} \end{bmatrix} \begin{bmatrix} \underline{U}_2 \\ \underline{I}_2 \\ \underline{I}_3 \end{bmatrix}, \tag{3}$$

les impédances équivalentes à vide ($\underline{Z}_{e10}$) et en court-circuit ($\underline{Z}_{e1cc}$) ont les expressions:

$$\underline{Z}_{e10} = \frac{\underline{A}_{11}\underline{Z}_3 - \underline{A}_{11}\underline{A}_{33} + \underline{A}_{13}\underline{A}_{31}}{\underline{A}_{21}\underline{Z}_3 - \underline{A}_{21}\underline{A}_{33} + \underline{A}_{23}\underline{A}_{31}}, \tag{4}$$

respectivement

$$\underline{Z}_{e1cc} = \frac{\underline{A}_{12}\underline{Z}_3 - \underline{A}_{12}\underline{A}_{33} + \underline{A}_{13}\underline{A}_{32}}{\underline{A}_{22}\underline{Z}_3 - \underline{A}_{22}\underline{A}_{33} + \underline{A}_{23}\underline{A}_{32}}, \tag{5}$$

si le quadripôle est alimenté en sens direct.

Dans la même Note [3] on a prouvé que l'équation (1) est satisfaite seulement si

$$\underline{Z}_3 = \frac{|\underline{A}|}{\underline{A}_{11}\underline{A}_{22} - \underline{A}_{12}\underline{A}_{21}}, \tag{6}$$

où

$$|\underline{A}| = \det[\underline{A}], \quad \text{avec} \quad [\underline{A}] = [\underline{A}_{ij}], \quad (i, j = 1, 2, 3). \tag{7}$$

Selon les résultats obtenus dans [3], ce sont seulement des QGLN nonréciproques qui sont capables à satisfaire la relation (6) qui assure le comportement unidirectionnel du quadripôle général. Compte tenu que ce comportement ne dépend pas de l'impédance $\underline{Z}_1$ du récepteur (dans le sens bloqué), on peut considérer que tels QGLN sont à forte unidirectionnalité.

On aboutit à des conclusions analogues si le QGLN transmet unidirectionnellement l'énergie électromagnétique de la porte (*2*), (*2'*) vers la porte (*1*), (*1'*).

Par conséquent *la condition nécessaire et suffisante afin qu'un QGLN soit à forte unidirectionnalité est que l'impédance* $\underline{Z}_3$ *soit donnée par (6).* Tels QGLN sont obligatoirement *non-réciproques.*

O b s e r v a t i o n s. 1° On peut obtenir le même résultat en imposant aux paramètres fondamentaux $\underline{A}_{ij}$, $(i,j{=}1,2)$, du quadripôle primitif [4] attaché au QGLN, la condition de type (1).

2° Si dans le cas des quadripôles en sens restreint la condition d'unidirectionnalité implique la nécessité que les paramètres fondamentaux satisfassent la relation (1), dans celui des QGLN la même condition est assurée seulement par le caractère non-réciproque du quadripôle, les paramètres fondamentaux de celui-ci ne devant pas satisfaire aucune autre restriction.

3° Compte tenu de la condition (6), il résulte qu'un QGLN ayant les paramètres fondamentaux $\underline{A}_{ij}, (i,j = 1,2,3)$, donnés, possède des propriétés unidirectionnelles seulement pour une certaine valeur, bien precisée, de l'impédance $\underline{Z}_3$ de la branche de couplage entre les portes (1), $(1')$ et (2), $(2')$ du quadripôle.

4° Dans le cas des QGLN ayant la branche de couplage entre les portes d'accès en court-circuit,la condition qu'ils soient à forte unidirectionnalité este $|\underline{A}| = 0$.

3. Quadripôles généraux linéaires, non-autonomes, à faible unidirectionnalité

On convient à denommer à faible unidirectionnalité un QGLN qui réalise le transfert de l'énergie électromagnétique seulement dans un seul sens et pour une certaine valeur de l'impédance du récepteur dans le sens bloqué.

Si on admet, par exemple, que le sens de transmission de l'énergie électromagnétique est du côté de la porte (1), $(1')$ vers la porte (2), $(2')$ et, d'une façon implicite, que le sens opposé est celui bloqué, on fait appel à l'expression de l'impédance équivalente à la porte (2), $(2')$ comme fonction des paramètres fondamentaux du QGLN, de l'impédance de la branche de couplage entre les portes d'accès et de l'impédance du récepteur, le quadripôle en étant inversé [5]:

$$\underline{Z}_{e2} = \frac{(\underline{A}_{22}\underline{Z}_3 - \underline{A}_{22}\underline{A}_{33} + \underline{A}_{23}\underline{A}_{32})\underline{Z}_1 + \underline{A}_{12}\underline{Z}_3 - \underline{A}_{12}\underline{A}_{33} + \underline{A}_{13}\underline{A}_{32}}{(\underline{A}_{21}\underline{Z}_3 - \underline{A}_{21}\underline{A}_{33} + \underline{A}_{23}\underline{A}_{31})\underline{Z}_1 + \underline{A}_{11}\underline{Z}_3 - \underline{A}_{11}\underline{A}_{33} + \underline{A}_{13}\underline{A}_{31}}. \tag{8}$$

La transmission de l'énergie électromagnétique de la porte (2), $(2')$ vers la porte (1), $(1')$ est bloquée si $\underline{Z}_{e2} \to \infty$, par exemple lorsque

$$\underline{Z}_1 = \frac{-\underline{A}_{11}\underline{Z}_3 + \underline{A}_{11}\underline{A}_{33} - \underline{A}_{13}\underline{A}_{31}}{\underline{A}_{21}\underline{Z}_3 - \underline{A}_{21}\underline{A}_{33} + \underline{A}_{23}\underline{A}_{31}}. \tag{9}$$

On constate aisément que, à l'encontre des QGLN à forte unidirectionnalité (v. le **§ 2**), qui se comportent comme tel pour n'importe quelle valeur de l'impédance $\underline{Z}_1$, le comportement unidirectionnel d'un même type de quadripôle est réalisé pour une certaine valeur, déterminée, de $\underline{Z}_1$. Il est naturel de denommer un tel QGLN comme un quadripôle *à faible unidirectionnalité.*

La relation (8) est, ainsi qu'on peut facilement constater, une transformation linéaire [6] qui réalise la transformation conforme du demi-plan $\Re e(\underline{Z}_3) \geq 0$ en un

cercle situé dans le plan (R_1, jX_1) dont l'équation est possible à obtenir en solutionnant d'abord la relation (9) par raport à $\underline{Z}_3$:

$$\underline{Z}_3 = \frac{(\underline{A}_{21}\underline{A}_{33} - \underline{A}_{23}\underline{A}_{31})\underline{Z}_1 + \underline{A}_{11}\underline{A}_{33} - \underline{A}_{13}\underline{A}_{31}}{\underline{A}_{21}\underline{Z}_1 + \underline{A}_{11}}, \tag{10}$$

en imposant ensuite la condition évidente $\Re e(\underline{Z}_3) \geq 0$. Tous calculs effectués on aboutit à la conclusion que étant donné un QGLN caractérisé par les paramètres fondamentaux $\underline{A}_{ij}, (i, j = 1,2,3)$, et l'impédance $\underline{Z}_3$, l'impédance $\underline{Z}_1$, qui confère au quadripôle considéré la propriété d'être à faible unidirectionnalité, peut prendre des valeurs seulement à l'intérieur et sur la frontière du domaine délimité par le cercle:

$$\begin{aligned} &\Re e[\underline{A}^*_{21}(\underline{A}_{21}\underline{A}_{33} - \underline{A}_{23}\underline{A}_{31})](R_1^2 + X_1^2) + \Re e[\underline{A}^*_{11}(\underline{A}_{21}\underline{A}_{33} - \underline{A}_{23}\underline{A}_{31}) + \\ &+\underline{A}^*_{21}(\underline{A}_{11}\underline{A}_{33} - \underline{A}_{13}\underline{A}_{31})]R_1 - \Im m[\underline{A}^*_{11}(\underline{A}_{21}\underline{A}_{33} - \underline{A}_{23}\underline{A}_{31}) - \\ &-\underline{A}^*_{21}(\underline{A}_{11}\underline{A}_{33} - \underline{A}_{13}\underline{A}_{31})]X_1 + \Re e[\underline{A}^*_{11}(\underline{A}_{11}\underline{A}_{33} - \underline{A}_{13}\underline{A}_{31})] = 0. \end{aligned} \tag{11}$$

Par conséquent *la condition nécessaire et suffisante afin qu'un QGLN donné soit à faible unidirectionnalité est que l'impédance $\underline{Z}_1$ du récepteur, dans le sens bloqué, ait l'expression (8).* Une telle situation est réalisable seulement si le domaine d'existence de l'impédance $\underline{Z}_1$ est délimité par le cercle ayant l'équation (11), en précisant toutefois que seulement la surface du cercle ci-dessus située dans le demi-plan $\Re e(\underline{Z}_1) \geq 0$ a un sens physique.

O b s e r v a t i o n s. 1° A l'encontre des QGLN à forte unidirectionnalité, qui obligatoirement sont non-réciproques, les QGLN à faible unidirectionnalité sont soit non-réciproques, soit réciproques.

2° Le procédé utilisé ci-dessus permet à obtenir la solution d'autres problèmes intéressants. Par exemple on peut déterminer les conditions dans lesquelles un QGLN, caractérisé par les paramètres fondamentaux $\underline{A}_{ij}$, $(i, j=1,2,3)$ et l'impédance $\underline{Z}_3$, se comporte comme un court-circuit. Dans ce but on utilise l'expression de l'impédance équivalente à la porte (1), $(1')$ du quadripôle [5]:

$$\underline{Z}_{e1} = \frac{(\underline{A}_{11}\underline{Z}_3 + \underline{A}_{13}\underline{A}_{31} - \underline{A}_{11}\underline{A}_{33})\underline{Z}_2 + \underline{A}_{12}\underline{Z}_3 + \underline{A}_{13}\underline{A}_{32} - \underline{A}_{12}\underline{A}_{33}}{(\underline{A}_{21}\underline{Z}_3 + \underline{A}_{23}\underline{A}_{31} - \underline{A}_{21}\underline{A}_{33})\underline{Z}_2 + \underline{A}_{22}\underline{Z}_3 + \underline{A}_{23}\underline{A}_{32} - \underline{A}_{12}\underline{A}_{33}}, \tag{12}$$

qui devient nulle si

$$\underline{Z}_2 = -\frac{\underline{A}_{12}\underline{Z}_3 + \underline{A}_{13}\underline{A}_{32} - \underline{A}_{12}\underline{A}_{33}}{\underline{A}_{11}\underline{Z}_3 + \underline{A}_{13}\underline{A}_{31} - \underline{A}_{11}\underline{A}_{33}}. \tag{13}$$

Cette expression est, même dans ce cas, une transformation linéaire [6] qui réalise la transformation conforme du demi-plan $\Re e(\underline{Z}_3) \geq 0$ en un cercle situé dans le plan (R_2, jX_2). On obtient l'équation de ce cercle en déterminant $\underline{Z}_3$ de la relation (13) à savoir:

$$\underline{Z}_3 = \frac{(-\underline{A}_{13}\underline{A}_{31} + \underline{A}_{11}\underline{A}_{33})\underline{Z}_2 + \underline{A}_{12}\underline{A}_{33} - \underline{A}_{13}\underline{A}_{32}}{\underline{A}_{11}\underline{Z}_2 + \underline{A}_{12}} \tag{14}$$

et en imposant, ensuite, la condition $\Re e(\underline{Z}_3) = 0$. Il résulte

$$\Re e[\underline{A}_{11}^*(\underline{A}_{11}\underline{A}_{33} - \underline{A}_{13}\underline{A}_{31})](R_2^2 + X_2^2) + \Re e[\underline{A}_{11}^*(\underline{A}_{12}\underline{A}_{33} - \underline{A}_{13}\underline{A}_{32}) +$$

$$+\underline{A}_{12}^*(\underline{A}_{11}\underline{A}_{33} - \underline{A}_{13}\underline{A}_{31})]R_2 - \Im m[\underline{A}_{11}^*(\underline{A}_{12}\underline{A}_{33} - \underline{A}_{13}\underline{A}_{32}) - \tag{15}$$

$$-\underline{A}_{12}^*(\underline{A}_{11}\underline{A}_{33} - \underline{A}_{13}\underline{A}_{31})]X_2 + \Re e[\underline{A}_{12}^*(\underline{A}_{12}\underline{A}_{33} - \underline{A}_{13}\underline{A}_{32})] = 0.$$

Evidemment seulement le sous-domaine contenu à l'intérieur et sur la frontière de ce cercle qui satisfait à la condition $\Re e(\underline{Z}_2) \geq 0$ a un sens physique.

3° Il est assez facile de particulariser les résultats obtenus dans ce paragraphe pour le cas où la branche de couplage entre les portes d'accès du quadripôle est en court-circuit.

4. Conclusions

1° On prouve que, d'une façon analogue aux quadripôles en sens restreint, les quadripôles généraux possèdent, en certaines situations, des propriétés unidirectionnelles.

2° Les quadripôles généraux linéaires, non-autonomes, ont des propriétés qui les confèrent un fonctionnement à forte unidirectionnalité, tout comme les quadripôles en sens restreint, seulement si ils sont non-réciproques, l'impédance $\underline{Z}_3$ ayant l'expression (6) pour n'importe quelle valeur de $\underline{Z}_1$ – l'impédance du récepteur en sens bloqué.

3° Dans le même temps les quadripôles généraux linéaires, non-autonomes, ont des propriétés qui les confèrent un fonctionnement à faible unidirectionnalité soit qu'ils sont réciproques ou non-réciproques, si l'impédance $\underline{Z}_1$ du récepteur en sens bloqué est donnée par (9). En outre un tel régime de fonctionnement est réalisable du point de vue physique seulement si le domaine d'existence de l'impédance $\underline{Z}_1$ est délimité par le cercle ayant l'équation (11) situé dans le demi-plan $\Re e(\underline{Z}_1) \geq 0$.

Reçue le 27 octobre 1997

Université Technique „Gh. Asachi", Jassy,
Chaire d'Electrotechnique générale
et Machines électriques
et
Chaire d'Electrotechnique

BIBLIOGRAPHIE

1. Şora C., *Introducere în studiul generatorului Hall.* Ed. Acad., Bucureşti, 1969.
2. Sigorsky V.P., *Théorie générale des quadripôles* (en russe). Ed. Acad. Sci. Ukraïne, Kiev, 1995.
3. Belaus D., *Sur la possibilité de réaliser l'égalité des impédances équivalentes à la porte d'entrée, à vide et en court-circuit, d'un quadripôle général linéaire, non-autonome.* Bul. Inst. polit., Iaşi, **XLIII (XLVII)**, *3-4*, s. III, 19-25 (1997).
4. Rosman H., *Sur les conditions de réciprocité et de symétrie d'un biporte général linéaire, non-autonome, en régime permanent harmonique.* Bul. Inst. polit., Iaşi, **XL (XLIV)**, *3-4*, s. III, 23-30 (1994).

5. R o s m a n H., *Les domaines d'existence de l'impédance équivalente à la porte d'entrée d'un quadripôle général en régime permanent harmonique.* Mem. secţ. şt. Acad. Română, s. III, **XI**, *1*, 193-206 (1988).
6. S t o i l o v S., *Teoria funcţiilor de o variabilă complexă.* Ed. Acad., Bucureşti, 1994.

CUADRIPOLI GENERALI LINIARI, NEAUTONOMI, UNIDIRECŢIONALI, ÎN REGIM PERMANENT ARMONIC

(Rezumat)

Se demonstrează că, analog cuadripolilor în sens restrans, cuadripolii generali liniari, neautonomi, sunt capabili de a poseda proprietăţi unidirecţionale. Este vorba de cuadripoli generali cu unidirecţionalitate tare, care sunt în mod obligator nereciproci, precum şi de cuadripoli generali cu neliniaritate slabă, care pot fi reciproci sau nereciproci.

In timp ce cuadripolii generali cu unidirecţionalitate tare realizează astfel de regimuri pentru orice valoare a impedanţei $\underline{Z}_1$ a receptorului în sensul blocat de transmisie a energiei electromagnetice, cei cu unidirecţionalitate slabă sunt capabili să aibă o comportare unidirecţională numai pentru o valoare bine determinată a impedanţei $\underline{Z}_1$.

BULETINUL INSTITUTULUI POLITEHNIC DIN IAŞI
Tomul XLIV (XLVIII), Fasc. 1-2, 1998
Secţia III
ELECTROTEHNICĂ. ENERGETICĂ. ELECTRONICĂ

D.C. 621.3.016.2

POWERS COMPUTING IN THE TIME DOMAIN: A HARTLEY TRANSFORM APPROACH

BY

ANCA-MIHAELA LAZĂR

A method that uses the Hartley series for computing and defining the powers in circuits is proposed. When nonsinusoidal signals are involved, the case of nonsinusoidal voltage and/or nonsinusoidal current are studied. The connections with other achievements in the field, along with an example, are also presented.

1. Introduction

The previous attempts concerning the definition of powers in nonsinusoidal situations used the Fourier series and the Fourier transform of the current and the voltage because there are well developed and efficient algorithms (from the mathematical point of view) and therefore they can be easily programmed.

Due to the existence of high speed A/D converters for acquisition of the signals represented by the voltage and the current we can store the evolution in time of these signals. Using the acquired samples one can make any kind of desired computing. Therefore we can define any type of power (even the ones blamed for their lack of physical meaning). The criteria for selecting a specific definition are, in the author's opinion, the ones of utility for further use and the cost (from the point of view of measuring and computing of a certain quantity).

The Fourier transform, widely used in these cases, in spite of its well known and effective algorithms, has a major drawback due to its redundancy: the memory locations and the computing time are twice the ones really needed to characterise any approximated function.

Until 1983 the Hartley transform was less used in spite of the fact that the work of R.V.L. H a r t l e y was first published in 1942 [1]. The main reason for this was probably the analogy with the Fourier transform and the ignored fact of its lack of redundancy (and therefore more efficient means of storing and computing data). From the computing of powers point of view it was almost totally ignored in spite of the 10 percents of the papers remembered in the references [2],...,[5].

2. The Hartley Series and the Hartley Transform: a Short Theoretical Background

The kernel of this transform was introduced in [1] and is named **cas** (from *c*osine *a*nd *s*ine). It is defined by

$$\operatorname{cas}(t) = \cos(t) + \sin(t). \tag{1}$$

A complementary cas function, denoted cas′ (because it is identical with the derivative of the cas function), may be also defined:

$$\operatorname{cas}'(t) = \cos(t) - \sin(t). \tag{2}$$

This is in fact, taking into account the parity of the sine and cosine functions, $\operatorname{cas}(-t)$, that is

$$\operatorname{cas}'(t) = \operatorname{cas}(-t). \tag{3}$$

In the same manner can be defined the Hartley series for a periodic function:

$$x(t) = \sum_{n=-\infty}^{\infty} \gamma_n \operatorname{cas}(n\nu_0 t). \tag{4}$$

The coefficients γ_n are given by

$$\gamma_k = \frac{1}{T} \int_t^{t+T} x(t) \operatorname{cas}(k\nu_0 t)\, \mathrm{d}t, \tag{5}$$

where $\nu_0 = 2\pi/T$ and T is the period.

It is worth noticing the fact that the coefficients are all real numbers[1].

3. Powers Computing by Means of the Hartley Series – A Point of View

3.1. Case of Sinusoidal Signals

Let us consider the voltage

$$u(t) = \sqrt{2}U \sin \nu t \tag{6}$$

[1]The implications of the use of the Hartley series are better evidenced by the following observation. Let us consider the Fourier series of a periodical signal [6]:

$$x(t) = \frac{A_0}{2} + \sum_{n=1}^{\infty} \cos n\omega t + \sum_{n=1}^{\infty} B_n \sin n\omega t$$

or, using another representation,

$$x(t) = X_0 + \sum_{n=1}^{\infty} \sqrt{2} X_n \sin(n\omega t + \alpha_n),$$

where the coefficients A_0, A_n, B_n, X_0, X_n and α_n are computed with well known formulas [6]. Using the cas function leads to more simple computing since less parameters are involved, as seen from their definition.

and the current

$$i(t) = \sqrt{2}I\sin(\nu t + \varphi). \tag{7}$$

Taking into account the representation of the above signals using the cas function we can write:

$$i(t) = \sqrt{2}I\sin(\nu t + \varphi) = \sqrt{2}/2I[\mathrm{cas}(\nu t + \varphi) - \mathrm{cas}(-\nu t - \varphi)] \tag{8}$$

and

$$u(t) = \sqrt{2}U\sin(\nu t) = \sqrt{2}/2U[\mathrm{cas}(\nu T) - \mathrm{cas}(-\nu t)]. \tag{9}$$

The instantaneous power is given by the expression:

$$p(t) = u(t)i(t) = \frac{1}{2}UI[\mathrm{cas}(\nu t + \varphi) - \mathrm{cas}(-\nu t - \varphi)][\mathrm{cas}(\nu t) - \mathrm{cas}(-\nu t)]; \tag{10}$$

after elementary computing we get:

$$p(t) = \frac{1}{2}UI[\mathrm{cas}\,\varphi + \mathrm{cas}(-\varphi) - \mathrm{cas}(2\nu t + \varphi) - \mathrm{cas}(-2\nu t - \varphi)], \tag{11}$$

or. taking into account (3),

$$p(t) = \frac{1}{2}UI[\mathrm{cas}\,\varphi + \mathrm{cas}'\,\varphi - \mathrm{cas}(2\nu t + \varphi) - \mathrm{cas}'(2\nu t + \varphi)]. \tag{12}$$

A simple observation[2] allows us to state the fact that in the last formula there are two signals and their quadrature components:

$$p(t) = \frac{1}{2}UI\left[\mathrm{cas}\,\varphi - \mathrm{cas}(2\nu t + \varphi) + \mathrm{cas}\left(\varphi + \frac{\pi}{2}\right) - \mathrm{cas}\left(2\nu t + \varphi + \frac{\pi}{2}\right)\right]. \tag{13}$$

Let us notice the fact that the representation using the cas function evidence the quadrature components without supplementary computing and this is, without any doubt, an advantage.

3.2. Case of the Sinuisoidal Voltage and Nonsinusoidal Current

In what follows we shall try to define powers when the voltage is sinusoidal and the current is nonsinusoidal because it looks like this is the most common case.

Let us suppose that the voltage is described by (6) and the current by the attached Hartley series of a periodic signal:

$$i(t) = \sqrt{2}\sum_{-\infty}^{\infty} I_h\,\mathrm{cas}(h\nu t), \tag{14}$$

where

[2] $\mathrm{cas}'(t) = \mathrm{cas}(\cdot\ \cdot 2 + t)$.

$$I_h = \frac{1}{T}\int_{t}^{t+T} i(t)\,\mathrm{cas}(h\nu t)\,\mathrm{d}t. \tag{15}$$

The voltage can be written using the cas function (s. rel. (9)).

In order to simplify the computing, we shall consider in what follows just one of the components of the Hartley series of the current, the one generically denoted by h. Obviously the other components lead to the same relations. Because the current has an infinite number of components, the instantaneous power will also have an infinite number of components. One of them can be written as:

$$p_h(t) = u(t)i_h(t). \tag{16}$$

The whole instantaneous power is obtained by summing all the components. Therefore,

$$\begin{aligned} p_h(t) &= UI_h[\mathrm{cas}(h\nu t)\,\mathrm{cas}(\nu t) - \mathrm{cas}(h\nu t)\,\mathrm{cas}(-\nu t)] = \\ &= UI_h\{\mathrm{cas}[-(h-1)\nu t] - \mathrm{cas}[-(h+1)\nu t]\} = \\ &= UI_h[\mathrm{cas}'(h-1)\nu t - \mathrm{cas}'(h+1)\nu t]. \end{aligned} \tag{17}$$

The last formula evidences the fact that there are two oscillations, of frequencies $(h+1)\nu$ and $(h-1)\nu$, which is in concordance with the result of A.E. E m a n u e l [7].

What is essentially different is the way of computing. If one intends to design a system that computes directly the different powers, less hardware and computing time will be needed because: a) the I_h coefficients are all real numbers; b) the functions that are arguments for the cas function are of the type ht and not $ht + \varphi_h$.

It is worth remembering that E m a n u e l, in spite of using relations written only in the time domain and involving the Fourier series, transfers the complications from the frequency domain, due to the form of each spectral component, $h\omega t + \varphi_h$, because φ_h must be computed for each component.

The equation (16), which gives the instantaneous power $p_h(t)$, allows us to observe that the components are also in quadrature:

$$p_h(t) = UI_h\left\{\mathrm{cas}\left[(h-1)\nu t + \frac{\pi}{2}\right] - \mathrm{cas}\left[(h+1)\nu t + \frac{\pi}{2}\right]\right\}. \tag{18}$$

3.3. Case of Nonsinusoidal Signals

Let us consider the Hartley series of the voltage and the current:

$$u(t) = \sum_{-\infty}^{\infty} \sqrt{2}U_n\,\mathrm{cas}(n\nu t), \qquad i(t) = \sum_{-\infty}^{\infty} \sqrt{2}I_m\,\mathrm{cas}(m\nu t). \tag{19}$$

In what follows $p_{nm}(t)$ will denote the instantaneous power given by the n-th component of the voltage and the m-th component of the current. We can write:

$$p_{nm}(t) = 2U_n I_m \operatorname{cas}(n\nu t)\operatorname{cas}(m\nu t) =$$

(20)

$$= U_n I_m[\operatorname{cas}(n+m)\nu t - \operatorname{cas}'(n+m)\nu t + \operatorname{cas}(m-n)\nu t + \operatorname{cas}'(m-n)\nu t].$$

One must notice, even in this case, that the components in quadrature are present, too:

$$p_{nm}(t) = U_n I_m \left\{\operatorname{cas}(n+m)\nu t - \operatorname{cas}\left[(n+m)\nu t + \frac{\pi}{2}\right] + \right.$$

(21)

$$\left. + \operatorname{cas}(m-n)\nu t + \operatorname{cas}\left[(m-n)\nu t + \frac{\pi}{2}\right]\right\}.$$

An interesting observation can be made when $n = m$. Equation (20) can be written:

$$p_{nn}(t) = U_n I_n[\operatorname{cas}(2n\nu t) - \operatorname{cas}'(2n\nu t) + 2]. \tag{22}$$

The $2U_n I_n$ type products are possible only when the indices of the components are the same.

An example of the results of the computing using Mathcad 5.0 will be given for a sinusoidal voltage with 1 V amplitude and a 1 A pulse current (with 50% filling factor) both with 1 s periods. The odd components are obviously zero.

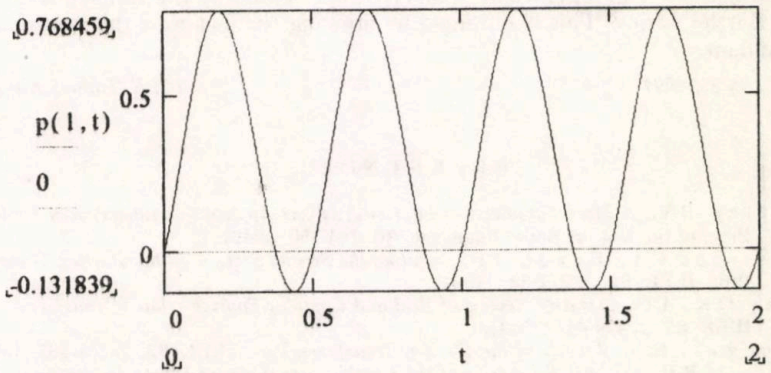

Fig. 1.– The p_1 component of the instantaneous power.

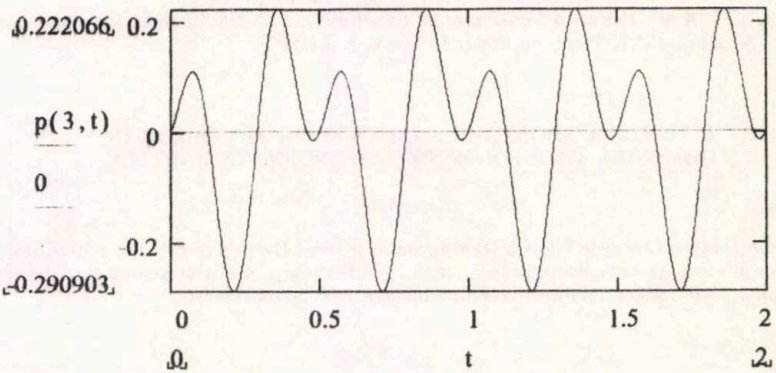

Fig. 2.– The p_3 component of the instantaneous power.

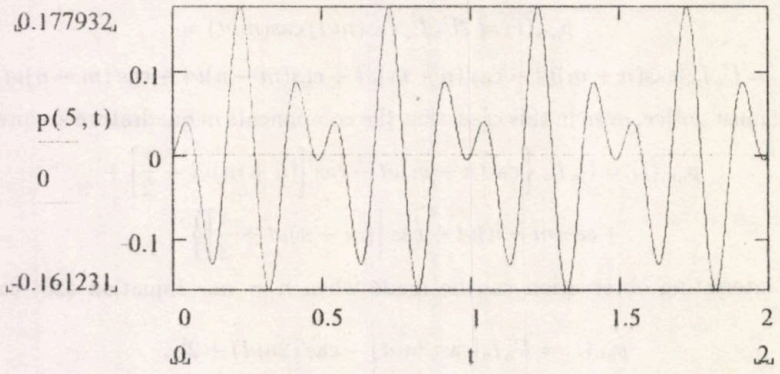

Fig. 3.- The p_5 component of the instantaneous power.

4. Conclusion

A method that allows to evidence the quadrature components and to compute the instantaneous power in an efficient manner is represented by the Hartley transform and the Hartley series. This is obtained by noticing the fact that this transform is not redundant.

Received, July 24, 1997

ICPE-Trafil S.A., Jassy

REFERENCES

1. Hartley R.V., *A More Symmetrical Fourier Analysis Applied to Transmission Problems.* Proc. of the Inst. of Radio Engineers, **30**, 144-150 (1942).
2. Olejniczak K.J., Heydt G.T., *Scanning the Special Section on the Hartley Transform.* Proc. IEEE, **82**, *3*, 372-380 (1994).
3. Ersoy O.K., *A Comparative Review of Real and Complex Fourier-related Transforms.* Proc. IEEE, **82**, *3*, 429-447 (1994).
4. Bracewell R.N., *Aspects of the Hartley Transform.* Proc. IEEE, **82**, *3*, 381-387 (1994).
5. Millane R.P., *Analytic Properties of the Hartley Transform and their Implications.* Proc. IEEE, **82**, *3*, 413-428 (1994).
6. Mocanu C.I., *Teoria circuitelor electrice.* E.D.P., Bucureşti, 1979.
7. Emanuel A.M., *Power in Nonsinusoidal Situations - a Review of Definitions and Physical Meaning.* IEEE Trans. on Power Delivery, **5**, *3* (1990).

O POSIBILĂ ABORDARE A CALCULULUI PUTERILOR ÎN DOMENIUL TIMP FOLOSIND TRANSFORMATA HARTLEY

(Rezumat)

Sunt prezentate avantajele folosirii transformatei şi seriei Hartley în calculul puterii instantanee. Se pun în evidenţă componentele ortogonale, justificându-se motivele pentru care calculele şi memoria unui posibil sistem destinat acestui scop sunt folosite mai eficient.

BULETINUL INSTITUTULUI POLITEHNIC DIN IAŞI
Tomul XLIV (XLVIII), Fasc. 1–2, 1998
Secţia III
ELECTROTEHNICĂ. ENERGETICĂ. ELECTRONICĂ

C.D. 621.3.018.6

OSCILLATIONS MÉCANIQUES DANS UN SYSTÈME LINÉAIRE ÉLECTROMÉCANIQUE
ÉTUDE DES SIGNAUX ÉLECTRIQUES

PAR

MARIANA BUZDUGA

On continue l'essai de caractériser le phénomène d'oscillations mécaniques d'un galvanomètre placé dans un circuit série muni d'une diode tunnel (DT) par l'étude de la concordance entre les paramètres des signaux électriques du circuit réel et ceux obtenus par simulation.

On effectue la correction du modèle et on obtient par simulation des solutions très proches de celles réelles pour les deux cas: avec et sans mouvement. On arrive aussi à justifier le phénomène de modulation des oscillations de relaxation sous l'influence du mouvement de la bobine mobile.

L'analyse critique des limites du modèle adopté permet à mettre en évidence l'influence du type d'approximation de la caractéristique de la DT sur les nonconcordances entre les signaux et les solutions correspondantes du point de vue de l'amplitude.

1. Introduction

Le phénomène étudié concerne l'apparition des oscillations mécaniques entretenues de l'ensemble mobile d'un galvanomètre magnétoélectrique se trouvant dans un circuit série muni d'une diode tunnel (DT), une résistance, R, et une source de cc, E, réglables.

Dans des études antérieures on a établi les conditions dans lesquelles ces oscillations apparaissent, en utilisant un modèle à basse fréquence où la caractéristique $i(u)$ de la DT est approximée par un polynôme incomplet du troisième degré.

Les équations qui décrivent ce circuit permettent l'obtention des solutions numériques pour les variables: $\alpha(t)$ – déplacement angulaire; $\mathrm{d}\alpha/\mathrm{d}t$ – vitesse de déplacement; $u(t)$ – tension sur la DT; $i(t)$ – courant dans le circuit. Ces solutions sont périodiques, de basse fréquence.

Si en ce qui concerne les variables $\alpha(t)$ et $\mathrm{d}\alpha/\mathrm{d}t$ les solutions numériques sont en concordance avec les résultats des expériments, pour $i(t)$ et $u(t)$ on observe des écarts essentiels entre les signaux et les solutions correspondantes. Une correction du modèle adopté s'impose. Dans ce qui suit on fournit une explication des phénomènes physiques observés et on propose un modèle corrigé.

Les signaux $i(t)$ et $u(t)$ sont liés par la caractéristique $i(u)$ de la diode tunnel

(DT), approximée dans le modèle par le polynôme:

$$i(u) = -a_1 u + a_3 u^3; \tag{1}$$

par conséquent on a choisi seulement $u(t)$ pour développer l'étude ci-dessous.

2. Correction du modèle

Le signal $u(t)$ observé contient des oscillations quasi-rectangulaires ayant une fréquence de l'ordre des dizaines de kHz, qui se déforment en synchronisme avec le mouvement de l'aiguille du miliampèremètre, ayant la fréquence et le rapport cyclique variables. L'oscillogramme de la Fig. 1 suggère le changement permanent de $u(t)$.

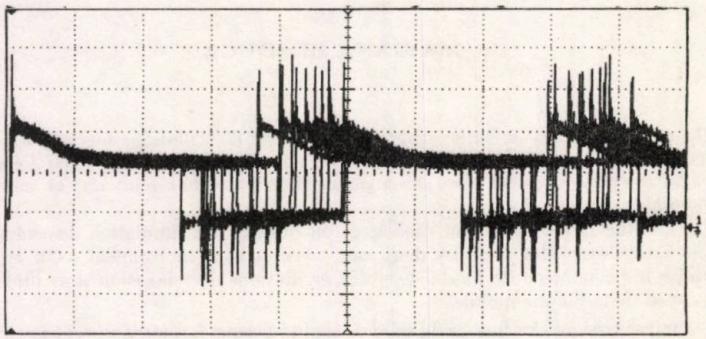

Fig. 1

On réalise la correction du modèle tenant compte de l'observation que, dans le domaine de fonctionnement considéré, il y a aussi des conditions pour l'apparition des oscillations électriques de relaxation. On ajoute à l'ancien modèle [1] les éléments qui décrivent le fonctionnement aux fréquences plus élevées et on obtient le schéma représenté dans la Fig. 2.

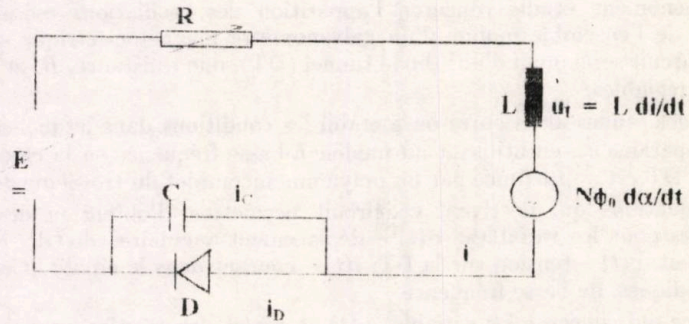

Fig. 2

Pour ce modèle on a les relations:

$$i_c = C_1 \frac{du}{dt}, \qquad i_D = i - i_c \tag{2}$$

de sorte que les équations différentielles sont:

$$E = Ri + u + L\frac{\mathrm{d}i}{\mathrm{d}t} + N\Phi_0\frac{\mathrm{d}\alpha}{\mathrm{d}t} \tag{3}$$

– pour le circuit électrique et

$$J\frac{\mathrm{d}^2\alpha}{\mathrm{d}t^2} + B\frac{\mathrm{d}\alpha}{\mathrm{d}t} + C\alpha = N\Phi_0(i_D + i_c) \tag{4}$$

– pour le système mécanique.

On utilise aussi les relations de régime permanent:

$$E = Ri_0 + u_0, \qquad C\alpha_0 = N\Phi_0 i_0; \tag{5}$$

pour les composantes variables des signaux les équations différentielles qui décrivent le système deviennent:

$$LC_1\frac{\mathrm{d}^2u'}{\mathrm{d}t^2} + \left[RC_1 + L\frac{\mathrm{d}i'(u')}{\mathrm{d}u'}\right]\frac{\mathrm{d}u'}{\mathrm{d}t} + u' + Ri'(u') = -N\Phi_0\frac{\mathrm{d}\alpha'}{\mathrm{d}t}, \tag{6}$$

$$J\frac{\mathrm{d}^2\alpha'}{\mathrm{d}t^2} + B\frac{\mathrm{d}\alpha'}{\mathrm{d}t} + C\alpha' = N\Phi_0\left[i'(u') + C_1\frac{\mathrm{d}u'}{\mathrm{d}t}\right]. \tag{7}$$

Si on utilise l'approximation (1), alors les équations (6), (7) prennent la forme:

$$LC_1\frac{\mathrm{d}^2u'}{\mathrm{d}t^2} + \left(RC_1 - a_1L + 3a_3Lu'^2\right)\frac{\mathrm{d}u'}{\mathrm{d}t} + (1 - Ra_1 + Ra_3u'^2)u' = -N\Phi_0\frac{\mathrm{d}\alpha'}{\mathrm{d}t}, \tag{8}$$

$$J\frac{\mathrm{d}^2\alpha'}{\mathrm{d}t^2} + B\frac{\mathrm{d}\alpha'}{\mathrm{d}t} + C\alpha' = N\Phi_0\left(-a_1u' + a_3u'^3 + C_1\frac{\mathrm{d}u'}{\mathrm{d}t}\right). \tag{9}$$

Solutionner ce système représente une démarche difficile à cause, à part la non-linéarité, de la grande différence entre les fréquences de variation des variables (2 Hz pour $\alpha'(t)$ face à 30 kHz pour $u'(t)$). Par conséquent on a essayé d'obtenir des résultats partiels, pour pouvoir valider le modèle à savoir:

1° En l'absence du mouvement, le terme libre de l'équation (8) est nul. La solution numérique de l'équation homogène, représentée dans la Fig. 3, décrit les oscillations de relaxation qui existent dans un circuit similaire mais fixe.

On peut obtenir dans le circuit réel un signal ayant les mêmes caractéristiques, dont l'oscillogramme est représentée dans la Fig. 4, quand on bloque la partie mobile, empêchant ainsi le mouvement.

2° Si on remplace le terme libre de l'équation (8) avec un autre, sinusoïdal, de la même amplitude mais de fréquence beaucoup plus grande, on peut obtenir la solution numérique représentée dans la Fig. 5. On observe aisément que les variations de la fréquence et du rapport cyclique ont la même forme que celles du signal réel. Par conséquent on a considéré que le nouveau modèle est capable de décrire d'une façon satisfaisante le comportement du circuit dans le régime considéré.

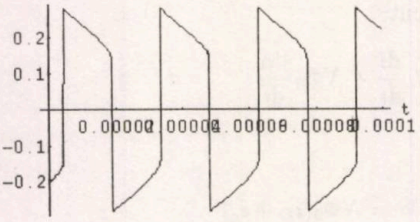

Fig. 3

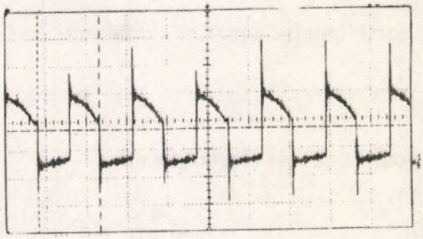

Fig. 4

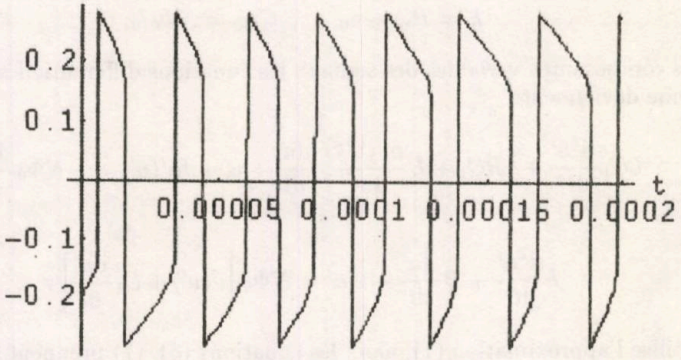

Fig. 5

3. Description des phénomènes physiques dans le système

Pour expliquer le comportement du système on a tenu compte des propriétés des oscillations de relaxation, en absence du mouvement. La forme et la fréquence de celles-ci sont fonctions des éléments du circuit. Les coordonnées (U_Q, I_Q) du point de fonctionnement Q (Fig. 6) représentent les valeurs moyennes des oscillations de relaxation des signaux électriques. Le changement de la position de celui-là va entrainer un changement du rapport cyclique et de la fréquence. Cette influence est mise en évidence dans les Figs. 7 et 8, en fonction de E, qui, à son tour, modifie U_Q conformément à la relation:

$$E = RI_Q + U_Q. \tag{10}$$

On peut donc prévoir qu'un déplacement périodique de Q va entrainer un changement périodique des paramètres f et RC, avec des amplitudes qui dépendent de l'ampleur et de la position de l'excursion de Q sur la zône de pente négative de la caractéristique $i(u)$ de la DT.

L'analyse de l'équation (8) permet d'observer qu'on peut assimiler le terme de basse fréquence, qui correspond à la tension induite dans la bobine du miliampèremètre, à une variation lente, ΔE, de la tension d'alimentation. L'effet immédiat d'une telle variation est le déplacement alternatif de la droite de charge parallèle à elle même, donc le déplacement périodique du point de fonctionnement Q.

On peut affirmer, en conclusion, que sous l'influence de la tension induite dans la bobine du miliampèremètre à cause du mouvement, le point de fonctionnement, Q, effectue un déplacement périodique, qui a comme effet une variation synchrone avec le mouvement, ayant la fréquence et le rapport cyclique des oscillations de relaxation.

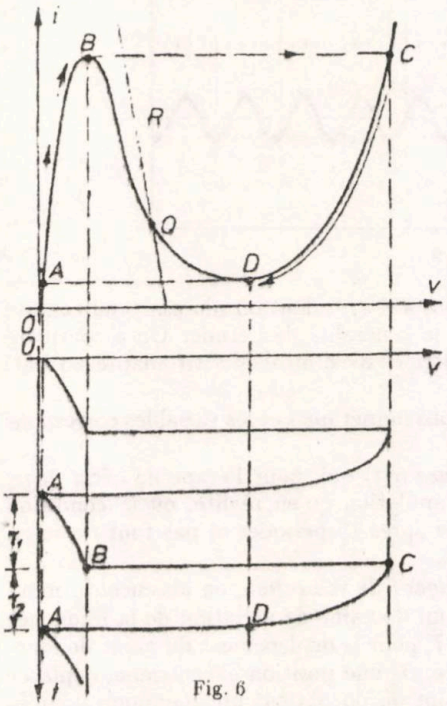

Fig. 6

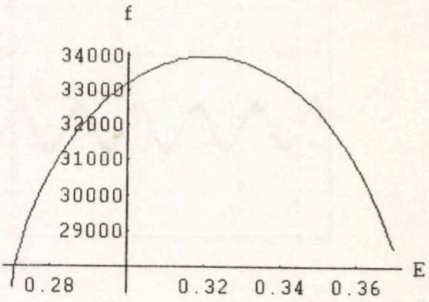

Fig. 7

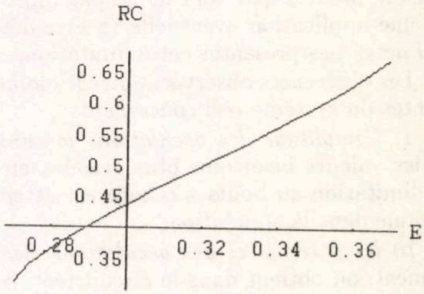

Fig. 8

Par conséquent la valeur moyenne du signal $u(t)$ doit avoir une variation en fonction du temps identique à celle de l'abscisse U_Q. On a obtenu, en effet, dans le circuit réel, par filtrage passe-bas, un signal synchrone avec le mouvement, correspondant à la valeur moyenne de $u(t)$, dont on présente l'oscillogramme dans la Fig. 9. La présence de ce signal constitue une confirmation pour l'interprétation donnée au phénomène.

On observe aussi que la présence ou l'absence des oscillations de relaxation dans le circuit électrique ne modifie pas la réponse de la partie mécanique. Dans ces conditions on peut étendre la valabilité du modèle en basse fréquence, en sachant que, dans les équations de ce modèle, les variables électriques correspondent maintenant aux valeurs moyennes U_Q, I_Q.

4. Analyse des limites du modèle adopté

Les observations effectuées pendant les expériments montrent une bonne concordance entre la théorie et les résultats obtenus par voie expérimentale en ce qui concerne les domaines d'existence des oscillations mécaniques et la fréquence des variables.

On doit faire l'observation que le galvanomètre utilisé pour les expérimentations

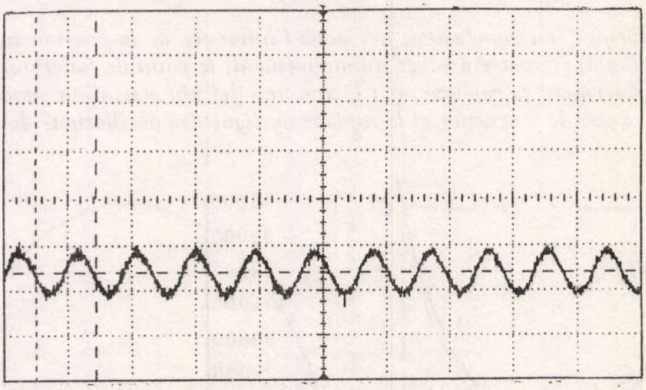

Fig. 9

présentait des butées, limitant le mouvement à $\pm\pi/4$, dont on n'a pas tenu compte dans le modèle, par soin de ne pas limiter la généralité de l'étude. On a considéré qu'une application éventuelle va être développée avec un dispositif adapté au but, qui ne va pas présenter cette limitation.

Les différences observées entre les solutions numériques et les variables correspondantes du système réel concernent:

a) *l'amplitude des oscillations mécaniques* $\alpha(t)$ qui, pour l'étape de démarrage, a des valeurs beaucoup plus grandes en simulation qu'en réalité, où la condition de limitation au bouts d'echelle est atteinte après 15 périodes et pas tout de suite, comme dans la simulation;

b) *les paramètres des oscillations électriques de relaxation*, en absence du mouvement; on obtient dans le circuit réel: α) un domaine de variation de la fréquence deux fois plus étendu, par rapport à la Fig. 7, pour le déplacement du point de fonctionnement Q sur la zône de pente négative; β) une position excentrique, déplacée vers des tensions supérieures à celle du point où on obtient un maximum pour la fréquence, donc une forme asymétrique du graphique de la Fig. 7; γ) une variation plus importante de la valeur maximum de la fréquence avec R; δ) une forme légérement différente des oscillations observées par rapport aux solutions numériques (v. les Figs. 3 et 4); ε) approximativement une même plage de variation du rapport cyclique dans les deux cas, pour le déplacement du point Q dans le domaine entier de pente négative.

Ces nonconcordances sont le résultat de l'approximation assez grossière que le polynôme (1) réalise pour la caractéristique de la DT, comme on peut constater dans la Fig. 10.

Vu que les deux courbes ont des pentes différentes pour une même abscisse, U_Q, le déplacement du point Q, suite à une excitation ΔE, ne sera pas le même dans les deux cas, ce qui entraine des différences dans les amplitudes des signaux.

La variation de l'abscisse U_Q en fonction de E, représentée dans la Fig. 11, est décrite par la relation (10). La pente de cette courbe est déterminante pour la réponse du circuit électrique au signal de réaction produit par la partie mécanique, donc pour la réponse du système en ensemble. On observe que les différences sont plus génantes pour des petites valeurs des signaux et pour une position du point Q située au milieu de la caractéristique.

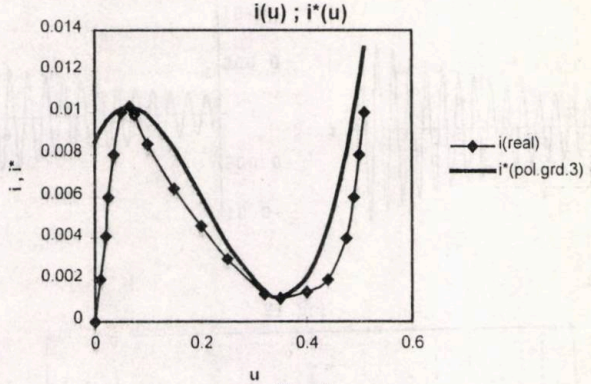

Fig. 10

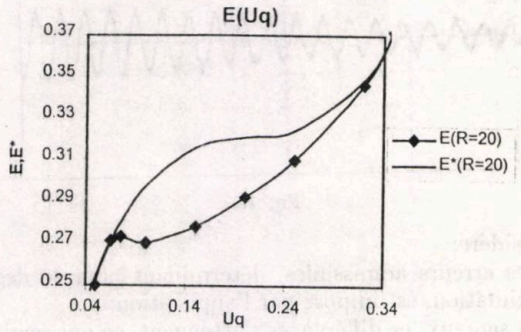

Fig. 11

En simulation, la courbe $E(U_Q)$ ayant une pente faible autour du point central, les valeurs des signaux $U_Q(t)$, $\mathrm{d}\alpha/\mathrm{d}t$ et $\alpha(t)$ vont vite augmenter dès le début, de sorte que les conditions de limitation par les butées sont atteintes après la première période, ce que n'a pas lieu dans le circuit réel.

Dans le cas des forts signaux les différences doivent s'atténuer jusqu'à leur disparition pour une excursion sur tout le domaine de pente négative.

Pour prouver que les différences mentionnées ci-dessus son dues au choix du type d'approximation de la caractéristique de la DT on a introduit dans le modèle mathématique une approximation linéaire, ayant la même pente que celle de la caractéristique réelle dans le point considéré, Q. Pour l'étape de démarrage, quand les signaux sont faibles et l'approximation peut être considérée valable, on a obte ı les solutions numériques pour $U_Q(t)$ et $\alpha(t)$ représentées dans la Fig. 12 *a* et *b*. Elles ont des valeurs très proches de celles des variables du circuit réel, pour lequel on représente dans la Fig. 13 l'oscillogramme de $U_Q(t)$.

On peut obtenir une amélioration du modèle en utilisant des approximations d'ordre supérieur pour la caractéristique $i(u)$, ce qui mène pourtant à compliquer les équations du système.

Pour l'étape actuelle on n'a pas considéré nécessaire d'insister sur ce point car:

a) chaque si··ation concrète impose un modèle détaillé, spécifique au dispositif à

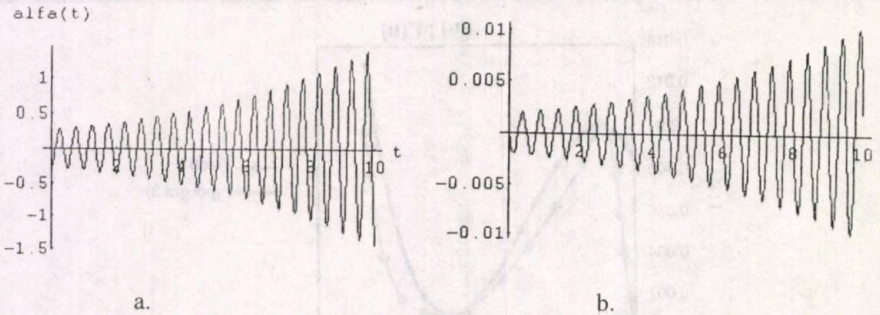

a. b.

Fig. 12

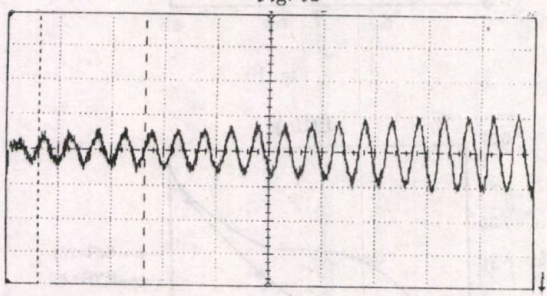

Fig. 13

pente négative considéré;

b) le niveau des erreurs admissibles, déterminant pour le degré nécessaire du polynôme d'approximation, est imposé par l'application;

c) pour de forts signaux les différences s'atténuent, ce qui rend le modèle acceptable dans des applications peu prétentieuses.

5. Conclusions

L'analyse de la tension sur la diode tunnel du circuit étudié permet de constater que dans le système coexistent des oscillations de relaxation et des oscillations mécaniques du cadre du miliampèremètre.

On effectue la correction du modèle adopté et on obtient des solutions numériques pour $u(t)$ très semblables au signal réel, dans les deux cas: avec et sans oscillations mécaniques.

On montre aussi, en utilisant les données concernant les propriétés des oscillations de relaxation, que sous l'action de la tension induite dans la bobine par le mouvement, la droite de charge du circuit effectue un déplacement alternatif, ayant comme conséquence le déplacement périodique du point de fonctionnement, Q. L'effet de ce deplacement est le changement périodique des paramètres (fréquence et rapport cyclique) des oscillations de relaxation.

La validation du modèle est obtenue d'une part par la comparaison des solutions partielles avec les signaux réels et d'autre part par la confirmation des hypothèses concernant les phénomènes physiques, par l'obtention en pratique du signal prévu théoriquement.

On effectue aussi une analyse critique des limites du modèle et on montre que les

erreurs d'amplitude des solutions sont dues au choix du type de l'approximation de la caractéristique $i(u)$ de la diode tunnel.

La validation des modèles, avec l'identification de leurs limites, permet dorénavant leur utilisation pour simulation, dans le but d'analyser les facteurs qui influencent les oscillations étudiées.

Reçue le 19 août 1997

Université Technique „Gh. Asachi", Jassy,
Chaire de Mesures électriques
et Matériaux électriques

BIBLIOGRAPHIE

1. B u z d u g a M., *Sur les condition d'apparition des oscillations mécaniques dans un système électromécanique. I. Etablissement des équations de mouvement.* Bul. Inst. polit., Iaşi, **XL(XLIV)**, *1-4*, s.III (1994).
2. S a n d u D.D., *Probleme moderne de tehnica impulsurilor.* Ed. Acad., Bucureşti, 1980.
3. S a v i n Gh., G r o v u M., *Elektromechanische Schwingungen, die mit nichtlinearen aktiven Netzwerken selbsterregt werden.* Archiv für Elektrot., **62**, 12 (1980).
4. S a v i n Gh., R o s m a n H., *Circuite electrice neliniare şi parametrice.* Ed. Tehnică, Bucureşti, 1973.

OSCILAŢII MECANICE ÎNTR-UN SISTEM ELECTROMECANIC LINIAR
Studiul semnalelor electrice

(Rezumat)

Se continuă analiza fenomenului de oscilaţii electromecanice ce apar într-un circuit cu diodă tunel (DT) şi un mecanism magnetoelectric, cu studiul semnalelor electrice.

Se corectează modelul iniţial şi se obţin, prin simulare, soluţii numerice foarte asemănătoare cu semnalele reale în ambele situaţii: cu şi fără mişcare. Se justifică, de asemenea, fenomenul de modulare a oscilaţiilor de relaxare sub acţiunea mişcării bobinei mobile.

Analiza critică a limitelor modelului adoptat permite să se pună în evidenţă influenţa tipului de aproximare a caracteristicii $i(u)$ a DT asupra neconcordanţelor între semnale şi soluţiile corespunzătoare din punctul de vedere al amplitudinii.

BULETINUL INSTITUTULUI POLITEHNIC DIN IAŞI
Tomul XLIV (XLVIII), Fasc. 1–2, 1998
Secţia III
ELECTROTEHNICĂ. ENERGETICĂ. ELECTRONICĂ

D.C. 621.372.061.1

COMPENSATION OF DISCRETE, LINEAR, TIME VARYING SYSTEMS

BY

DANIELA TĂRNICERIU and VALERIU MUNTEANU

A synthesis method for linear time variant (LTV) discrete systems is proposed. The structure of a discrete controller, which is cascaded with the known time varying process, is inferred, so that the ensemble behaves as a linear time invariant (LTI) system satisfying certain design requirements. Simulation results are included to illustrate the proposed method.

1. Introduction

In practice, the processes to be controlled – plants – have time varying parameters and they have to be driven according to certain requirements. In what follows, the plant is assumed to be described by a linear difference equation with time variant coefficients. The synthesis is based on the cascading of the plant with a regulator able to control it according to imposed requirements. In [1],...,[4] the synthesis of LTV digital filters is performed using either a criterion to minimize the difference between the given and the approximated response, or the frozen time approximation technique. Both situations result in errors because, for certain time intervals the plant is considered as a time invariant system. In [5],...,[8] the synthesis of a regulator for linear continuous systems has been proposed. In the present explored method, the regulator that controls the time varying process is synthesized so that the regulator–plant cascade presents a time invariant behaviour. So, the classical synthesis methods for linear discrete systems with time invariant parameters may be used [9],...,[12]. Based on the design requirements, the difference equation for an LTI system satisfying the proposed conditions is determined. Then, according to the structure of the LTV process, a regulator will be synthesized, so that the cascade behaves as the LTI system above inferred. The regulator is easy to implement, by means of a parallel bank of LTI systems of first order, followed by amplifiers with variable gain. These gains depend on the plant structure. The first section of this paper provides a background for a new method to obtain the poles and residia of a linear time invariant system, on which the proposed synthesis method is based. The second section presents theoretical results along with the assumptions they entail.

which can be used in the practical synthesis of controllers. In the third section it is shown, through simulation studies, the effectiveness of the proposed method. To conclude, one can say that the presented method is generally and it can be easily implemented.

2. Relation between Poles and Residia of a Linear Discrete Time Invariant System

Let us consider a discrete time invariant system described by a difference equation of first order:

$$y[n] - a_1 y[n-1] = x[n], \; a_1 \neq 0. \tag{1}$$

Under zero initial conditions:

$$y[-1] = y[-2] = \cdots = 0, \qquad x[-1] = x[-2] = \cdots = 0, \tag{2}$$

the output $y[n]$ can be computed as follows:

$$y[n] = \sum_{k=0}^{n} x[k] a_1^{n-k}. \tag{3}$$

Let d be the delay operator with the following propriety:

$$d^k y[n] = y[n-k]. \tag{4}$$

With (4) relation (1) may be written in an equivalent form as:

$$y[n] = \frac{x[n]}{1 - a_1 d}. \tag{5}$$

From (3) and (5) it results:

$$\frac{x[n]}{1 - a_1 d} = \sum_{k=0}^{n} x[k] a_1^{n-k}. \tag{6}$$

Let us consider now a discrete LTI system, described by a difference equation of N^{th} order:

$$y[n] + a_1 y[n-1] + a_2 y[n-2] + \cdots + a_N y[n-N] = x[n], \tag{7}$$

with $a_i \neq 0$, for $i = 1, 2, \ldots, N$. Under zero initial conditions and if the system has only distinct real poles, one can write:

$$y[n] = x[n] \sum_{j=1}^{N} \frac{A_j}{1 - p_j d}, \tag{8}$$

where p_j and A_j are named the poles and the residia of the system, respectively. Considering (6), relation (8) becomes:

$$y[n] = \sum_{k=0}^{n} \sum_{j=1}^{N} A_j x[k] p_j^{n-k}. \tag{9}$$

Substituting $y[n], y[n-1], ..., y[n-N]$, obtained from (9), in (7), we get, by identification:

$$\sum_{j=0}^{N} A_j = 1, \tag{10}$$

$$\sum_{i=0}^{N} a_i p_j^{N-i} = 0, \; a_0 = 1, \tag{11}$$

for any $j = 1, 2, ..., N$ and

$$\sum_{j=1}^{N} A_j p_j^{-m} = 0, \; m = \overline{1, N-1}. \tag{12}$$

The relationships between the poles and residia of a system with distinct poles are represented by (10),...,(12).

3. Controller Equations

Let us assume that the difference equation of the plant is of the form:

$$y[n] + b_1[n]y[n-1] + b_2[n]y[n-2] + \cdots + b_M[n]y[n-M] = x_1[n], \tag{13}$$

where $y[n]$ is the output quantity and $x_1[n]$ is an intermediate quantity. The linear difference equation (13) may be rewritten using the delay operator d (s. (4)) as follows:

$$(1 + b_1[n]d + b_2[n]d^2 + \cdots + b_M[n]d^M)y[n] = x_1[n]. \tag{14}$$

For the sake of simplicity we note:

$$L(d, n) = \sum_{i=0}^{M} b_i[n]d^i, \; b_0[n] = 1. \tag{15}$$

With (15), relation (14) may be compactly written as:

$$L(d, n)y[n] = x_1[n]. \tag{16}$$

Let us consider that the controller is described by the operational equation:

$$C(d, n)x[n] = x_1[n], \tag{17}$$

where $x[n]$ is the input and $C(d, n)$ is for the moment an unknown operator. $C(d, n)$ has to be determined so that controller plant cascade, shown in Fig. 1, exhibits linear

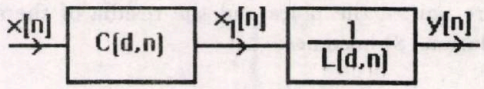

Fig. 1.- Block diagram of controller – plant cascade.

discrete time invariant behaviour, described by difference equation (7). From (16) and (17) it results:

$$L(d,n)y[n] = C(d,n)x[n]. \tag{18}$$

Substituting (8) and (15) in (18) we get:

$$C(d,n)x[n] = \sum_{i=0}^{M}\sum_{j=1}^{N} \frac{b_i[n]A_j d^i}{1-p_j d}x[n]. \tag{19}$$

After some mathematical manipulations, the relation above becomes:

$$C(d,n)x[n] = \begin{cases} \sum_{j=1}^{N} L(p_j^{-1},n)\dfrac{A_j}{1-p_j d}x[n], & \text{for } M \le N-1, \\ \sum_{j=1}^{N} L(p_j^{-1},n)\dfrac{A_j}{1-p_j d}x[n] - b_M[n]\sum_{j=1}^{N} A_j p_j^{-M}, & \text{for } M = N. \end{cases} \tag{20}$$

According to (20), the controller will be implemented by parallel connection of discrete time invariant systems of first order, followed by amplifiers with variable gain $A_j L(p_j^{-1}, n)$, as shown in Fig. 2.

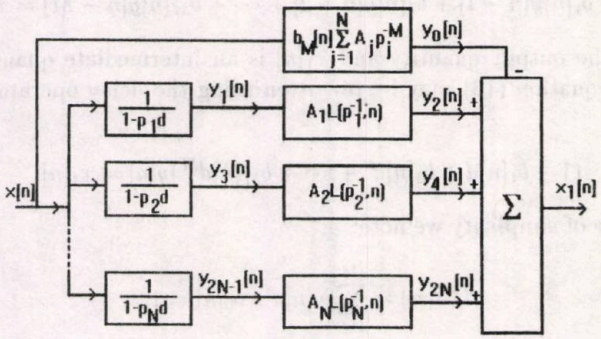

Fig. 2.- The structure of the controller.

4. Simulation Case Study

To verify the effectiveness of the proposed synthesis method, computer simulations have been made. As an example, the plant is considered to be described by the difference equation of first order:

$$y[n] + \frac{2n-1}{2n+1}y[n-1] = x_1[n]. \tag{21}$$

The difference equation of the time invariant system satisfying the prescribed requirements is:

$$y[n] - 1.2y[n-1] + 0.35y[n-2] = x[n]. \tag{22}$$

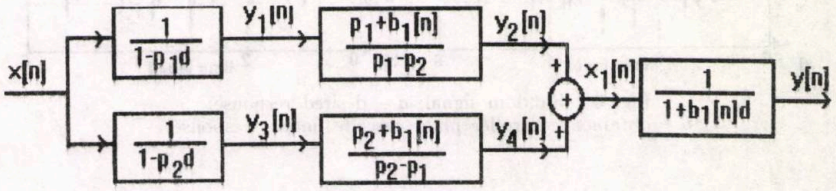

Fig. 3.- Controller–plant structure for the considered example.

The equivalent discrete time invariant system is shown in Fig. 3. The following equations may be written from the block diagram:

$$y_1[n] - p_1 y_1[n-1] = x[n], \quad y_3[n] - p_2 y_3[n-1] = x[n];$$

$$y_2[n] = \frac{p_1 + b_1[n]}{p_1 - p_2} y_1[n], \quad y_4[n] = \frac{p_2 + b_1[n]}{p_2 - p_1} y_3[n]; \tag{23}$$

$$x_1[n] = y_2[n] + y_4[n], \quad y[n] + b_1[n]y[n-1] = x_1[n],$$

where $p_1 = 0.7, p_2 = 0.5$ and $b_1[n] = (2n+1)/(2n-1)$. In simulation study, three cases for the input signal have been considered. They are a unit step, a periodic signal and a random sequence, respectively. Figs. 4 *a*, 5 *a* and 6 *a* exhibit the signals obtained at the output of the system, described by relation (22), for the considered inputs. The output signals of the regulated system, shown in Fig. 3, are presented in Figs. 4 *b*, 5 *b* and 6 *b*, respectively. The simulation results emphasize that the proposed synthesis method is able to control various plants.

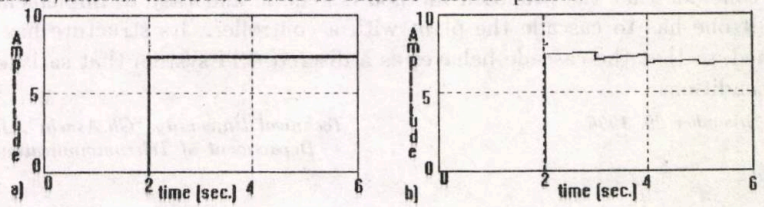

Fig. 4.- Unit step: *a* – desired response; *b* – obtained controller–plant cascade output response.

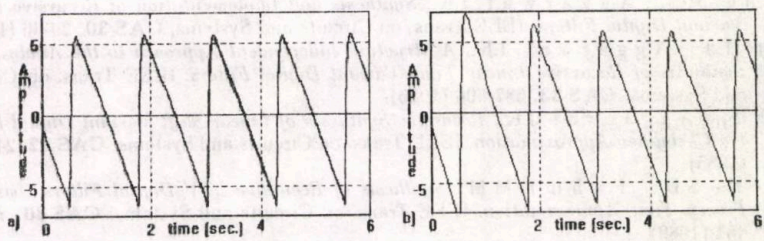

Fig. 5.- Periodic signal: *a* – desired response; *b* – obtained controller–plant cascade output response.

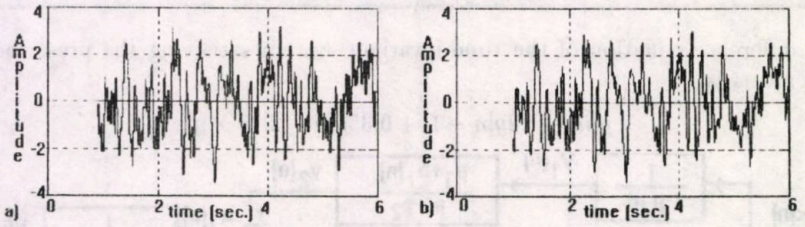

Fig. 6.– Random signal: *a* – desired response;
b – obtained controller-plant cascade output response.

5. Conclusions

The proposed method is a general one and easy to implement. To perform it one has to cascade the known system with time varying parameters with a controller. Its structure has been designed, so that the cascade behaves as a linear time invariant system that satisfies the desired requirement. The stages of the design are:

1° The order of the linear difference equation describing the regulated system with time varying parameters is inferred. Let this be M.

2° The linear difference equation of a linear time invariant system of order $N \geq M$ is determined under the imposed requirements.

3° The difference equation of the open-loop system, inferred in the second stage, is also determined.

4° The structure of a discrete regulator, described by a difference equation with time varying parameters, is constructed so that the regulated system cascaded with the regulator results in discrete time invariant system from the third step. Finally, one can conclude that the proposed method is general and easy to implement. To perform it one has to cascade the plant with a controller. Its structure has been determined, so that the cascade behaves as a discrete LTI system that satisfies the desired conditions.

Received. December 29. 1996

Technical University "Gh.Asachi", Jassy,
Department of Telecommunications

REFERENCES

1. Huang N.C., Aggarwal J.K., *Synthesis and Implementation of Recursive Linear Variant Digital Filters.* IEEE Trans. on Circuits and Systems, **CAS 30**, 29-36 (1983).
2. Leon T.J., Aggarwal J.K., *A Structure Independent Approach to the Analysis and Synthesis of Recursive Linear Time Variant Digital Filters.* IEEE Trans. on Circuits and Systems, **CAS 33**, 687-696 (1986).
3. Park S., Aggarwal J.K., *Recursive Synthesis of Linear Shift Variant Digital Filters via Chebyshev Approximation.* IEEE Trans. on Circuits and Systems, **CAS 32**, 245-251 (1985).
4. Peters S.D., Fahmi M.M., *Synthesis of Recursive LTV Digital Filters Using the Frozen Time Approximation.* IEEE Trans. on Circuits and Systems, **CAS 36**, *3*, 448-451 (1989).
5. Kirszemblat A., *Generalized Operational Calculus for Linear Parameter Systems.* Ann. de Telecom., France *11-12* (1969).

6. Munteanu V., Alexandru N., *Synthesis of Automatic Linear Systems with Time Varying Parameters* (I). Bul. Inst. polit., Iaşi, **XXI (XXV)**, *3-4*, s. III (1975).
7. Munteanu V., Alexandru N., *Synthesis of Automatic Linear Systems with Time Varying Parameters* (II). Bul. Inst. polit., Iaşi, **XXII (XXVI)**, *3-4*, s. III (1976).
8. Stubberud A., *Linear Time Variable System Synthesis Techniques in Modern Control Systems Theory*. C.T. Leondes, McGraw-Hill, New York, 1965.
9. Tărniceriu D., Grigoraş V., *Digital Filter Synthesis* (in Romanian). Ed. „Gh.Asachi", Iaşi, 1995.
10. Åström K.J., Wittenmark B., *Adaptive Control*. Addison-Wesley, New York, 1989.
11. Crochière R.E., Rabiner L.R., *Multirate Digital Signal Processing*. Prentice Hall, Englewood Cliffs, NJ, 1983.
12. Oppenheim A.V., Schafer J.F., *Discrete Time Signal Processing*. Prentice Hall, Englewood Cliffs, NJ, 1989.

COMPENSAREA SISTEMELOR DISCRETE, LINIARE, VARIANTE IN TIMP

(Rezumat)

Se propune o nouă metodă de sinteză a sistemelor discrete, liniare, variante în timp. Este dedusă structura unui controler care, cascadat cu procesul variant în timp cunoscut, să se comporte ca un ansamblu liniar invariant capabil să satisfacă anumite cerinţe de proiectare impuse. Prin simulări pe calculator se ilustrează corectitudinea metodei propuse.

BULETINUL INSTITUTULUI POLITEHNIC DIN IAŞI
Tomul XLIV (XLVIII), Fasc. 1–2, 1998
Secţia III
ELECTROTEHNICĂ. ENERGETICĂ. ELECTRONICĂ

D.C. 621.391.15

ON THE FAULT COLLAPSING IN COMBINATIONAL CIRCUITS

BY
DAMIAN IMBREA, N. COJAN and CLARISSA GÂTLAN

If the objective of the testing experiment is limited to the fault detection only, then the number of single stuck-at faults to be analysed can be reduced by fault collapsing based on equivalence and dominance relations [1]. The fault collapsing is often confined to fanout-free regions of the circuits and achieves a substantial reduction of the initial set of faults (about 50 percent). The standard algorithm for fault collapsing in digital circuits is T o's algorithm. An enhancement of this algorithm is introduced in [2].

However, the fault classes obtained by analysing the fanout-free regions only, are not maximal. Reconvergent fanout may create faults in different fanout-free regions and these faults are left uncollapsed. Extending the fault collapsing across fanout-free regions require additional analysis. The algorithms proposed in [3] and [4] are examples of such collapsing techniques.

The proposed method for extending the fault collapsing across fanout-free regions is based on logical implication and redundancy identification techniques without test pattern generation.

1. Definitions and Notations

Let C be a combinational circuit with primary input vector X and primary output vector Z. $Z(X)$ denotes the mapping realized by C. We will denote by T a specific input vector, and by $Z(t)$ the response of C to t. The presence of a fault f transforms C into a new circuit, C_f. Here we assume that C_f is a combinational circuit with function $Z_f(X)$. We will denote l_v the fault line l stuck-at-v, where v is a binary value.

D e f i n i t i o n 1. *Two faults α and β are said to be functionally equivalent if and only if $Z_\alpha(X) = Z_\beta(X)$. We will denote $\alpha \leftrightarrow \beta$.*

Let T_α and T_β be the sets of all tests that detects α and β, respectively. If $\alpha \leftrightarrow \beta$, then $T_\alpha = T_\beta$.

D e f i n i t i o n 2. *A fault α dominates the fault β, if and only if α and β are functionally equivalent under T_β (i.e., $Z_\alpha(t) = Z_\beta(t)$ for every $t \in T$). We say that the fault α is test implied by the fault β and denote $\beta \rightarrow \alpha$. If $\beta \rightarrow \alpha$, then $T_\beta \subseteq T_\alpha$.*

Note that definitions 1 and 2 are not limited to faults of the same category.

D e f i n i t i o n 3. *A line l dominates the line j if and only if every path from j to the primary outputs passes through l.*

Based on definitions 1 and 2 we can prove the statements of the following

L e m m a 1. *Let α and β two faults that belong or not to the same category:*
(1) *If $\alpha \leftrightarrow \beta$ and $\beta \leftrightarrow \gamma$ then $\alpha \leftrightarrow \gamma$.*
(2) *If $\alpha \rightarrow \beta$ and $\beta \rightarrow \gamma$ then $\alpha \rightarrow \gamma$.*
(3) *If $\alpha \leftrightarrow \beta$ and $\beta \rightarrow \gamma$ then $\alpha \rightarrow \gamma$.*
(4) *If $\alpha \rightarrow \beta$ and $\beta \leftrightarrow \gamma$ then $\alpha \rightarrow \gamma$.*
(5) *If $\alpha \rightarrow \beta$ and $\beta \rightarrow \gamma$ then $\alpha \leftrightarrow \beta$.*

2. Identification of Equivalent Faults

L e m m a 2. *If line l dominates the line j and $(j = u) \Rightarrow (l = v)$, where u and v are binary values, then $j_u \leftrightarrow l_v$.*

P r o o f. Let t be a test that detects the fault j_u. Then t activates j_u (by setting $j = \overline{u}$ in the fault-free circuit C) and propagates the resulting error $\overline{u}/u$ to primary outputs; u is the signal value at line j in the faulty circuit C_{ju}. Since $(j = u) \Rightarrow (l = v)$ and the error passes through l, the error at line l is $\overline{v}/v$. Thus, the test t activates the fault l_v. But t propagates the error $\overline{v}/v$ from l to the primary outputs. Therefore t detects l_v, hence $j_u \rightarrow l_v$.

Let us assume that t detects l_v. In the fault-free circuit C, t sets $l = \overline{v}$ and this implies $j = \overline{u}$. Thus, t activates the fault j_u. In the faulty circuit C_{ju}, the test t propagates the error from j to l because $(j = u) \Rightarrow (l = v)$. Then, t propagates the error from l to primary outputs because t detects l_v, hence $l_v \rightarrow j_u$. According to Lemma 1 (5), $l_v \leftrightarrow j_u$.

If one of the two faults is undetectable then both are undetectable.

Based on Lemma 1 and Lemma 2 we can identify equivalent single stuck-at faults that belong to the same fanout-free region or to different fanout-free regions.

E x a m p l e 1. In the circuit of Fig. 1, all lines belong to the same region except b.
a) $e_0 \leftrightarrow k_1$ because $(e = 0) \Rightarrow (k = 1)$ and k dominates e (Lemma 2);
b) $b_0 \leftrightarrow z_1$ because $(b = 0) \Rightarrow (z = 1)$ and z dominates b (Lemma 2);
c) $e_0 \leftrightarrow f_1$ because $e_0 \leftrightarrow k_1$ and $f_1 \leftrightarrow k_1$ (Lemma 1).

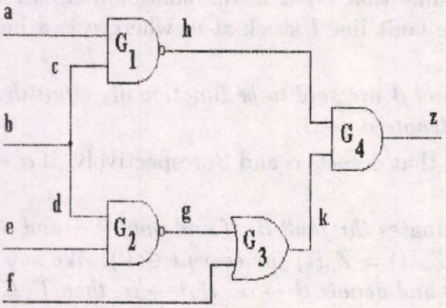

Fig. 1

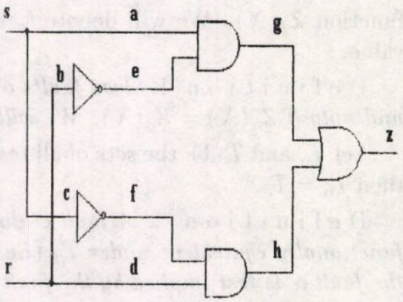

Fig. 2

However, Lemma 1 and Lemma 2 may not identify all equivalent single stuck-at faults within a fanout-free region. The following example shows such cases.

E x a m p l e 2. In the circuit from Fig. 2, all lines belong to the same fanout-free region (FFR) except s and r. The following equivalent fault classes are obtained using Lemma 1 and Lemma 2: $\{a_0, b_1, e_0, g_0\}$ $\{d_0, c_1, f_0, h_0\}$, $\{b_0, e_1\}$, $\{c_0, f_1\}$ and $\{g_1, h_1, z_1\}$.

Now, we find out other equivalent fault classes using redundancy identification techniques.

Let us denote by C' the circuit of Fig. 2. The presence of the fault a_1 transforms C into a new combinational circuit C_{a1}. The fault d_1 is undetectable in C_{a1}. It means that d_1 and the double fault $\{a_1, d_1\}$ are equivalent. The fault a_1 is also undetectable in the circuit C_{d1}. Therefore a_1 and $\{a_1, d_1\}$ are equivalent faults. Based on Lemma 1 (1) we can conclude that $a_1 \leftrightarrow d_1$.

In a similar way we may prove that b_0 and c_0 are equivalent faults. Thus, the equivalence fault classes in the circuit of Fig. 2 are: $\{a_0, b_1, e_0, g_0\}$; $\{d_0, c_1, f_0, h_0\}$; $\{b_0, e_1, c_0, f_1\}$; $\{a_1, d_1\}$; $\{g_1, h_1, z_1\}$.

For fault analysis it is sufficient to consider only one representative fault from every equivalence class. This type of reduction of the set of faults to be analysed based on equivalence relations is called *equivalence fault collapsing.*

3. Identification of Test Implied faults

L e m m a 3. *If line l dominates the line j and all paths between j and l have the same inversion parity p, $p \in \{0, 1\}$, then:*

$$j_0 \rightarrow l_p, \quad j_1 \rightarrow l_{\overline{p}}.$$

P r o o f. If a test t detects the fault j_0 then the propagated error on line l must have the form $\overline{p}/p$. Then, t propagates the error from l to primary outputs. Hence t detects the fault l_p and therefore the fault l_p dominates the fault j_0 ($j_0 \rightarrow l_p$). In a similar way, we can prove that the fault $l_{\overline{p}}$ dominates the fault j_1 ($j_1 \rightarrow l_{\overline{p}}$).

Based on Lemma 3 we can identify dominance relations between faults that belong to the same or different fanout-free regions.

The test implied faults (or dominating faults) can be removed from the set of faults we consider for test generation. This type of reduction of set of faults to be analysed based on dominance relations is called *dominance fault collapsing.*

In the following example we collapse the single stuck-at faults based on the three lemmas presented in this paper and redundancy identification techniques.

E x a m p l e 3. There are 12 lines in the circuit of Fig. 3. The number of possible single stuck-at faults is 24. The equivalence and dominance relations between these faults are represented in Fig. 4.

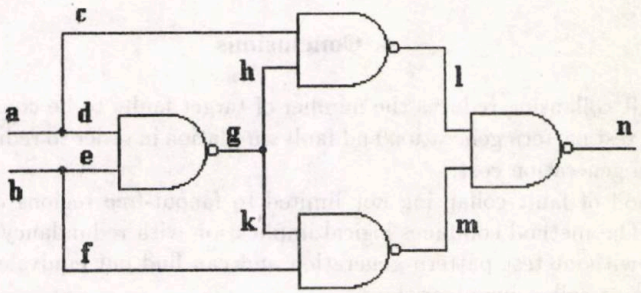

Fig. 3

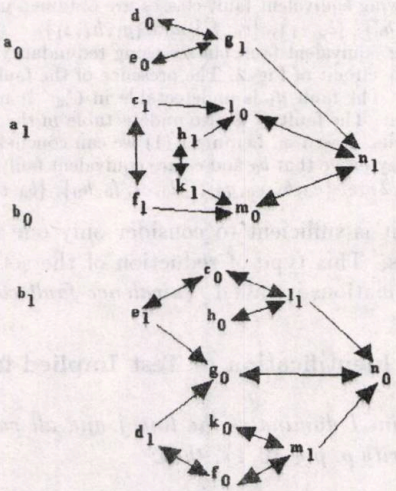

Fig. 4

The fault classes and representative faults are as follow:

$\{a_0\}$	a_0
$\{a_1\}$	a_1
$\{b_0\}$	b_0
$\{b_1\}$	b_1
$\{d_0, e_0, g_1, n_1, l_0, m_0\}$	d_0 (or e_0, or g_1)
$\{c_1, f_1, l_0, m_0, n_1\}$	c_1 (or f_1)
$\{h_1, k_1, l_0, m_0, n_1\}$	h_1 (or k_1)
$\{e_1, c_0, h_0, l_1, g_0, n_0\}$	e_1 (or c_0, or h_0, or l_1)
$\{d_1, f_0, k_0, m_1, g_0, n_0\}$	d_1 (or f_0, or k_0, or m_1).

The following equivalent faults are found out using redundancy identification techniques: $c_1 \leftrightarrow f_1$, $h_1 \leftrightarrow k_1$, $e_1 \leftrightarrow c_0$ and $d_1 \leftrightarrow f_0$. For test generation we may consider only the nine above representative faults. The reduction of the initial set of faults is 62.5 percent.

4. Conclusions

The fault collapsing reduces the number of target faults to be considered before performing test pattern generation and fault simulation in order to reduce the overall test pattern generation cost.

A method of fault collapsing not limited to fanout-free regions only has been proposed. The method combines logical implication with redundancy identification techniques without test pattern generation and can find out equivalent faults that escape to most collapsing algorithms.

In large circuits that have many reconvergent fanout stems, the fault collapsing method proposed in this paper may be much more efficient than one limited to

fanout-free only.

Received August 28, 1996

Technical University "Gh.Asachi", Jassy,
Department of Applied Electronics

REFERENCES

1. Abramovici M., Breuer M.A., Friedman A.D., *Digital Systems Testing and Testable Design*. Computer Science Press, New York, 1990.
2. Akachai Sang-in, Cheung Y.K., *A Method of Representative Fault Selection in Digital Circuits for ATPG*. IEEE ISCAS, London, 1994, **1**, 73-76.
3. Lioy A., *Advanced Fault Collapsing*. IEEE Design and Test of Computer, 64-71 (1992).
4. Lioy A., *On the Equivalence of Fanout Point Faults*. IEEE Trans. on Computers, **42**, *3*, 268-271 (1993).

ASUPRA COLAPSĂRII DEFECTELOR ÎN CIRCUITELE COMBINAŢIONALE

(Rezumat)

Reducerea numărului de defecte singulare stuck-at ce trebuie explicit considerate la generarea testelor se numeşte *colapsare*. Această operaţie se realizează pe baza relaţiilor de echivalenţă şi de dominanţă dintre defecte. Majoritatea algoritmilor de colapsare se limitează la regiunile fără fanout ale circuitelor şi clasele de defecte astfel obţinute nu sunt maximale.

Un fanout reconvergent poate creea defecte echivalente care aparţin aceleiaşi regiuni fără fanout sau la regiuni fără fanout diferite şi care sunt lăsate necolapsate de majoritatea algoritmilor de colapsare. Metoda propusă identifică astfel de defecte şi se bazează pe implicaţii logice şi identificare a redundanţei fără generarea testelor.

In cazul circuitelor mari şi care au un număr mare de stemuri cu fanout reconvergent, această metodă de colapsare poate realiza o reducere a setului de defecte ce trebuie explicit analizate semnificativ mai mare faţă de metodele limitate numai la regiunile fără fanout.

BULETINUL INSTITUTULUI POLITEHNIC DIN IAŞI
Tomul XLIV (XLVIII), Fasc. 1–2, 1998
Secţia III
ELECTROTEHNICĂ. ENERGETICĂ. ELECTRONICĂ

D.C. 537.74

THE METROLOGICAL PERFORMANCE OF THE PROXIMITY FUZZY-SYMBOLIC SENSOR

BY
C. SĂRMĂŞANU and M. CREŢU

A functional approach for description of the metrological performance of the sensor in the numerical–symbolic conversion is proposed. In that view, three functions are defined to characterize the imprecision of the sensor. As application, a proximity fuzzy-symbolic sensor has been implemented.

1. Introduction

The fuzzy-symbolic sensors are based on a numerical–symbolic conversion [1],...,[3]. This conversion is a representation of words by fuzzy subsets of a precise measurement numerical domain. In reality, the measurement process is not ideal, and the numerical values given back by the sensor are imprecise. The aim of this paper is to take into account the metrological performance of the sensor in the numerical–symbolic conversion. The problem is to recognize the different errors (systematic, regular and aberrant errors) which affect the sensor. It requires information about the sensor's operation, whose performance must be known.

2. Description of the Sensor Metrological Performance

For characterize the sensor performance we propose a functional approach which is coherent with the fuzzy-subset theory [4]. The imprecision of the sensor are defined by three functions, namely: a) the *precision function*, which is the probability distribution of the experimental measurements and reflects the estimation performance of the sensor for regular operating; b) the *detection function*, which describes the detection performance and can be interpreted as an *a priori* probability of regular measurements; c) the *validity function*, which characterizes the validity of the measure and can be interpreted as an *a posteriori* probability of *regular* measurements.

These functions could be obtained by theoretical calculus or by experimental analysis. It is necessary to underline that the detection function requires knowledge of the sensor's performance, which depends on the operating configuration. The validity function requires internal or external data, providing information on the

observed situation, in order to do a coherence test of the measured value, which leads to a validity rating of the measurement [5].

We propose to process the imprecision measurement in accordance which each error (systematic, regular and aberrant errors) and to take in account these errors in the numerical–symbolic conversion. The idea is to associate to a symbolic value a membership function that integrates elements of different nature (external information about the designated purpose for symbolic representation, imprecision measurements).

So, to process the *systematic errors*, we will utilize a special function f_s. This function may simply be a subtraction by a constant or a multiplication by a scale factor in the case of correction of systematic errors by a standard, a parametric function depending on external physical quantities or a correction table, in the most complex cases.

In the crisp approach, the border between two concepts is quite abrupt. Therefore, because of the statistical variation of the numerical value, the symbolic one obtained in return varies a lot. The management of *regular errors* may take in account the precision of the sensor in the construction of the fuzzy partition by smoothing the transition between concepts (similar to a frequential filtering). With that end in view we propose to convolute the meaning of concepts by the *precision function*, which constitutes the impulse response of the symbolic sensor.

In what follows an example is given for a proximity sensor [6], which illustrates this procedure. The concept *close* is defined by the Gaussian interval 2.5...7.5 cm. Let us consider his following precision function:

$$f_p = \begin{cases} 1 & \text{if } x \in \left[5 - \frac{\varepsilon}{2},\ 5 + \frac{\varepsilon}{2}\right], \\ 0 & \text{if } x \notin \left[5 - \frac{\varepsilon}{2},\ 5 + \frac{\varepsilon}{2}\right]. \end{cases} \tag{1}$$

If we have a precision of $\varepsilon = 2$ mm around the 5 cm measurement, the modified concept is presented in Fig. 1.

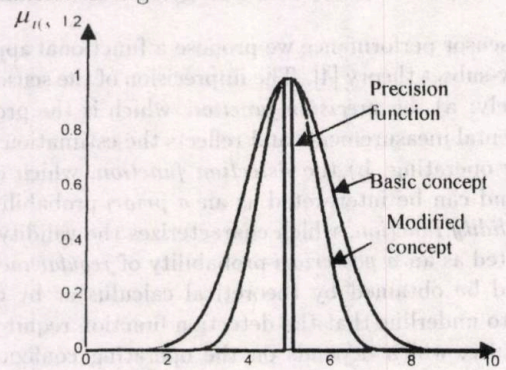

Fig. 1.– Accuracy of proximity sensor $\varepsilon = 2$ mm.

In this case the sensor was quite efficient and the change is slight. In order to understand the effect of the convolution by the precision function on the basic concept we consider two extreme cases (Figs. 2 *a*, *b*) for a precision of $\varepsilon = 1$ cm, respectively $\varepsilon = 3$ cm. In the second case, the fuzzy concept does not have a modal value and this low membership grade expresses the low credibility of the symbolical value, which is in accordance with the precision of the sensor. This information is also an incitement to redefine the basic concept.

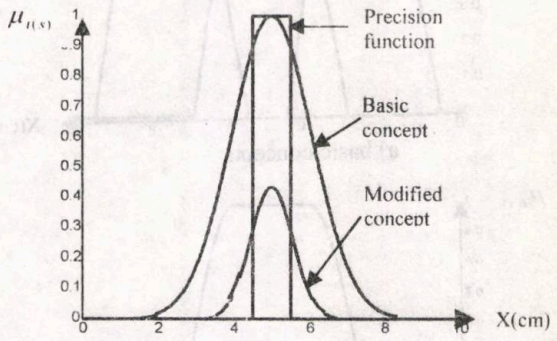

a) $\varepsilon = 1cm$

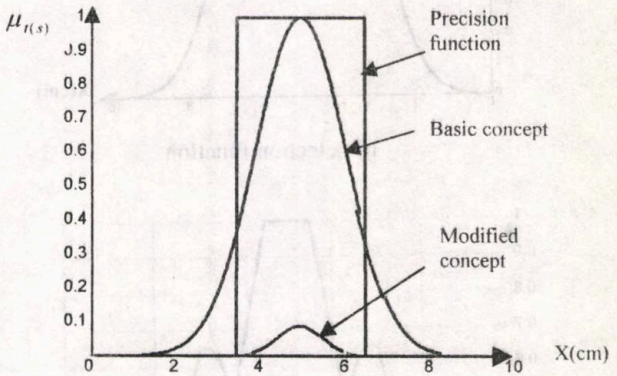

b) $\varepsilon = 3cm$

Fig. 2.– Accuracy of proximity sensor $\varepsilon = 1$ cm and $\varepsilon = 3$ cm.

Aberrant measurement errors correspond to values that share nothing with the observed reality. We will distinguish two cases: the first case is the *a priori* aberrant values, determined by the non-membership to a nominal operating area, must lead to a small membership grade of concepts, according to their small confidence value. For this case we propose to multiply the meaning of concepts by the detection function that constitutes information about the normal operating area of the sensor (Figs. 3 *a*, *b*, *c*).

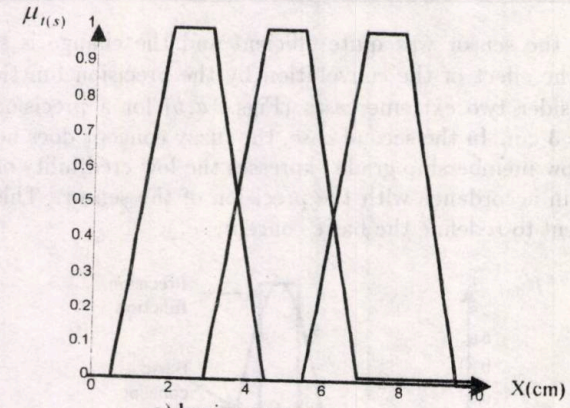

a) basic concepts

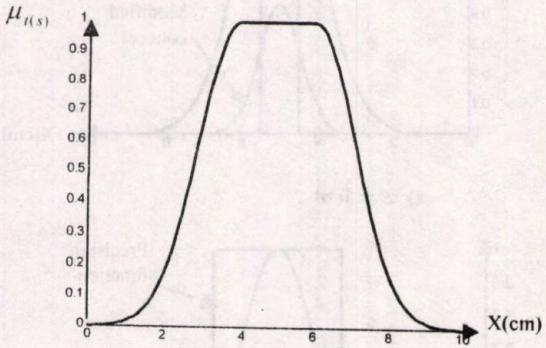

b) detection function

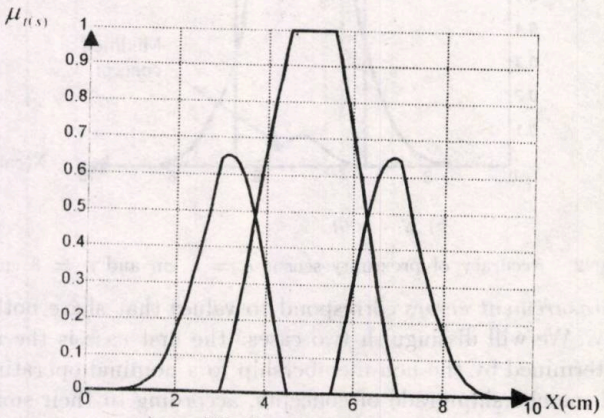

c) modified concepts

Fig. 3.- Action of the detection function to a basic proximity concept.

The second case is the *a posteriori* aberrant measurement errors, which are values belonging to the nominal operating area of the sensor but which share nothing with the observed reality. To detect these faults, information about the acquired values, which will be characterized by a validity function, is required. The validity is obtained by crosschecking with other internal or external information about the measurement processing. Finally, the meaning of the modified concepts is deduced by multiplication of the basic concepts by the validity function.

3. Fuzzy-Symbolic Proximity Sensor

Assuming the previous section, the block diagram of a fuzzy-symbolic proximity sensor is presented in Fig. 4.

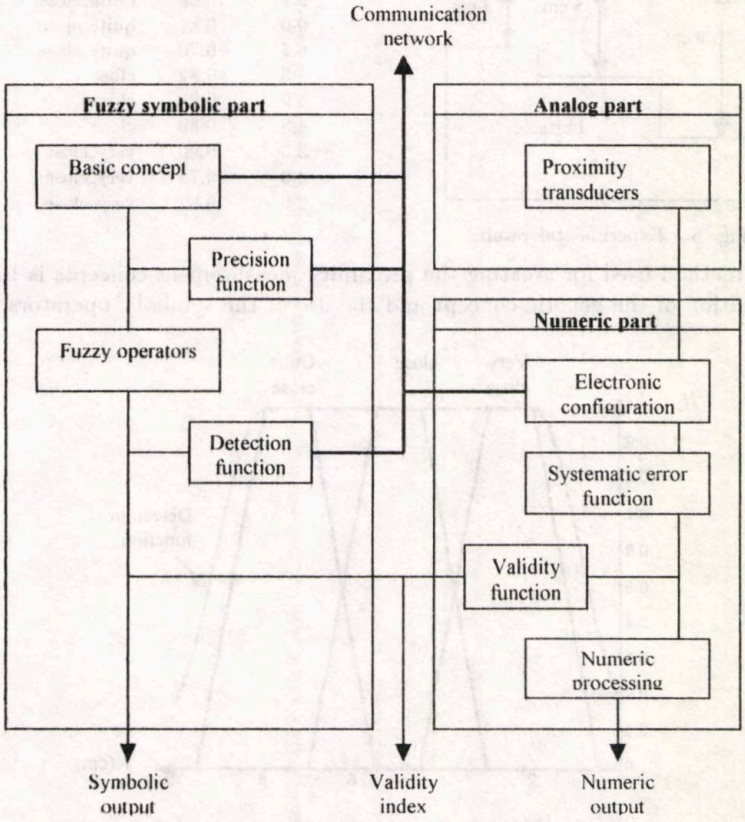

Fig. 4.– The block diagram of a fuzzy-symbolic proximity sensor.

The analogical part makes the usual proximity sensing. The numerical part acquires a numerical measurement of proximity with possible correction and compensation of the measures. The fuzzy-symbolic part generates the meanings of the

concepts by taking in account the measurement imprecision. The precision, detection and validity function depends on the configuration of the sensor and act with specific operators (convolution, multiplication) in the numerical-symbolic conversion. The output of the sensor consists in numerical measurements and their validity and a symbolic description of the proximity measurement. The membership grade of the proximity measurements is shown as a validity index of the concept fusing symbolic uncertainty and numerical measurement imprecision.

The experimental results obtained with this sensor for a robot over a plane supporting an obstacle are given in Fig. 5.

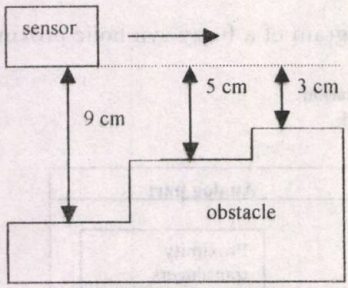

X, [cm]	Validity	Symbol
9.2	0.69	quite_close
9.0	0.81	quite_close
8.7	0.70	quite_close
5.3	0.82	close
5.0	0.98	close
4.8	0.89	close
3.0	0.90	very_close
3.3	0.78	very_close
2.9	0.82	very_close

Fig. 5.- Experimental results.

The method used for creating the proximity measurement concepts is based on the definition of the generic concept and the use of the symbolic operators [5], [7], [8].

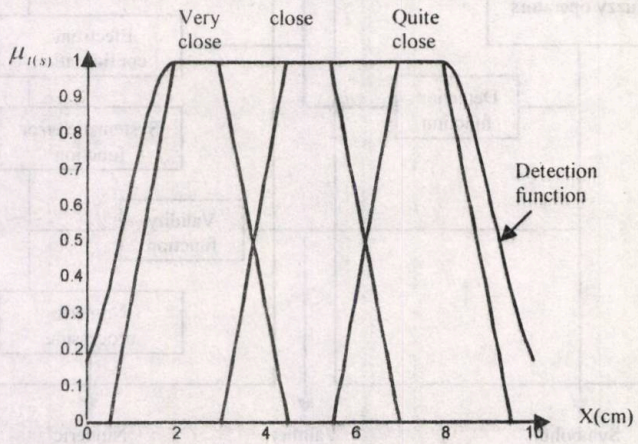

Fig. 6.- Creation of proximity measurement concepts.

The detection function f_d is equal to 1 in the interval [0.04 cm, 12 cm] so that it does not affect the membership grades in this range (Fig. 6). The validity of measurements is obtained by the computation of the average proximity measurement,

x_a, and the average proximity measurement with 5% of error, x_e:

$$f_v = \frac{x_a}{x_e}. \tag{2}$$

A validity close to 1 means a good validity for the considered measurement, whereas a value close to 0 corresponds to a not very reliable measurement.

4. Conclusion

Using the symbolic sensors, the numerical data about the proximity are ultimately turned into a qualitative response. In reality, the measurement process is not an ideal one and the numerical values given back by the sensor are imprecise. The fuzzy subset theory for the management of the measurement errors are used. So, the proposed fuzzy-symbolic proximity sensor allows conventional sensing, description, adaptation to the measurement context and treatment of errors.

Received, October 16, 1997

Technical University "Gh.Asachi", Jassy,
Department of Electrical
Measures and Materials

REFERENCES

1. Benoit E., Foulloy L., *Symbolic Sensors.* IMEKO TC7 Internat. Symp. on AIMaC'91, Kyoto, Japan, 1991, 131-136.
2. Benoit E., Foulloy L., *Symbolic Sensors: One Solution to the Numerical-Symbolic Interface.* Internat. Workshop on Qualitative Reasoning and Decision Support System, Toulouse, France, 1991.
3. Sărmăşanu C., *Sur un capteur symbolique de proximité.* Bul. Inst. polit., Iaşi, **XLI (XLV)**, *1-4*, s. III (1995).
4. Zadeh L.A., *The Role of Fuzzy-logic in the Management of Uncertainty in Expert System.* Fuzzy-sets Syst., **11**, 199-227 (1983).
5. Mauris G., Benoit E., Foulloy L., *Fuzzy Symbolic Sensors - From Concept to Application.* Measurement, J. of the Internat. Meas. Confed. IMEKO, *12*, 357-384 (1994).
6. Sărmăşanu C., Creţu M., *A Two-dimensional Fuzzy-symbolic Proximity Sensor.* Proc. of the Internat. Conf. on Develop. a. Appl. Systems, D&AS'96, Suceava, 1996.
7. Sărmăşanu C., Creţu M., Niţă L., Postolache O., *Senzori de proximitate fuzzy-simbolici. Generarea reperelor scării.* SIELMEC'97, Chişinău, Rep. Moldova, 1997.
8. Sărmăşanu C., Creţu M., Niţă L., *Posibilităţi de dilatare şi comprimare a scării în măsurarea fuzzy-simbolică a proximităţii.* SIELMEC'97, Chişinău, Rep. Moldova, 1997.

PERFORMANŢELE METROLOGICE ALE SENZORILOR DE PROXIMITATE FUZZY-SIMBOLICI

(Rezumat)

Se propune o abordare funcţională a performanţei metrologice a senzorului în conversia numeric–simbolică. În acest scop s-au definit trei funcţii care caracterizează imprecizia senzorului. Ca aplicaţie s-a implementat un senzor fuzzy-simbolic de proximitate.

BULETINUL INSTITUTULUI POLITEHNIC DIN IAŞI
Tomul XLIV (XLVIII), Fasc. 1–2, 1998
Secţia III
ELECTROTEHNICĂ. ENERGETICĂ. ELECTRONICĂ

D.C. 538.23

CHUA TYPE HYSTERESIS MODEL

BY
MARINEL TEMNEANU and CRISTINA TEMNEANU

A C h u a type model is proposed in order to characterise the specific behviour of magnetic materials both in high and low frequencies. There is also presented an analytical equivalent expression based on the most common available magnetic parameters, Steinmetz coefficient and exponent. Experimental measurements were made for different values of peak induction. As a result, it is confirmed that the proposed C h u a type model has satisfactory reproductibility of the typical magnetization characteristics commonly observed in practice.

1. Introduction

Recently, considerable effort has been done in order to represent the magnetization characteristics for the computer oriented design of magnetic devices. The models representing magnetization characteristics may be classified into two types. One is a P r e i s a c h type model, which assumed that each of domains has a rectangular hysteresis loop and interaction between domains can be introduced by assuming local field acting on domains. The other is a C h u a type model, which is based on the fact that a trajectory of flux linkage versus current is uniquely determined by the last point at which the time derivative of flux linkage change sign.

The C h u a type model exhibits many important hysteretic properties like the presence of minor loops and the increase of the loop area (representing the iron losses) with frequency. Furthermore, it has been reported that a C h u a type model can be derived by the Fourier series expansion of the field intensity under the sinusoidal time varying magnetic flux density.

This paper proposes a C h u a type model that can be successfully used for the characterization of the specific behaviour of magnetic materials both in high and low frequencies.

2. Theoretical Considerations

The specific model belonging to C h u a [1] assumes that:

$$H = \frac{1}{\mu} B + \frac{1}{s} \cdot \frac{\partial B}{\partial t}, \tag{1}$$

where H, B, μ, s and t denote the field intensity, flux density, permeability, hysteresis coefficient and time, respectively.

From an experimental point of view, the magnetization is accomplished in essence through the time varying flux density. There are two major aspects to consider:

1° The $B_{max}(H_{max})$ curve is a nonlinear one, so the permeability function $\mu(H)$ must reflect this situation.

2° There are different $B(H)$ paths according to the sign of time derivative of flux density (the $B(H)$ function is a multiple branch one). In C h u a type models describing equation (1) this behaviour is reflected by the presence of the second term which takes different signs on the ascending or descending branch of the hysteresis loop.

The magnetization trajectory is uniquely determined by the sign of $\partial B/\partial t$ as well as the rate of change $\partial B/\partial t$.

The determination of model parameters (μ and s) is very simple. A trace of the peak points of B versus H yields a single valued (single branch) function of permeability μ, because the term $\partial B/\partial t$ in (1) becomes zero when the flux density arrives at the positive or negative extremum value (Fig. 1). C h u a and other authors [2], [3], consider that similarly, a trace of the peak points of the $\partial B/\partial t$ versus H trajectories yields a single valued function of the hysteresis coefficient s (Fig. 2). This assumption is based on the experimental observation that B is zero when the field intensity takes the coercive value and the time derivative of magnetic flux density arrives at the positive or negative maximum value.

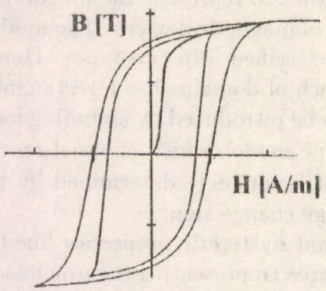

Fig. 1

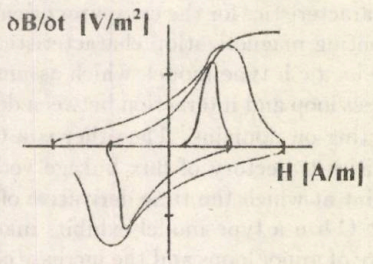

Fig. 2

Even if this assumption is correct the $s(H)$ or $s(B)$ function is not a single branch one. Taking a closer look at the magnetization characteristics, we will see that the hysteresis loop is not symmetric to the fundamental characteristic of magnetization. This means that for the same value of magnetic flux density, s depends on the sign of $\partial B/\partial t$ (takes different values for the ascending or descending branch of the loop). By consequence, the hysteresis parameter s must be determined as a function of B and $\partial B/\partial t$.

Another important observation that can be made is the following. When we try to simulate the behaviour of magnetic materials in very low frequency, classic C h u a type models are unusable. In eq. (1), when frequency is decreasing to zero, $\partial B/\partial t$ becomes negligible small, and $H = B/\mu$. Graphically, this means that at very

low frequencies, the hysteresis loop approaches till confusion to the fundamental characteristic of magnetization. Because the enclosed area of the hysteresis loop reflects the iron losses, this means also that, for low frequencies, these losses are zero. Or, experimentally, the dynamic hysteresis loop approaches, when frequency decrease to zero, to the static hysteresis loop, which is smaller than the dynamic one but definitively still a multi-branch curve. In order to solve this problem we propose a new C h u a model definition as follows:

$$H = \frac{1}{\mu}B + H_{st} + \frac{1}{s}\cdot\frac{\partial B}{\partial t}, \tag{2}$$

where H_{st} represents the static contribution in field intensity expression. The determination of H_{st} as a function of B and $\partial B/\partial t$ is possible if fundamental characteristic of magnetization (or initial DC megnetization curve) and static hysteresis loop is known. In many cases the last one is not available. We can consider, in these cases, that the static loop can be replaced with the iron loss equivalent ellipse [4]. The equation of this ellipse, represented in Fig. 3, is:

$$\left(\frac{B}{B_m}\right)^2 + \left(\frac{H}{H_c}\right)^2 = 1, \tag{3}$$

where B_m and H_c are peak magnetic flux density and coercive magnetic field intensity respectively.

Eq.(2) becomes:

$$H = \frac{1}{\mu}B + \frac{1}{s}\cdot\frac{\partial B}{\partial t} + \operatorname{sgn}\left(\frac{\partial B}{\partial t}\right)H_c\sqrt{1-\left(\frac{B}{B_m}\right)^2}. \tag{4}$$

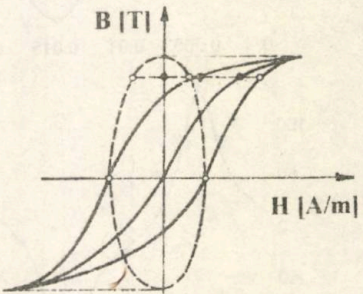

Fig. 3

Taking into account that the area of the iron loss equivalent ellipse represents the hysteresis loss per cycle, which can be expressed using the Steinmetz formula by:

$$W_{V,st} = \eta B_m^n, \tag{5}$$

we can derive the following analytical expression for the hysteresis loop:

$$H = \frac{1}{\mu}B + \frac{1}{s}\cdot\frac{\partial B}{\partial t} + \operatorname{sgn}\left(\frac{\partial B}{\partial t}\right)\frac{\eta}{4\pi}B_m^{n-1}\sqrt{1-\left(\frac{B}{B_m}\right)^2}, \tag{6}$$

where η and n are the Steinmetz coefficient and exponent, usually available in any manufacturers catalogue.

3. Experimental Results

There are presented the results obtained by using the expression (6) in the modelisation process of Silectron alloy behaviour [6]. The model parameters were calculated

using an algorithm presented in [5]. In Figs. 4 and 5 are represented the waveform of magnetic flux density B, [T], and magnetic field intensity H, [A/m], versus time t, [s], and magnetic flux density B, [T], versus magnetic field intensity H, [A/m]. We imposed a sinusoidal variation of flux density with peak value $B_m = 1$ T (Fig. 5), and respectively $B_m = 1.8$ T (Fig. 4). For both situations the frequency was $f = 50$ Hz.

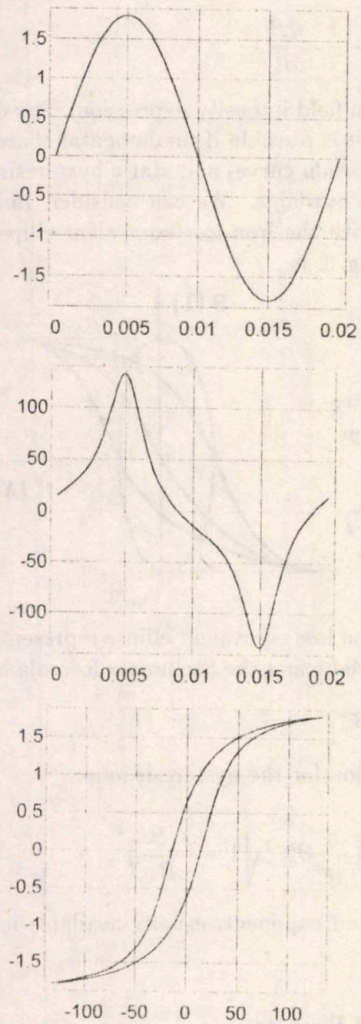

Fig. 4.– $B(t)$, $H(t)$, $B(H)$ for $B_m = 1.8$ T.

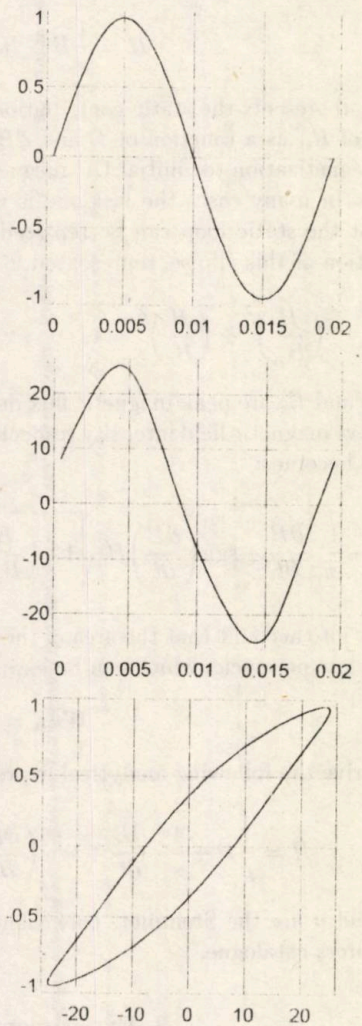

Fig. 5.– $B(t)$, $H(t)$, $B(H)$ for $B_m = 1$ T.

4. Conclusions

A C h u a type model that can be successfully used for the characterization of the specific behaviour of magnetic materials both in high and low frequencies is proposed. There are also presented an analytical equivalent expression, based on the most common available magnetic parameters, Steinmetz coefficient and exponent and some experimental results.

Received. October 16, 1997

Technical University "Gh.Asachi", Jassy,
Department of Electrical
Measures and Materials

REFERENCES

1. C h u a L.O., B a s s S.T.C., *A Generalized Hysteresis Model.* IEEE Trans. Circuit Theory, **CT-19**, *1*, 36-48 (1972).
2. S a i t o Y., N a m i k i M., H a y a n o S., T s u y a N., *Experimental Verification of a Chua Type Magnetization Model.* IEEE Trans. Magn., **25**, *4*, 2968-2970 (1989).
3. S a i t o Y., F u k u s h i m a K., H a y a n o S., T s u y a N., *Application of a Chua Type Model to the Loss and Skin Effect Calculations.* IEEE Trans. Magn., **23**, *5*, 2227-2229 (1987).
4. S a v i n Gh., R o s m a n H., *Circuite electrice neliniare și parametrice.* Ed. Tehnică, București, 1973.
5. T e m n e a n u M., F o ș a l ă u C., T e m n e a n u C., *Modelarea comportării aliajului tip* $Fe_{77.5}Si_{7.5}B_{15}$ *cu ajutorul modelelor tip Chua.* Sielmec, Chișinău, 1997, vol. **II**, 235-238.
6. T e m n e a n u M., Postgraduate Report, Techn. Univ. „Gh.Asachi", Jassy, 1997.

UN MODEL DE TIP CHUA AL CICLULUI DE HISTEREZIS

(Rezumat)

Se urmărește rezolvarea unor dificultăți întâlnite de către utilizatorii modelării matematice de tip C h u a a caracteristicilor magnetice de material. Este propus un nou model din această clasă împreună cu o modalitate de formulare a expresiei analitice de definire a acestuia în funcție de coeficientul și exponentul lui Steinmetz, disponibili în marea majoritate a cataloagelor de producător.

BULETINUL INSTITUTULUI POLITEHNIC DIN IAŞI
Tomul XLIV (XLVIII), Fasc. 1-2, 1998
Secţia III
ELECTROTEHNICĂ. ENERGETICĂ. ELECTRONICĂ

D.C. 621.389:57

A TRIAXIS BROADBAND MAGNETIC FIELD METER FOR BIOMEDICAL APPLICATIONS

BY
VALERIU DAVID, M. ANTONIU and EMIL VREMERĂ

A magnetic field meter having an isotropic directional characteristic, suitable for measurements of perturbative fields that can have dangerous effects on biological systems is described. The instrument is characterized by a great sensitivity and a frequency range from 40 Hz to more than 100 kHz.

1. Introduction

The effects of the interaction of electromagnetic fields with the biological tissues depend on the frequency range of the exposure fields. A classification of the exposure fields was made [1] in fields with frequencies less than 100 kHz and fields of frequencies greater than 100 kHz. The measurement of the electromagnetic fields with greater frequencies than 100 kHz can be made using an isotropic broadband electric field probe [2] or a long term survey system [3]. Because of the continuous exposure of human beings to the fields created by the power system and VDUs, a special interest presents the determination of the electromagnetic pollution between 20 Hz and 100 kHz. That is why efforts have been directed to the measurement of electromagnetic environment, the study of electromagnetic radiations effects on beings, also the design of electric systems in order to minimize these perturbations ("biological compatibility"). It is known that the measurement of the magnetic field in range less than 100 kHz is realized, generally, with two field meters. One of them works in the band 20 Hz...2 kHz and the other one in the band 2 kHz...400 kHz [4], [5]. For this reason the authors propose an isotropic magnetic field meter which covers alone the frequency range less than 100 kHz [6].

2. The Principle of the Instrument

The two main requests for the electromagnetic sensors are a great sensitivity and a frequency broadband for which the transfer function should be simple. If the last request is realized, it is possible to use only one sensor for a great frequency range. In this situation, another advantage is represented by the possibility to per-

form time domain measurements. Moreover, instruments used for the measurement of electromagnetic fields in biomedical applications have to fulfil the following two conditions:

1° To have an isotropic directional characteristic, since the polarization of the measured field and the direction of propagation are usually unknown.

2° To allow the recording of the field magnitude for a longer time because of its temporal variations.

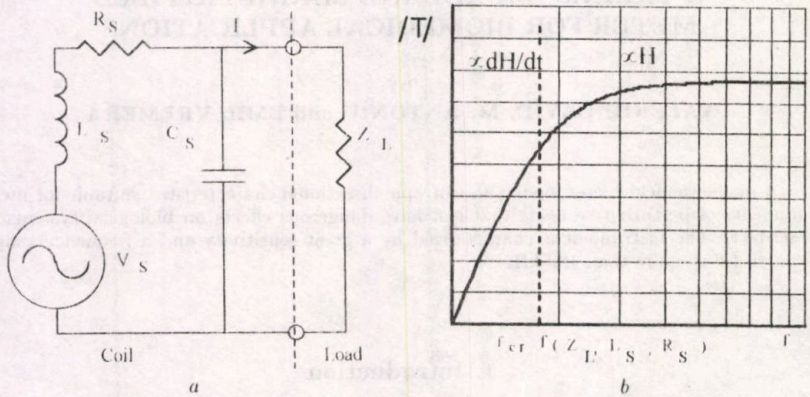

Fig. 1.– The equivalent electrical diagram and the transfer function for a magnetic field sensor.

If we consider the equivalent circuit of one magnetic field sensor [7] (Fig. 1), it is noticed that the transfer function has two distinct regions ($\propto dH/dt$ and $\propto H$). The first is proportional to the time derivative of the field strength and the second is proportional to the field strength. These two parts are separated by the critical frequency [8]:

$$f_{cr} = \frac{R}{2\pi L_S}, \tag{1}$$

where L_S is the coil inductance and R – the coil resistance connected in series with the load resistance. In the first situation (Z_L having a large value), C_S limits the higher frequency. In the second case (Z_L very small), C_S has no influence upon the transfer function.

The increase in sensitivity is made by loading the coil with voltage or current amplifiers. Thus, an active sensor is obtained. For the proposed sensor, the functioning on the region proportional to the magnetic field strength is preferred, namely $f > f_{cr}$. The decrease of the critical frequency is achieved by increasing L_S and connecting the coil to a differential current amplifier. If the coil is made on a core of relative permeability μ_r, winding N turns, its inductance and resistance being [9]:

$$L_S = \mu_0 \mu_r \frac{A}{l} N^2 \beta^{-2/5} \quad (a), \qquad R_S = N\pi D \frac{\rho_{Cu}}{S_{Cu}} \quad (b), \tag{2}$$

where: A is the cross section area of the coil, l – length of the core, β – correction factor, D – coil diameter, ρ_{Cu} – resistivity of copper and S_{Cu} – copper wire cross section area.

For the coil placed in a time varying magnetic field the induced voltage is:

$$V_S = -\frac{\mathrm{d}\phi}{\mathrm{d}t} = -\frac{\mathrm{d}}{\mathrm{d}t}\int_A \mathbf{B}\mathbf{n}^0\,\mathrm{d}A. \tag{3}$$

For a magnetic field of intensity:

$$\underline{H} = H_m e^{j\omega t}, \tag{4}$$

perpendicular to the cross sectional area of the coil, equation (3) becomes:

$$\underline{V_S} = -j\omega N A \mu_0 \mu_r \underline{H}. \tag{5}$$

If $f \gg f_{cr}$, the current

$$\underline{I} = \frac{\underline{V_S}}{j\omega L_S} = \frac{l\beta^{2/5}}{N}\underline{H} \tag{6}$$

is independent of frequency and of μ_r, being proportional to H. The lower frequency of the sensor is limited by f_{cr}:

$$f_{min} \gg f_{cr}. \tag{7}$$

When the coil is loaded by a differential current amplifier, (7) becomes:

$$2\pi f_{min} L_S \gg R_S. \tag{8}$$

From (2) and (8) a new expression for the lower limit is obtained:

$$f_{min} \gg \frac{2\rho_{Cu}}{\pi\mu_0 S_{Cu}} \cdot \frac{l\beta^{2/5}}{\mu_r N D}. \tag{9}$$

For a given core, the decrease of f_{min} may be obtained increasing N.

It is known that the high-frequency limitation tends to be related to the transit times on the coil:

$$f_{max} \ll \frac{c}{\pi D N}, \tag{10}$$

where c is the speed of light.

The proposed instrument (Fig. 2) is realized by three mutually perpendicular coils, connected each to a differential current amplifier. The immunity of the sensor to the electric field and a good common mode rejection can be achieved by shielding and balancing the configuration [10]. In order to eliminate the errors due to the spatial distribution of the field, the dimensions of the sensor have to be small [11].

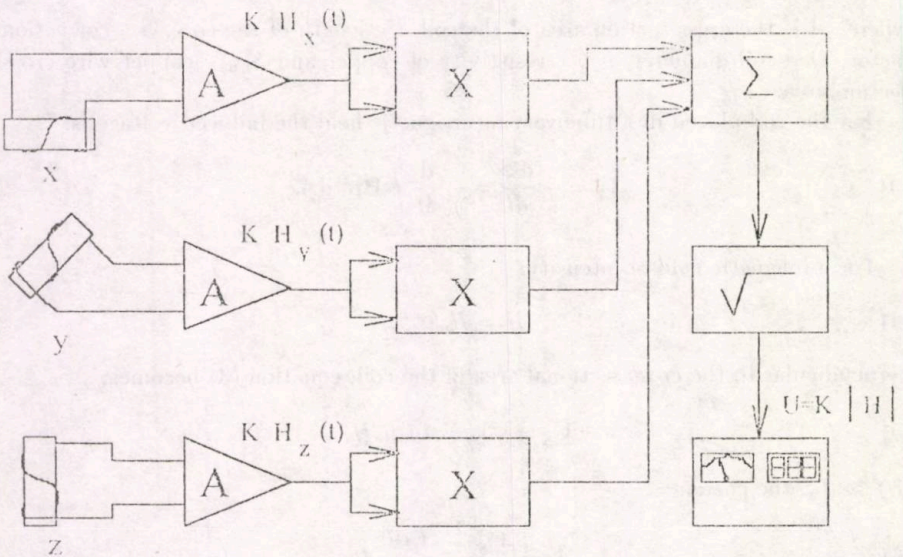

Fig. 2.– The simplified block diagram of the instrument.

Each sensor has $L_S = 65$ mH and $R_S = 10.2\ \Omega$. Therefore, the critical frequency is 25 Hz. The sensor can be used to measure magnetic fields above 35 μA/m and its sensitivity is about 30 V/A m^{-1}.

The output voltages obtained from the three differential current amplifiers are multiplied, added and the RMS value (H) of the magnetic field strength is obtained with a circuit of extraction of the square root:

$$U = KH = K\sqrt{H_x^2 + H_y^2 + H_z^2}, \tag{11}$$

where K is a constant and H_x, H_y, H_z are the magnetic field components.

3. Conclusions

A triaxis magnetic field meter of great sensitivity, that covers alone a frequency range from 40 Hz to more than 100 kHz, is proposed.

The instrument is recommended for the measurement of the perturbative fields that can have dangerous effects on the biological tissues. It can be also used for characterizing the environment or a source from the magnetic point of view.

Received, July 25, 1997

Technical University "Gh. Asachi", Jassy,
Department of Electrical
Measures and Materials

REFERENCES

1. Sienkiewicz Z., *Biological Effects of Electromagnetic Fields and Radiation.* Proc. IEE Internat. Conf. on EMC, York, UK, 1994, 17-21.

2. K a u d a M., D r i v e r L.D., *An Isotropic Electric-Field Probe with Tapered Resistive Dipoles for Broad-Band Use, 100 kHz to 18 GHz*. IEEE Trans. on Microwave Theory and Techniques, **MTT-35**, 2, 126-130 (1987).
3. B a u m a n n J., *Long-term Survey of the Background Electromagnetic Environment in Switzerland*. 10th Internat. Zürich Symp. and Techn. Exhib. on EMC, March 9-11, 1993, 1-4.
4. A r s e n e a u R., Z e l l e J.J., *A Tri-axis Electromagnetic Field Meter*. IEEE Trans. on Instrumentations and Measurement, **39**, 1, 23-26 (1990).
5. W a h l P., K r o n S., *MPR2 and Related E- and H-Field Measurements*. Proc. of the 1994 EMC/ESD Int'l Conf., Anaheim, California, USA, 73-75.
6. D a v i d V., A n t o n i u M., V r e m e r ă E., *A Triaxis Broadband Magnetic Field Meter*. IEEE Digest, Conference on Precision Electromagnetic Measurements (CPEM 1996), Braunschweig, Germany, June 17-20, 1996, 433-434.
7. B a u m C.E., *Fast Electrical and Optical Measuremants*. Vol.I, Dordrecht, The Netherlands, Martinus Nijhoff Publishers, 1986, 73-144.
8. S t u c h l y M.A., L e P o n c h e r H., G i b b o n s D.T., T h a n s a n d o t e A., *Active Magnetic Field Sensor for Measurements of Transients*. IEEE Trans. on Electromagnetic Compatibility, **33**, 4, 275-280 (1991).
9. L u k o s c h u s D.G., *Optimization Theory for Induction-Coil Magnetometers at Higher Frequencies*. IEEE Trans. on Geoscience Electronics, **GE-17**, 3, 56-63 (1979).
10. H a u s e r J.P., *A 20 Hz to 200 kHz Magnetic Flux Probe for EMI Surveys*. IEEE Trans. on EMC, **32**, 1 (1990).
11. M i s a k i a n M., F e n i m o r e C., *Distributions of Measurement Error for Three-Axis Magnetic Field Meter During Measurements Near Appliances*. IEEE Trans. on Instr. and Measurement, **45**, 1, 244-249 (1996).

UN MĂSURĂTOR TRIAXIAL DE BANDĂ LARGĂ AL CÂMPULUI MAGNETIC CU APLICAŢII BIOMEDICALE

(Rezumat)

Se prezintă un măsurător de camp magnetic avand o caracteristică de directivitate izotropică, fiind indicat pentru măsurarea campurilor electromagnetice perturbatoare ce pot avea efecte nocive asupra sistemelor biologice.

Instrumentul este caracterizat printr-o mare sensibilitate şi are un domeniu de frecvenţă cuprins intre 40 Hz şi mai mult decat 100 kHz.

BULETINUL INSTITUTULUI POLITEHNIC DIN IAŞI
Tomul XLIV (XLVIII), Fasc. 1–2, 1998
Secţia III
ELECTROTEHNICĂ. ENERGETICĂ. ELECTRONICĂ

D.C. 621.313.17

ON THE TRANSDUCERS USED IN D.C. MOTORS WITH STATIC SWITCHING

BY

I. SUCHAR

Some results concerning the study of the series ferroresonant circuit with orthogonally driven nonlinear coil placed in the field of a moving permanent magnet are studied. Using these results a ferroresonant transducer for the position of the rotor of a d.c. motor with static switching [18], is proposed.

1. Introduction

The collector–brushes assembly of a d.c. motor is responsible for determining the relative position of the axes of the magnetic fields produced by the rotor and for the switching of the current in the induced winding.

The existence of the collector and the brushes is a major constraint to the fields of utilization of the d.c. motors because the need of permanent servicing and the lack of reliability, especially in wet atmosphere and chemically aggressive or dusty environments. The sparks which may appear during switching lead to R.F. interference, limit the speed and make impossible the use of d.c. motors in environments with great risk of explosion.

By replacing the traditional collector–brushes assembly with a solid-state commutation system, a d.c. motor "without collector" is obtained [3], [4], [10], [11], also known as "contactless" d.c. motor [7], [15], "brushless" d.c. motor [9], [16], [22], d.c. motor with electronic switching [8], [13], [14], or d.c. motor with solid-state commutation [2], [17], [20].

In a d.c. motor with solid-state commutation there are gathered the advantages of the a.c. brushless motors (simplicity, robustness and high reliability in long term functioning) with the ones of the classical d.c. motors (smooth tuning in a wide range of the speed and strong starting torque).

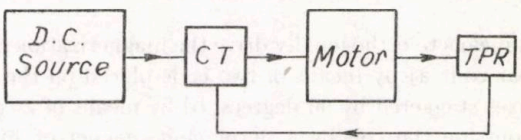

Fig. 1

The block diagram of a d.c. motor is given in Fig. 1. The main differences compared to a d.c. motor with collector and brushes are the followings: a) the induced winding is placed on the stator and is build in the same manner as a polyphased symmetrical winding, the rotor being a permanent magnet with the role of the inductor; b) the switching of the current in the induced winding is made without contacts (solid-state commutation), using a solid-state switch; c) the moments when the solid-state commutation is made are determined by a transducer of the position of the rotor.

2. Technical Solutions for the Transducers of the Position of the Rotor

The role of the transducer is to sense the position of the axis of the magnetic field of the rotating inductor towards the axis of the magnetic field of the stator and to deliver that information as an electrical signal to the input of the switch to unlock it when necessary, in order to drive only those sections of the induced winding which successively take part in producing the electromagnetic torque in the same direction.

The transducer has to meet the following specifications [20]: a) the generated signal must depend only on the position of the rotor and not on the speed and the direction of rotation; b) must be contactless; c) the increasing and decreasing slope of the signal must be steep in order to provide a reliable and economical functioning of the electronic switch; d) the ratio between the maximum signal and the residual one from the output of the transducer must be at least 3; e) the energy used by the transducer must not be greater than the mechanical loses caused by the collector–brushes assembly and the electrical one caused by the contact resistance of the brushes which take place in the equivalent d.c. motors; f) the size of the transducer must not be greater than the size of the collector–brushes assembly; g) must allow easy tuning with the input of the switch; h) the specifications and the reliability must not be discredited by the environmental conditions.

There are several d.c. motors with solid-state commutation equipped with position transducers which use the light [7], [9], [3], [13], the energy of the electric field [7], [21], the energy of the magnetic field [5], [7], [11], [14], [15] or radioactive energy [21].

The advantages and the drawbacks of these transducers are shown in [20].

So, there is a large range of possibilities to choose the transducer type. Choosing the right transducer must take into account the specifications of the motor, the availability of the components and the skill of the designer.

3. On Orthogonally Driven Nonlinear Coils

There are two means to orthogonally drive the magnetization of the ferromagnetic core of a nonlinear coil: a) by means of two coils placed on the ferromagnetic core which have the axes staggered by 90 degrees; b) by means of a continuous magnetic field, generated outside the coil by a permanent magnet or by an electromagnet

powered by d.c. current.

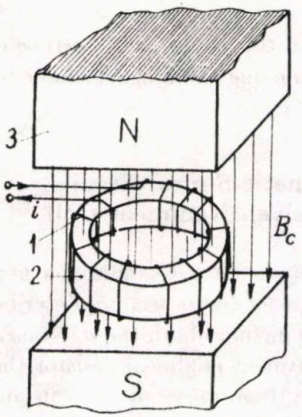

Fig. 2

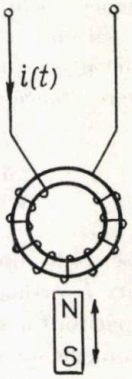

Fig. 3

In Fig. 2, the orthogonal magnetization is achieved by exciting the nonlinear coil *1* in the drive field between the poles N-S of the magnet *3*, so that the plane of the core *2* to be perpendicular on the direction of the magnetic induction lines B_c.

An alternative to this procedure of orthogonal magnetization is given in Fig. 3, where the permanent magnet rotates towards the fixed nonlinear coil.

In Fig. 4 a family of characteristics of magnetization $B(H)_{B_c=\text{const.}}$, for an isotropic ferromagnetic core made of cold laminated steel [6], is represented. It was magnetized in orthogonal field by means of the procedure shown in Fig. 2.

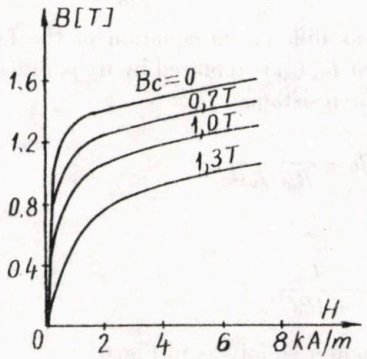

Fig. 4

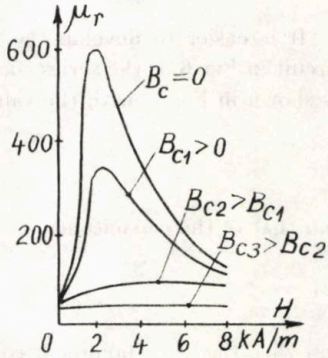

Fig. 5

It can be seen that when the induction (B_c) of the orthogonal driving rises simultaneously with the liniarization process of the magnetization characteristics, the ferromagnetic material saturates itself at progressively lower values of the induction B of the resultant field.

As B_c rises, a decrease of the relative magnetic permeability takes place and the trace of $\mu_r(H)_{B_c=\text{const.}}$ becomes more linear. From a certain value of the induction

of the orthogonal field, the permeability μ_f does not depend of the intensity of the main magnetic field H any more (Fig. 5).

It is well understood that if we refer to the procedure of orthogonal driving of the nonlinear coil presented in Fig. 3, by moving the magnet closer to the coil, the inductive reactance decreases.

4. On the Ferromagnetic Series Circuit with Orthogonally Driven Nonlinear Coil

The series ferroresonant circuit presented in Fig. 6 contains a nonlinear coil of inductivity L, orthogonally driven by means of the procedure described in Fig. 3, a linear capacitor C_0 and a resistor R_0 which includes both the resistance of the coil, a linear supplementary resistor and the equivalent nonlinear resistor that models the losses in the ferromagnetic core. Because these losses are less in an orthogonally driven nonlinear coil than in the same coil without the drive [1], in what follows is considered that the resistor R_0 is linear as a whole.

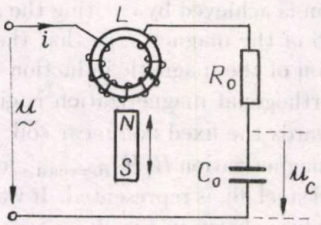

Fig. 6

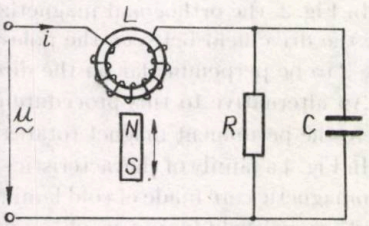

Fig. 7

It is easier to develop the nonlinear differential equation of the ferroresonant circuit in Fig. 6, if the series conexion of R_0-C_0 is replaced by its parallel equivalent, as shown in Fig. 7, with the value of the resistance

$$R = R_0 + \frac{1}{R_0 C_0^2 \omega^2} \tag{1}$$

and that of the capacitance

$$C = \frac{C_0}{1 + R_0^2 C_0^2 \omega^2}, \tag{2}$$

and with the same nonlinear coil and power supply as in Fig. 6.

The magnetization characteristic of the undriven nonlinear coil (drawn in Fig. 4 for $B_0 = 0$) can be approximated in a satisfactory manner by means of a third degree polynomial:

$$i = a_1 \Psi + a_3 \Psi^3, \tag{3}$$

where a_1, $[H^{-1}]$, and a_3, $[H^{-1}Wb^{-2}]$, are positive coefficients which depend on the magnetic properties of the used ferromagnetic core.

As in [12], the analytic expression of the magnetization characteristic of an orthogonally driven nonlinear coil can be obtained multiplying the coefficients a_1 and a_3 in (3) by a factor $b > 1$:

$$i = b_1\Psi + b_1 b_3 \Psi^3, \tag{4}$$

where

$$b_1 = a_1 b, \qquad b_3 = \frac{a_3}{a_1}. \tag{5}$$

For the circuit in Fig. 7, powered by the sinusoidal voltage $u = \sqrt{2}\,U \sin \omega t$, the following differential equation of Duffing type can be obtained:

$$\frac{\mathrm{d}^2 a}{\mathrm{d}^2 \tau^2} + k_1 \frac{\mathrm{d}a}{\mathrm{d}\tau} + \frac{1}{\lambda} a + \frac{k_2}{\lambda} a^3 = \sin \tau, \tag{6}$$

where

$$a = \frac{\Psi}{\Psi_n}, \tag{7}$$

with

$$\Psi_n = \frac{\sqrt{2}\,U\sqrt{1 + R^2 C^2 \omega^2}}{RC\omega^2}, \tag{8}$$

$$\lambda = \frac{C\omega^2}{b_1} = LC\omega^2. \tag{9}$$

– the normed inductivity of the magnetized coil,

$$L = \frac{1}{b_1} = \frac{\Psi}{i} \tag{10}$$

– the linear inductivity of the orthogonal magnetized coil which depends on the inclination of the characteristic of magnetization in the origin of the axes, and

$$k_1 = \frac{1}{RC\omega} = \frac{1}{R_0 C_0 \omega}, \tag{11}$$

$$k_2 = b_3 \Psi_n^2, \tag{12}$$

$$\tau = \omega t + \varphi. \tag{13}$$

Supposing that the higher harmonics are negligible for the fundamental term of the forced response we have the solution:

$$a = A\cos(\tau + \gamma), \tag{14}$$

which, replaced in (6), leads to the following equation of the family of resonance characteristics:

$$A^2 \left[k_1^2 + \left(\frac{3}{4} \cdot \frac{k_2}{\lambda} A^2 + \frac{1}{\lambda} - 1 \right)^2 \right] = 1. \tag{15}$$

Solving the last equation with respect to λ, we get:

$$\lambda = \frac{\frac{3}{4}k_2A^2 + 1}{1 \pm \sqrt{\frac{1}{A^2} - k_1^2}}. \tag{16}$$

In order to be able to draw the graph $F(\lambda, A)$, defined by (15), we can observe that, according to the implicit functions theory, we have:

$$\frac{dA}{d\lambda} = -\frac{\partial F/\partial \lambda}{\partial F/\partial A}, \tag{17}$$

so that the maximum value of the parameter A can be obtained from equation:

$$\frac{\frac{2}{\lambda^2}\left(\frac{3}{4}k_2A^2 + 1\right)\left(\frac{\frac{3}{4}k_2A^2 + 1}{\lambda} - 1\right)}{\frac{3k_2}{\lambda}\left(\frac{\frac{3}{4}k_2A^2 + 1}{\lambda} - 1\right) + \frac{2}{A^3}} = 0, \tag{18}$$

which represents the condition to have $dA/d\lambda = 0$, in fact $\partial F/\partial \lambda = 0$.

Solving (18) we get:

$$\lambda_{max} = \frac{3}{4}k_2A^2 + 1; \qquad A_{max} = \pm\frac{1}{k_1}. \tag{19}$$

Because $k_1 > 0$, and taking into account (11), we choose the positive value for A.

It is well known that the ferroresonant circuits have a "contactless relay-type" characteristic. To get the two distinct values for which the characteristic has two vertical tangents describing the ferroresonant jumps we must fulfill the equality

$$\frac{\partial F}{\partial A} = 0, \tag{20}$$

which means:

$$\frac{\lambda^2}{A^4} + \left(\frac{3}{2}k_2 - 1\right)\lambda + \frac{3}{2}k_2\left(\frac{3}{4}k_2A^2 + 1\right) = 0. \tag{21}$$

The last equation has two real and distinct roots if the discriminant is positive namely:

$$3k_2\left(\frac{3}{4}k_2 - 1 - \frac{2}{A^4} - \frac{3}{2}\cdot\frac{k_2}{A^2}\right) > 0. \tag{22}$$

Considering (22) an inequation in A^2 and solving it leads to the following condition:

$$\sqrt{1 + \sqrt{1 + \frac{9}{k_2}}} < A < \frac{1}{k_1}. \tag{23}$$

Another constraint for A can be obtained observing the fact that when $\lambda \to \infty$,

$$A \to \frac{1}{\sqrt{k_1^2 + 1}}. \tag{24}$$

The inequality (23) gives us the opportunity to individualize the useful range of values for the parameters R, L, C and ω of the ferroresonant circuit.

5. The Ferroresonant Jump Drives the Solid-State Commutation

The property of the series ferroresonant circuit with nonlinear coil having two stable values of the current – one with small amplitude and the other with high amplitude – is the main ideea of the ferroresonant transducer of the position of the rotor of a d.c. motor with solid-state commutation which will be studied in what follows.

In the transducer, made of one rotating and one fixed part, the jumps of the current are caused by the variation of the inductivity of the nonlinear coil by means of orthogonal drive, according to the procedure presented in Fig. 6.

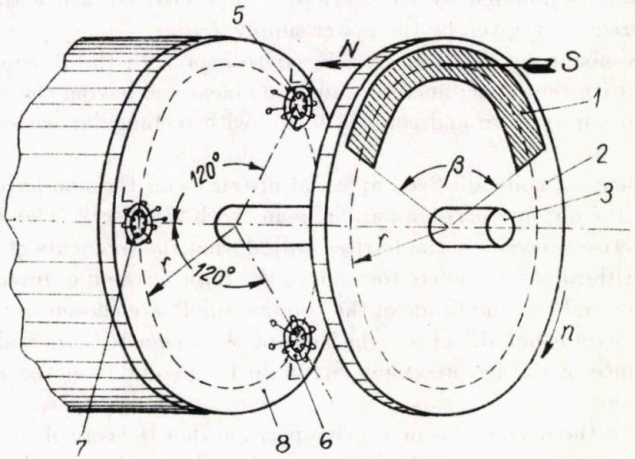

Fig. 8

According to Figs. 8 and 9 the rotating part is made of a bipolar magnet *1*, with the shape of a sector of circular ring with medium radius r and the center angle $\beta = 120°$, which will be named in what follows the angle of the sector of the signal. The magnet *1*, with the North pole on a plane and the South pole on the other plane, parallel with the first, is included in the disc *2* (which is not ferromagnetic), fixed on the shaft *3* of the rotor of the d.c. motor.

The angle ρ between the axes of the magnetic poles of the bipolar inductor of the d.c. motor and the axis of symmetry in the radial direction of the magnet *1* (which in fact is the same with the bisectrix of the angle β) is invariable during the functioning of the d.c. motor.

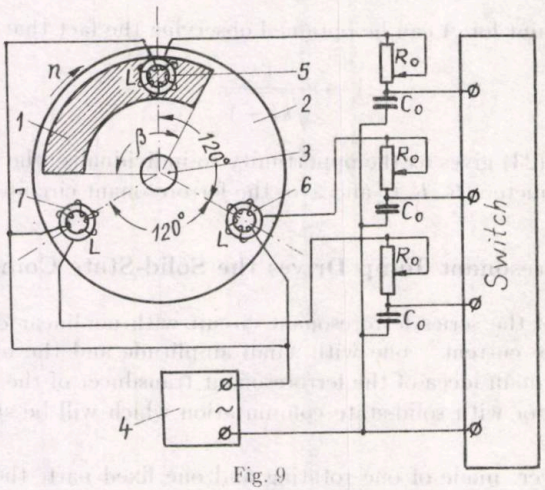

Fig. 9

The fixed part of the ferroresonant transducer is made from three identical series ferroresonant circuits powered by an alternative sinusoidal voltage with constant amplitude and frequency, given by the power supply *4*.

Every ferroresonant circuit contains a linear resistor with the resistance R_0, a linear capacitor with the capacitance C_0 and a nonlinear coil having the inductivity L, made without gap on torroidal cores of ferrite with rectangular hysteresis loop, [5],...,[7].

The three identical coils are fixed at equal distances on the non-ferromagnetic frontal shield of the d.c. motor, on a parallel plane with the disc *2*. The field of the magnet *1* magnetize succesively the ferrites only during the moments of time that corresponds to a third of a complete rotation of the rotor of the d.c. motor.

The frequency and the amplitude of the volatge supply are chosen so that, when the nonlinear coils are not driven by the field of the magnet *1*, the value of the inductive reactance of the ferroresonant circuit to be greater than the one of the capacitive reactance.

Supposing that the magnet *1* is in a such a position that the core of the nonlinear coil is not premagnetized, the normed inductivity has the maximum value:

$$\lambda_0 = L_0 C_0 \omega^2, \tag{25}$$

where

$$L_0 = \frac{1}{a_1} \tag{26}$$

represents the maximum linear inductivity of the coil in the absence of the drive field. In this situation the amplitude of the voltage drop on the capacitor C_0 has a small value

(27) $$U_1 = U - \frac{1}{\sqrt{k_1^2 + 1}},$$

determined by the minimum current flowing through the circuit, in the absence of the ferroresonance.

As long as $\lambda \in [\lambda_0, \lambda_{V_1}]$, when the magnet closes to the nonlinear coil, a small premagnetisation of the core of that coil occurs, when the stable functioning points of that ferroresonant circuit are placed on the branch *I* of the $U_c(\lambda)$ "relay-type characteristic" presented in Fig. 10, where λ_{V_1} and λ_{V_2} are the normed inductivities in the points for which the function $U_c(\lambda)$ has vertical tangents.

When the magnet is close enough to the nonlinear coil, so that $\lambda < \lambda_{V_1}$, the ferroresonant jump of the amplitude of U_c occurs, at a value $U_2 = U + k_1^{-1}$, greater than the previous one and the functioning point of the circuit is on the stable branch *II* of the characteristic. The voltage drop on the capacitor is hold at a high value as long as $\lambda \in [\lambda_{V_1}, \lambda_{V_2}]$.

If the magnet has been rotated with such an angle that $\lambda > \lambda_{V_2}$, a new jump of the amplitude of U_c from the high value to the lower one, corresponding to the branch *I* of the characteristic in Fig. 10, occurs.

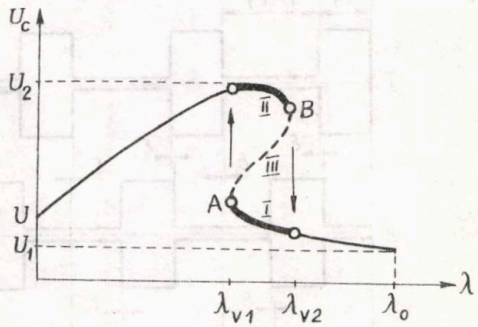

Fig. 10

The functioning of the ferroresonant circuit on the branch *III* of the $U_c(\lambda)$ characteristic is unstable and therefore there is no interest to study it.

The amplitude jumps of U_c depend on the position of the rotating magnet of the ferroresonant transducer relative to the fixed nonlinear coil and can be used to drive the current in the sections of the winding of the d.c. motor with solid-state commutation.

We must point out that the use of the ferroresonant transducer for the solid-state commutation is justified only if in the range of variation of the λ parameter the amplitude jumps of the voltage U_c take place in both ways, or, in other words, if the function $U_c(\lambda)$ has two vertical tangents in two distinct points (*A* and *B* – Fig. 10), where the stable branches are continued by the instable branch *III*.

The existence of the jumps of I in both ways is assured if the following conditions are simultaneously fulfilled:

$$\lambda_0 \geq \lambda_{V_2}, \tag{28}$$

$$\omega > \frac{1}{\sqrt{\frac{L_V C_0}{1 + R_0^2 C_0^2 \omega^2}}}, \tag{29}$$

$$R_0 + \frac{1}{R_0 C_0^2 \omega^2} \geq \left| \frac{\sqrt{3}}{\frac{1}{\omega L_V} - \frac{C_0 \omega}{1 + R_0 C_0^2 \omega^2}} \right|, \tag{30}$$

where L_V is the value of the inductivity of the orthogonally premagnetized coil, in the moment of the ferroresonant jump from the low amplitude current to the high one.

The voltage drops $u_c(t)$ of the capacitors C_0 (Fig. 9), which are the drive signals of the solid-state commutation, are rectangular pulses, represented in Fig. 11 with low and high values according to the values of the currents in the three ferroresonant states (I, II, III).

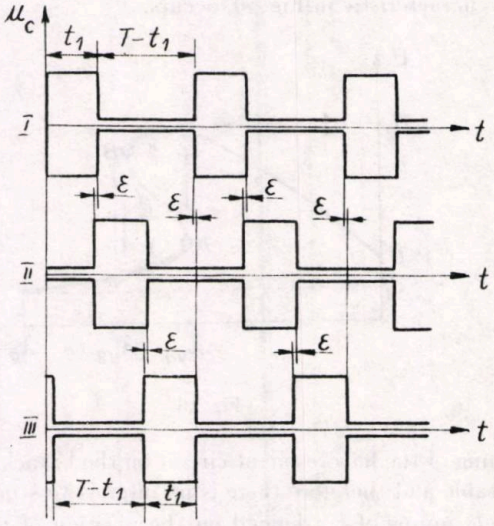

Fig. 11

The experimental results have shown that the duration of each pulse, t_1, is determined by β, the angular dimension of the sector of the signal and by the value of R_0.

We used the ferroresonant transducer for the the solid-state commutation of a d.c. motor described in [18].

The optimum value of the angle of the sector of the signal for the moments when the d.c. motor has zero torque can be computed with the formula [20]:

(31) $$\beta = \frac{2\pi}{pN_s},$$

where p is the number of the pairs of the poles of the d.c. motor, and N_s – the number of the sections of the induced winding.

The oscillograms in Figs. 12 and 13 present the shape of the drive signals of the studied transducer, when $\beta > 120°$ and respectively when $\beta = 120°$.

The experimental results have shown that for the d.c. motor in [18] it is advantageous to have a small overlapping, ε (s. Fig. 11), between two successive pulses as in the case of a combustion engine, when it is necessary to have an advance angle when firing.

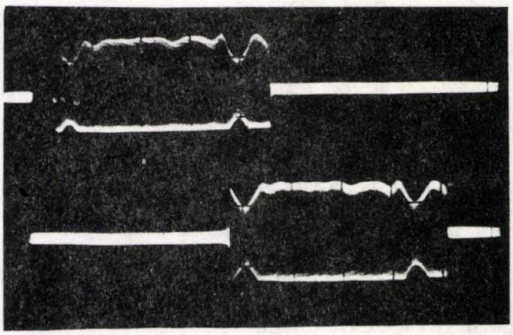

Fig. 12

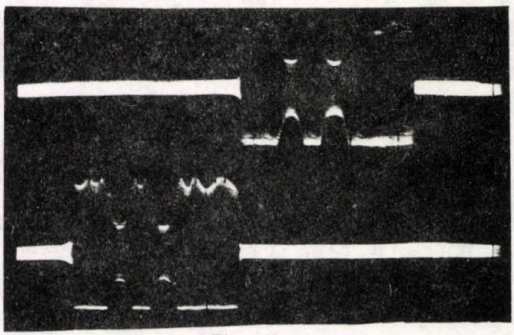

Fig. 13

The main advantages of the ferroresonant transducer of the position of the rotor are: a) absence of the contacts; b) ensuring a start torque; c) robustness and simplicity; d) is reliable in harsh environments; e) a low power consumption; f) the drive signals are steep and therefore the commutation is reliable and economical; g) the ratio between the amplitude of the maximum signal and the amplitude of the minimum signal is greater than the one of the other known position transducers and therefore there is no need for supplementary amplifiers.

Among disadvantages there are the following: a) the need of an oscillator with a frequency of tens of kHz and small output impedance to power the ferroresonant circuits; b) the rotating part increases the resistant torque of the d.c. motor; c) the need for equilibration of the rotating part of the transducer, because the mass of the magnet for the orthogonal driving of the nonlinear coils is different than the one of the nonmagnetic disc that holds the magnet.

The first disadvantages is common to all the inductive or capacitive transducers for position described in literature and the second disadvantage may become sometimes an advantage (e.g. for the mechanisms used in the sound technique).

Received, May 7, 1997

Technical University "Gh. Asachi", Jassy,
Department of General Electrotechnics
and Electrical Machines

REFERENCES

1. Angel Y., *Commande magnétique orthogonale des systèmes paramétriques.* Acta electronica, **4**, *3*, 359-380 (1960).
2. Bauerlein G., *A Brushless D.C. Motor with Solid-state Commutation.* I.R.E. Internat. Convention. Record, part VI, 1962, 184-190.
3. Bergtold F., *Neuer Gleichstrom - Kleinstmotor ohne Kollektor.* Funkschau, *17*, 470-474 (1965).
4. Cuesta A., *Motors auto-regulados sin colector.* Rev. Española de Electrónica, **17**, *188*, 70-71 (1970).
5. Dittrich W., Rainer E., *Electronikmotor DMc 3, ein neuer Kolektorloser Gleichstrom-Kleinstmotor.* Siemens- Ztschr., **40**, *9*, 690-693 (1966).
6. Dorožko L.I., Libkind M.S., *Reaktory s poperečnym podmagničivaniem.* Izd. Energia, Moskva, 1977.
7. Dubenski A.A., *Beskontaktnye dvigateli postoiannovo toka.* Izd. Energia, Moskva, 1967.
8. Favre R., *Les moteurs à commutation électronique.* Schweiz. Techn. Ztschr., *22/23*, 465-467 (1964).
9. Fink R.A., *The Brushless D.C. Motor: Link to System Versatility.* Control Eng., **17**, *6*, 75-78 (1970).
10. Grancoin B., *Moteurs à courant continu sans collecteur, à effet Hall.* Electronique Industrielle, *119*, 821-824 (1968).
11. Kröger G., *Kollektorlose Gleichstrommotoren.* Arch. für techn. Messen, *387*, Z 562-1, 79-82 (1968).
12. Lüder E., *Ein kontaktloser Schalter mit Hilfe des Ferroresonanzkreises.* ETZ-A, **90**, *7*, 158-161 (1969).
13. Mazda F.F., *Electronic Commutation for Small Motors.* Electrical Times, **160**, *12*, 45-49 (1971).
14. Moczala H., *Gleichstrom-Kleinstmotoren mit electronischer Kommutierung.* A.E.G.-Mitt., **55**, *2*, 1965, 114-117.
15. Ovčinnikov I.E., Lebedev N.I., *Beskontaktnye dvigateli postoiannogo toka avtomatičeskikh ustroistv.* Izd. „Nauka", Moskva–Leningrad, 1966.
16. Smith Ch.S., *Brushless D.C. Motors.* Electromechanical Design, **11**, *10*, 48-50 (1967).
17. Suchar I., Creţu A., *Traductor pentru comanda comutaţiei statice.* Patent Romania, *54720* (1971).
18. Suchar I., Creţu A., *Electromotor de curent continuu cu comutaţie statică.* Patent Romania, *74350* (1980).
19. Tasić B., Iliśković A., Tovarlazǎ D., *Fotoelektronisch gesteuerter Kollektorloser Gleichstrommotor.* Elektronik, *4*, 105-108 (1969).
20. Vasiliu Gh., Suchar I., Şerban Gh., *Micromotoare de curent continuu cu comutaţie statică.* Ed. Tehnică, Bucureşti, 1976.
21. Wilson T.G., Trickey P.H., *D.C. Machine with Solid-State Commutation.* Elect. Eng., **81**, *11*, 879-884 (1962).
22. Yates W.W., *Brushless D.C. Motors.* Machine Design, **38**, *5*, 136-142 (1966).

ASUPRA TRADUCTOARELOR FOLOSITE LA MOTOARELE DE CURENT CONTINUU CU COMUTAŢIE STATICĂ

(Rezumat)

Sunt expuse unele rezultate obţinute în studiul circuitului ferorezonant serie cu bobină neliniară comandată ortogonal de campul unui magnet care se deplasează în raport cu bobina neliniară imobilă. Utilizand aceste rezultate se studiază un traductor ferorezonant de poziţie a rotorului pentru comanda unui motor magnetoelectric cu comutaţie statică [18].

BULETINUL INSTITUTULUI POLITEHNIC DIN IAŞI
Tomul XLIV (XLVIII), Fasc. 1–2, 1998
Secţia III
ELECTROTEHNICĂ. ENERGETICĂ. ELECTRONICĂ

D.C. 621.313.333.021.2

ON TWO-PHASE SQUIRREL CAGE INDUCTION MACHINE WORKING, DRIVEN BY A PULSE WIDTH MODULATED CONVERTER AND SINUSOIDAL VOLTAGE

BY

EMIL-COSTEL TEODORU and MIRCEA GOGU

The rotational voltage influence on the phase current waveform, when a two-phase induction motor is fed in a particular way: one phase by a sinusoidal voltage and another by a PM converter is studied.

Statoric windings are orthogonal in space. Apparently, the electromagnetical interaction between them does not exists. In reality, these windings, fed by a two-phase sinusoidal voltages system, become the rotation induction voltages area, produced by the rotor motion.

The rotation induction voltage amplitude are linear dependent on rotor speed and excitation applied voltage, considering a given machine. Compounding the two stator winding voltages (excitation voltage and rotation induction voltage), a sinewave voltage results. So, the phase winding currents are also sinewave ones. Given the sinewave form of the phase voltages and the phase currents, the rotation induction voltage presence effects are not very conspicuous.

When the two-phase induction machine is fed by a two-phase pulse width modulated (PWM) converter, the phase rotation induction voltage and the PWM phase excitation voltage affect the phase current waveform. The phase current waveform becomes non-sinusoidal.

This phenomenon was clean-cut shown by several software simulations and practical experiments. The obtained results lead us to create an amelioration phase current waveform method, in order to decrease the high torque harmonics amplitude relatively to the fundamental torque harmonic.

1. Introduction

Let us consider a two-phase squirrel-cage induction motor with two identical windings, orthogonaly disposed in space, with the following respective winding functions:

$$w_a(\theta) = w_s \cos\theta, \qquad w_b(\theta) = w_s \cos\left(\theta - \frac{\pi}{2}\right). \tag{1}$$

Fig. 1 shows the fundamental two-phase squirrel-cage induction motor. When $u_a(t)$ and $u_b(t)$ sinewave voltages are applied (Fig. 1 *a*), a turning magnetic field occurs. In the same way a three phase symmetrical voltages system applied determines in a three-phase induction machine a turning magnetic field. The rotor speed

becomes n, nearly the synchronism speed. The rotor is fixed and the a winding is supplied from $u_a(t)$ voltage (Fig. 1 b) the alternating flux Φ_a determine a transformer voltage in rotor conductors and then the rotor currents appear. However the electromagnetic torque is zero. A winding rotor reaction flux Φ_y, along the supplied winding axis, appears. This flux is orthogonal on b winding axis, so the induction voltage does not exists. When the machine is started (like any single-phase motor) Φ_a flux produces a rotation voltage in addition to the fixed rotor transformer voltage.

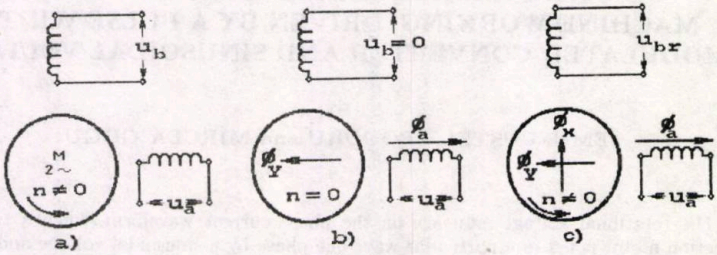

Fig. 1

The rotation voltage rotor currents create in b winding axis the Φ_x flux. This flux determines an induction voltage in b winding. The u_{br} voltage (at b winding terminals) is proportional to speed n in amplitude, and constant frequency (u_a voltage frequency equals), (Fig. 1 c).

The phase difference between u_{br} and u_a is 90° el. degr. An analogous reasoning may be done when b winding is supplied only.

Fig. 2 represents the instantaneous supply and rotation voltages values. In the same figure one can see a two-phase induction motor scheme, where the squirrel-cage rotor winding is equivalent to two orthogonal windings. The winding repartition functions are:

$$w_x(\theta) = w_r \cos(\theta - \theta_r), \qquad w_y(\theta) = w_r \sin(\theta - \theta_r). \tag{2}$$

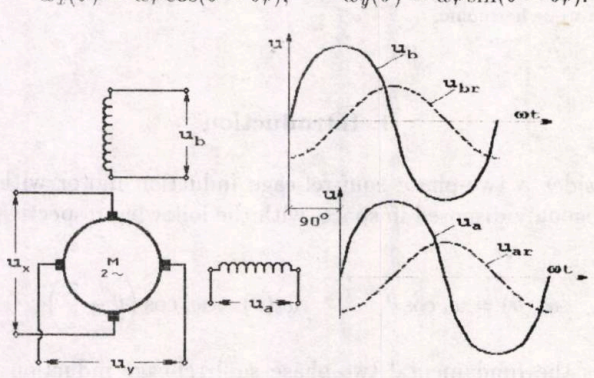

Fig. 2

Compounding the supply and rotation voltages, there are sinewave voltages who results. But the resulting voltage amplitude is different. The rotation induction

voltage influence can't be observed, because the currents amplitude and the phase difference between currents and resulting voltages are identically modified in both windings.

2. Two-phase Induction Motor Fed by a PWM Converter and Sinusoidal Voltage Experimental Results

When the two-phase induction machine is fed by a PWM converter (Fig. 3), the phase current wave-forms become non-sinusoidal. These wave-forms are offered by u_a and u_b excitation voltages and rotation induction voltage amplitudes. In this case, Fourier series are used to analyze the voltage and currents waveforms, studying separately the voltages and currents harmonics [8]. The induction machine working is described by following equation:

$$[u] = [R][i] + \mathrm{d}([L][i]). \tag{3}$$

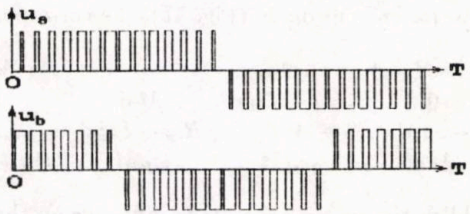

Fig. 3

During the two-phase squirrel-cage induction motor fed by PWM converter work, the converter construction-type determine four different acting situations (Figs. 4 and 5). For the first one, when pulses of the PWM voltage are present at the both stator windings terminals (Fig. 4 *a*), the instantaneous value equations are:

$$\begin{bmatrix} u_a \\ u_b \\ 0 \\ 0 \end{bmatrix} = \begin{bmatrix} R_{sa} + L_{sa}\,\mathrm{d} & 0 & 0 & M\,\mathrm{d} \\ 0 & R_{sb} + L_{sb}\,\mathrm{d} & M\,\mathrm{d} & 0 \\ -\omega_R M & M\,\mathrm{d} & R_{rx} + L_{rx}\,\mathrm{d} & -\omega_R M \\ M\,\mathrm{d} & \omega_R M & \omega_R M & R_{ry} + L_{ry}\,\mathrm{d} \end{bmatrix} \begin{bmatrix} i_a \\ i_b \\ i_x \\ i_y \end{bmatrix}, \tag{4}$$

where ω_R represents the real rotor speed.

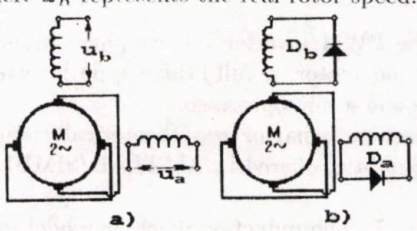

Fig. 4

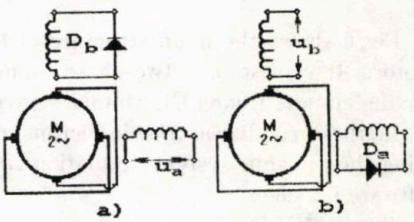

Fig. 5

For the second situation, when the inverse current diodes shunt stator winding terminals (Fig. 4 *b*), the equations are:

$$(5)\qquad \begin{bmatrix}0\\0\\0\\0\end{bmatrix}=\begin{bmatrix}R_{sa}+L_{sa}\,\mathrm{d} & 0 & 0 & M\,\mathrm{d}\\ 0 & R_{sb}+L_{sb}\,\mathrm{d} & M\,\mathrm{d} & 0\\ -\omega_R M & M\,\mathrm{d} & R_{rx}+L_{rx}\,\mathrm{d} & -\omega_R M\\ M\,\mathrm{d} & \omega_R M & \omega_R M & R_{ry}+L_{ry}\,\mathrm{d}\end{bmatrix}\begin{bmatrix}i_a\\i_b\\i_x\\i_y\end{bmatrix}.$$

When *a* stator winding is fed by the PWM voltage pulse and *b* stator winding is shunted by the inverse current diode (Fig. 5 *a*), one can write:

$$(6)\qquad \begin{bmatrix}u_a\\0\\0\\0\end{bmatrix}=\begin{bmatrix}R_{sa}+L_{sa}\,\mathrm{d} & 0 & 0 & M\,\mathrm{d}\\ 0 & R_{sb}+L_{sb}\,\mathrm{d} & M\,\mathrm{d} & 0\\ -\omega_R M & M\,\mathrm{d} & R_{rx}+L_{rx}\,\mathrm{d} & -\omega_R M\\ M\,\mathrm{d} & \omega_R M & \omega_R M & R_{ry}+L_{ry}\,\mathrm{d}\end{bmatrix}\begin{bmatrix}i_a\\i_b\\i_x\\i_y\end{bmatrix}.$$

At last, when *b* stator winding is fed by PWM voltage pulse and *a* stator winding is shunted by the inverse current diode (Fig. 5 *b*), the corresponding equations are:

$$(7)\qquad \begin{bmatrix}0\\u_b\\0\\0\end{bmatrix}=\begin{bmatrix}R_{sa}+L_{sa}\,\mathrm{d} & 0 & 0 & M\,\mathrm{d}\\ 0 & R_{sb}+L_{sb}\,\mathrm{d} & M\,\mathrm{d} & 0\\ -\omega_R M & M\,\mathrm{d} & R_{rx}+L_{rx}\,\mathrm{d} & -\omega_R M\\ M\,\mathrm{d} & \omega_R M & \omega_R M & R_{ry}+L_{ry}\,\mathrm{d}\end{bmatrix}\begin{bmatrix}i_a\\i_b\\i_x\\i_y\end{bmatrix}.$$

In order to establish the rotational voltage influence on the phase current waveform, one induction motor phase was supplied by a single-phase PM converter and another by a sinusoidal power source (Fig. 6).

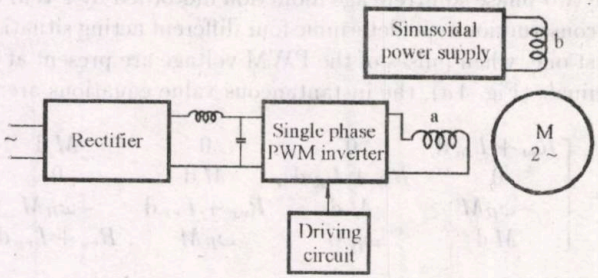

Fig. 6

Fig. 6 shows the main structure of the PWM inverter-fed two-phase induction motor. It consist of a two-phase induction motor, a full-bridge type inverter, a driving circuit, a fixed DC voltage source and a microprocessor.

In these conditions the induction machine behavior was theoretically studied using the dynamic system simulation capabilities offered by MATLAB/SIMULINK software package.

The SIMULINK model is shown in Fig. 7. The induction machine model shown in this figure is based on stator reference frame working machine equations; for this

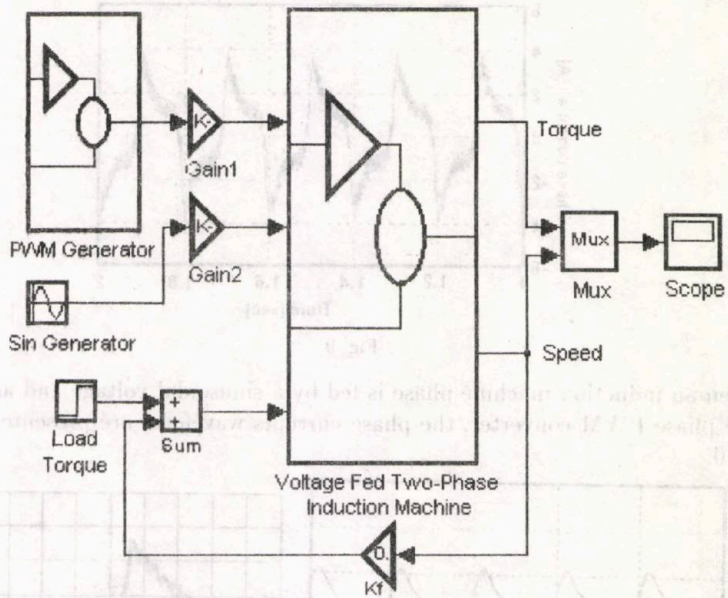

Fig. 7

case the software package blocks were used. But we can do this machine model in two other different ways: using SIMULINK *s*-function [5], or the "Dynamic Node Technique" method [6].

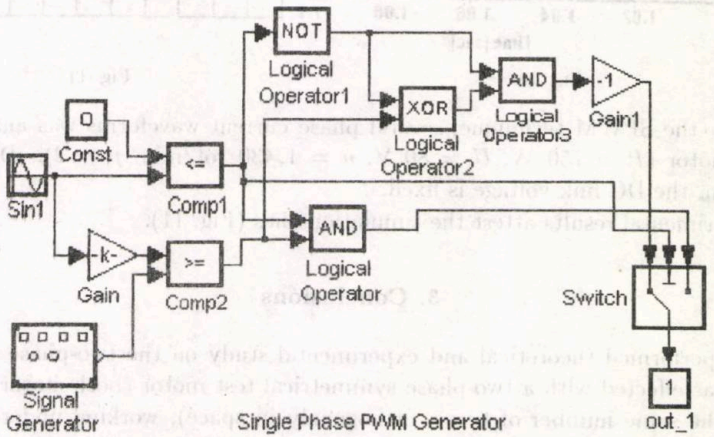

Fig. 8

Fig. 8 shows the single-phase PWM converter model, based on SPWM technique. It contains two generators: a sinewave generator (for the modulation wave) and a triangular one (the carrier wave). The intersections between sinusoidal and triangular waves, generate the commutations moments.

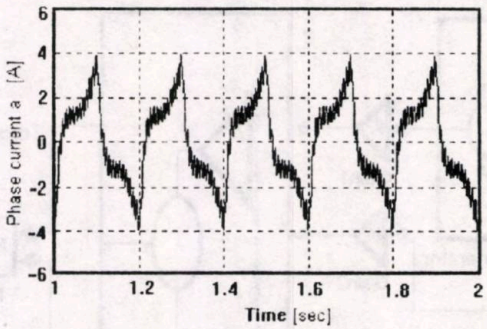

Fig. 9

When an induction machine phase is fed by a sinusoidal voltage and another by a single phase PWM converter, the phase currents waveform are presented in Figs. 9 and 10.

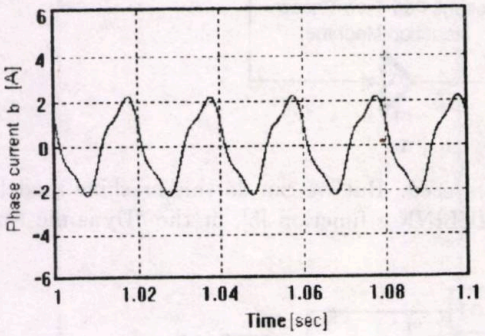

Fig. 10

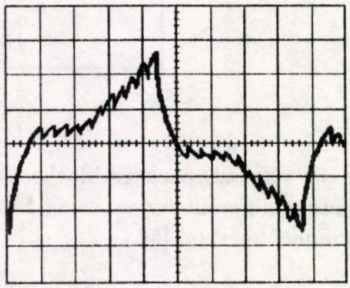

Fig. 11

Using the SPWM technique, several phase current waveforms was analyzed on a test motor (P = 750 W, U = 80 V, n = 1,430 rot/min, p = 2). During the operation, the DC link voltage is fixed.

Experimental results attest the simulation ones (Fig. 11).

3. Conclusions

The performed theoretical and experimental study on the two-phase induction motor was effected with a two-phase symmetrical test motor (both stator windings having the same number of turns, orthogonaly in space), working under balanced conditions (both excitation voltages are identically and fixed, their phase difference being fixed at 90 el. degr.).

Each stator winding operate under two voltages influence: excitation voltage and rotation one. So the phase currents will be the compounding result of two voltages.

When a two-phase squirrel-cage induction machine operate driven by PWM converter, the rotation induction voltage affects the phase current waveform, who moves

away from a sine one. This phenomenon determine an important current and torque harmonic content, in addition to the contribution of the commutation pulses.

This situation may be considerably ameliorate operating with an adequate PWM technique, a better switching algorithm and proper ratio. The last one depends on converter output voltage frequency variation range.

Notations

$d \equiv d/dt$ – rate of change;
f – fundamental frequency, [Hz];
i – instantaneous current, [A];
$[i]$ – instantaneous current matrix, [A];
I – current (rms value), [A];
$j = \sqrt{-1}$;
L – inductance, [H];
$[L]$ – inductance matrix, [H];
M_r – torque, [normalized value];
R – resistance, [Ω];
$[R]$ – resistance matrix, [Ω];
s – fundamental slip;
t – time, [sec.];
T – fundamental period, [sec.];
u – instantaneous voltage, [V];
$[u]$ – instantaneous voltage matrix, [V];
X – reactance, [Ω];
ω – angular velocity or frequency, [rad./sec.];
Θ – angular velocity, [rad./sec.];
θ – angular displacement, [rad.];
ν – order of harmonic.

Subscripts

a – stator winding a;
b – stator winding b;
M – mutual reactance;
r – rotor;
s – stator;
x – physical rotor x winding;
y – physical rotor y winding;
ν – order of harmonic;
t – triangular wave

Received April 4, 1997

Technical University "Gh.Asachi", Jassy,
Department of General Electrotechnics
and Electrical Machines

REFERENCES

1. A l e x a D., *Static Frequency Convertor for Supplying an Asynchronous Two-phase Motor.* IEEE Proc., **134**, *1*, 57-60 (1987).
2. G o g u M., T e o d o r u E.C., *About the Pulse Width Modulated (PWM) Voltage Source Invertor System for Two-phase Asymmetrical Induction Motors.* The Eight Nat. Conf. of Electrical Drives, Romania, Oct. 22-24, 1992, sect. B.16.
3. G o g u M., T ă r n i c e r i u D., T e o d o r u E.C., *About Harmonic Content of Current and Torque Pulsations of the Two-phase Induction Motors Fed by a Two-phase PWM Invertor.* The Internat. Conf. on Appl. and Theor. Electrotechnics, Craiova, Nov. 18-20, 1993, 116-121.

4. Gogu M., Teodoru E.C., *Rotation Voltage Influence over Two-phase Squirrel Cage Induction Motors Driven for PWM Converters Working.* Aegean Conf. on Electrical Machines and Power Electronics, Kuşadaşi, Turkey, 1995, 172-177.
5. Gogu M., Teodoru E.C., Gogu R., *A New Strategy for Two-phase Induction Motors.* Internat. Conf. on Electrical Machines, Vigo, Spain, **III**, 30-35, 1996.
6. Gogu M., Teodoru E.C., Păstrăvanu A., *PWM Two-phase Induction Motor Controlled System "SIMULINK" Models.* Baltic Electronics Conf., Tallin, Estonia, 1996, 351-354.
7. Thurston R.C., Legowski S., *A Simple and Accurate Method of Computing Average and RMS Currents in a Tree-phase PWM Invertor.* IEEE Trans. on Power Electronics. **8**, *2*, 192-199 (1993).
8. Gogu M., *Two-phase Squirrel-cage Induction Machine Working, Fed by a PWM Converter, Considering the Current Harmonics.* Bul. Inst. polit., Iaşi, **XLI (XLV)**, *1-4*, s. III (1995).
9. Do-Hyun Jang, Jong-Soo Won, *Voltage, Frequency and Phase-difference Angle Control of PWM Inverters-fed Two-phase Induction Motors.* IEEE Trans. on Power Electronics, **9**, *4*, 177-183 (1994).

ASUPRA FUNCŢIONĂRII MAŞINII ASINCRONE BIFAZATE ALIMENTATE DE LA UN CONVERTOR PWM ŞI O SURSĂ SINUSOIDALĂ

(Rezumat)

Se studiază funcţionarea motorului asincron bifazat la care o fază este alimentată cu tensiune sinusoidală iar a doua fază este alimentată de la un invertor PWM monofazat. Acest studiu este important pentru faptul că pune în evidenţă efectul deformant al tensiunii de rotaţie asupra curentului ce străbate o înfăşurare alimentată de la un invertor PWM şi asupra curentului ce parcurge înfăşurarea alimentată cu tensiune sinusoidală. Deşi efectul tensiunii de rotaţie se manifestă şi în cazul alimentării celor două faze cu tensiuni sinusoidale, forma curentului rămâne sinusoidală. Rezultatele obţinute prin simulare utilizând MATLAB/SIMULINK software sunt în concordanţă cu cele experimentale efectuate pe prototipul realizat. S-au conceput metode de ameliorare a formei curentului prin înfăşurările statorice la care rezultatele experimentale au fost confirmate prin simulare.

BULETINUL INSTITUTULUI POLITEHNIC DIN IAŞI
Tomul XLIV (XLVIII), Fasc. 1-2, 1998
Secţia III
ELECTROTEHNICĂ. ENERGETICĂ. ELECTRONICĂ

D.C. 621.314.2: 538.23

ANALOG BEHAVIOURAL SPICE MACROMODELING OF TRANSFORMERS

BY

ADRIAN MAXIM, DANIELLE ANDREU and JACQUES BOUCHER

A new method of SPICE macromodeling of the magnetic components is proposed. It is based on an electric equivalent circuit of the electromagnetic laws, where the magnetic field intensity and the magnetic flux density are simulated with corresponding voltages. The $B(H)$ anhysteretic nonlinear curve is piece-wise-linear approximated with a table controlled source, and the hysteresis is introduced with a Schmidt trigger circuit. Using the Analog Behavioural Modeling facilities of modern Spice simulators, an accurate and a highly computationally efficient model was developed.

1. Introduction

Active device SPICE models have become more and more complex and accurate. Hence, in many simulations the accuracy is determined by the passive device models. In power electronic circuit simulation, the models used for the magnetic components are of a great importance, especially at high current levels, when strong nonlinear characteristics are exhibited.

The simplest models for inductors and transformers are the linear L and K SPICE devices [1]. They give a low analysis time, but also a poor precision.

More complex nonlinear models have already been developed for magnetic components [2],...,[8], but none of them can describe a rectangular $B(H)$ hysteresis curve such as for an amorphous magnetic material.

A first order nonlinear macromodel was introduced in Intusoft SPICE [2], [3]. It's main advantage is that it is made up of only standard SPICE elements and so it can be used with all SPICE 2G6 compatible simulators. However, it gives a rather poor accuracy, as it considers only two constant values for the magnetic permeability: μLIN in the linear and μSAT in the saturation regime. Furthermore, the model introduce errors through using a false dependence of coercive force (H_c) on the flux density level (B). Also, it can't simulate a magnetic core working only in the saturation regime. There exists an enhanced version of this model that simulates the low frequency hysteresis as well [3], [4], but it still has all the other basic model disadvantages.

A more accurate nonlinear macromodel was built [3], [4]. This model simulates the dependence of permeability on the magnetic field intensity, and also the frequency influence on the coercive force. However, this model can't simulate amorphous magnetic materials that have abrupt $B(H)$ hysteresis curves.

The J i l e s - A t h e r t o n model is the most popular nonlinear model of magnetic components [5],...,[8]. It was included in many electric circuit simulators, such as PSPICE [1] and SABER [9]. As it is an internal SPICE model, the analysis time is much lower as the one of the Intusoft macromodel. Also the model parameters extraction from data sheet characteristics is done automatically with the PARTS extractor [1]. In this model the anhysteretic $B(H)$ curve is modeled with an empirical equation that fits very well with ferromagnetic behaviour, but can't describe amorphous material $B(H)$ curve. Moreover, in many highly nonlinear applications, long analysis times result and sometimes convergence problems appear.

As amorphous magnetic materials are increasingly used in power electronic circuits, a new SPICE macromodel for magnetic components, that can simulate rectangular $B(H)$ hysteresis curve, must be developed.

A simple and efficient way to develop a new accurate nonlinear model is to use the Analog Behavioural Modeling (ABM) facilities of modern SPICE type simulators [1] that enables the definition of nonlinear controlled sources. Using the ABM, the electromagnetic laws can be modeled with «in line equation» controlled voltage and current sources.

2. Transformer's ABM Macromodel Description

The key idea of this new ABM nonlinear model is to start with a simple ideal transformer model, that simulates the linear voltage and current laws, and then to add the nonlinear effects by introducing corresponding «in line equation» controlled sources. The fact that the resulting model is modular and each effect has its own model parameters represents the main advantage of this modeling strategy. Hence, the model parameters extraction algorithm becomes very simple and straightforward. The main features that will be added to the ideal model are: the magnetizing and leakage inductances, the parasitic capacitors, the copper and core losses and finally the $B(H)$ hysteresis curve with the ambient temperature dependence.

2.1. Transformer's Parasitic Elements

Fig. 1 shows the starting ideal transformer's model, which is made up of: Evoltage (controlled voltage source), that models the ideal voltage law (Vout = NVin) and Gcurrent (controlled current source), that models the ideal current law (Iout = Iin/N), where N is the winding turns ratio.

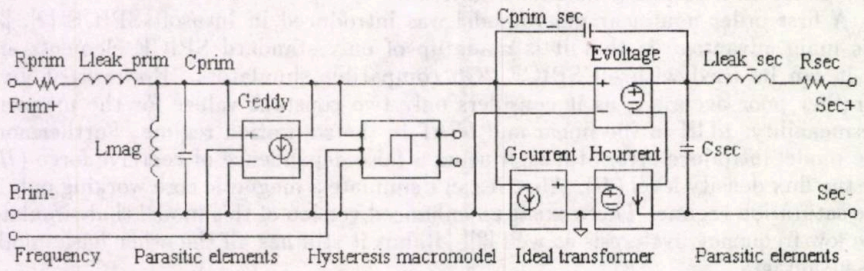

Fig. 1. - Ideal transformer's model, including the parasitic elements.

To obtain a real transformer equivalent circuit, the magnetizing (Lmag) and leakage (Lleak1, Lleak2) inductances, as well as the parasitic capacitances (Cprim, Csec, Cprim_sec) must be added [10].

2.2. Losses Modeling

There are three mechanisms that generate losses in a magnetic component: i^2R, eddy currents and hysteresis. The first one is modeled by the R_{prim} and R_{sec} winding's serial resistors. The eddy current losses are modeled by the R_{eddy} resistor, parallel connected with one of the two windings. This parallel configuration also models the frequency dependence of the eddy current losses. Finally, the hysteresis losses will be modeled by a saturable core model (COREsat) parallel connected with one of the two windings. It will generate the nonlinear current components that are added to the linear component and which will lead to the $B(H)$ hysteresis curve description.

2.3. Hysteresis Model

This new SPICE model of the hysteresis phenomena is based on an electric dual of the magnetic field intensity (H) and the magnetic flux density (B). So the electromagnetic laws are modeled with an electric equivalent circuit, that can be analysed by SPICE type simulators. The detailed electric model of the saturable core that generates the nonlinear $B(H)$ curve is presented in Fig. 2.

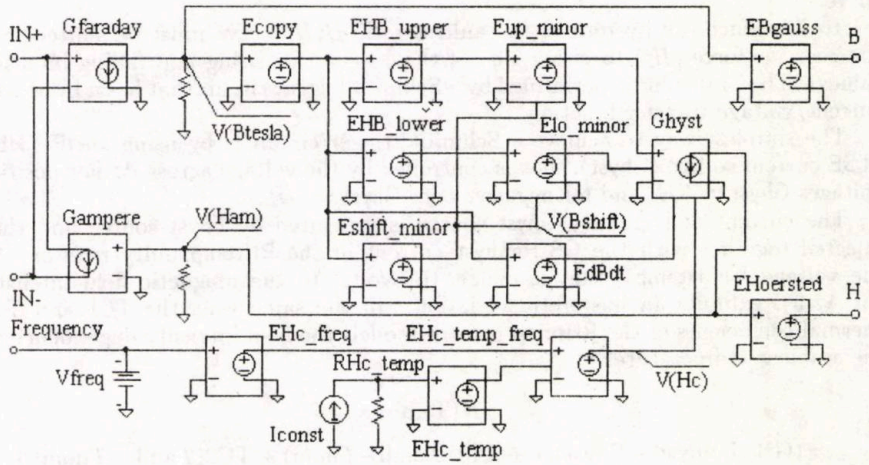

Fig. 2.– New ABM model of the saturable core.

The Faraday's law gives the dependence between the terminal voltage (v) and the magnetic flux density (B). For a uniform B distribution, the flux density becomes proportional to the terminal voltage integral:

$$(1) \qquad v = \frac{\mathrm{d}}{\mathrm{d}t} \iint_S B \,\mathrm{d}S \qquad \text{and consequently} \quad B = \frac{1}{N\,\mathrm{AREA}} \int v(t)\,\mathrm{d}t,$$

where AREA is the mean magnetic cross-section and N is the winding turns ratio.

Faraday's electromagnetic equation is modeled with the Gfaraday «in line equation» controlled source, that calculates the integral of the input terminal voltage. This current source delivers a unity resistance (RBtemp = 1) and so gives a corresponding voltage (in Volts) equal to the flux density (in Tesla):

$$(2) \qquad V(\mathrm{RBmag})\,[\mathrm{V}] = B\,[\mathrm{Tesla}].$$

Defining the TC1 and TC2 thermal coefficients of the RBtemp resistor, the V(RBtemp) voltage becomes dependent on the ambient temperature:

$$B(\text{Tamb}) = V(\text{RBtemp}) = \\ = \text{GBmag}\,[1 + \text{TC1}(T\text{amb} - T\text{nom}) + \text{TC2}(T\text{amb} - T\text{nom})^2]. \tag{3}$$

So the thermal dependence of magnetic flux density was modeled.

The EBgauss controlled voltage source with a 10,000 gain converts the flux density value from the MKS system [Tesla] to the CGS one [Gauss].

The Ecopy voltage follower source assures the isolation between the flux density and the field intensity computing subcircuits.

The nonlinear slope of the anhysteretic $B(H)$ curve is modeled with the GB_Hanhyst ABM TABLE source, that performs a piece-wise-linear approximation of the experimental curve. This is the major advantage of this new nonlinear model: it assures a point-by-point description of the $B(H)$ curve, and so it greatly increases the simulation accuracy. Furthermore this model can describe any kind of $B(H)$ curve.

To introduce the hysteresis, the anhysteretic $B(H)$ curve must be shifted with the coercive force (H_c) to either side of the Y-axis (for rising and falling intensity values). This shift can be performed by a Schmidt trigger circuit that has a hysteretic current/voltage transfer function.

The simplest way to achieve a Schmidt trigger circuit is by using an IF THEN ELSE current source (Ghyst), that is controlled by the voltage across it. For positive voltages Ghyst $= +H_c$ and for negative ones Ghyst $= -H_c$.

The current delivered by Ghyst source is measured by Fhyst source and then injected together with the GB_Hanhyst current in the RHtemp unity resistor. So the voltage V(RHtemp), that is equals (in Volts) to the magnetic field intensity (in A/m), exhibits an hysteretic variation. In the same way, the TC1 and TC2 thermal coefficients of the RHtemp resistor models the field intensity dependence on the ambient temperature:

$$H(\text{Tamb}) = \\ = (\text{GB_Hanhyst} + \text{Fhyst})(1 + \text{TC1}(T\text{amb} - T\text{nom}) + \text{TC2}(T\text{amb} - T\text{nom})^2]. \tag{4}$$

The EHoersted controlled source with a $10{,}000/4\pi$ gain converts the field intensity value from the MKS system, [A/m], to the CGS one, [Oersted].

Finally, the Ampère law is modeled with the Gampère «in line equation» ABM source, that imposes the current through the input winding:

$$NI = \oint_l H\,\mathrm{d}l \Rightarrow \text{Gampère} = I = \frac{0.4\pi\text{PATH}}{N} H, \tag{5}$$

where PATH is the mean magnetic path length, N – winding turns ratio and the magnetic field intensity is given by the V(RHtemp) voltage. Both Faraday's and Ampère's laws have now been modeled with corresponding «in line equation» ABM controlled sources.

The main advantage of this new nonlinear model is the fact that it enables a piece-wise-linear approximation of the $B(H)$ curve and so it eliminates the mathematical equation fitting used in the classic nonlinear SPICE magnetic component models.

3. Simulation Results

Using a PSPICE 6.3 circuit simulator, the proposed nonlinear model was compared with the classical SPICE ones and also with the experimental measurements.

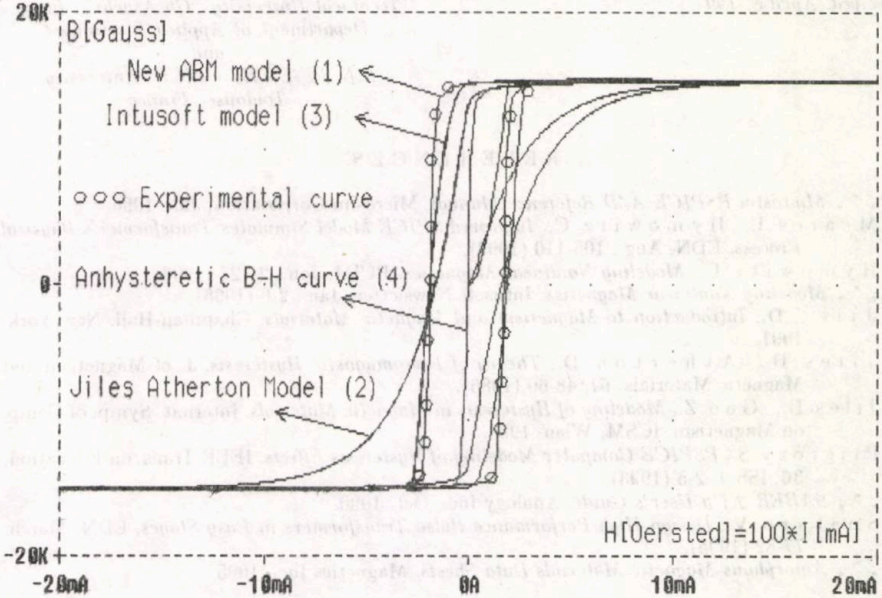

Fig. 3.- The $B(H)$ curve obtained with the classical and the new ABM SPICE models.

Fig. 3 presents the simulated $B(H)$ curve of an amorphous material (orthonol) [11] for the ABM model (*1*), for the PSPICE internal J i l e s - A t h e r t o n model (*2*) and for the simple Intusoft SPICE model (*3*). The anhysteretic $B(H)$ curve is also shown (*4*). The symbols denote the experimental $B(H)$ curve. It can been observed that the ABM model greatly increases the simulation accuracy.

4. Conclusions

Using the ABM facilities of the modern SPICE type simulators, the electromagnetic equations of the magnetic components were modeled by means of an equivalent electric circuit.

This new modeling method performs a piece-wise-linear approximation of the nonlinear $B(H)$ curve, instead of the classical model's empirical equation fitting. So the model is able to simulate any kind of magnetic materials.

The data sheets parameters (e.g. H_c, B_r, Path, Area, etc.) are directly specified as model parameters and so the parameters extraction algorithm was eliminated. Second order effects such as thermal variations of the magnetic field intensity and magnetic flux density have also been included.

The model is made up only of passive devices, controlled voltage and controlled current sources, which leads to a high computational efficiency model with no convergence problems.

This ABM method of magnetic components modeling is general and can be used in all the SPICE simulators that have ABM facilities: SPICE, IsSPICE, Berkeley SPICE3, etc.

Received, April 8, 1997

Technical University "Gh.Asachi", Jassy,
Department of Applied Electronics
and
E.N.S.E.E.I.H. - I.N.P. University,
Toulouse, France

REFERENCES

1. . . *Microsim PSPICE A/D Reference Manual.* Microsim Corporation, Jan. 1996.
2. Meares I., Hymowitz C., *Improved SPICE Model Simulates Transformer's Physical Process.* EDN, Aug., 105-110 (1993).
3. Hymowitz C., *Modeling Nonlinear Magnetics.* PCIM, Jan., 21-27 (1996).
4. . . *Modeling Nonlinear Magnetics.* Intusoft Newsletter, Jan., 2-6 (1995).
5. Jiles D., *Introduction to Magnetism and Magnetic Materials.* Chapman-Hall, New York, 1991.
6. Jiles D., Atherton D., *Theory of Ferromagnetic Hysteresis.* J. of Magnetism and Magnetic Materials, *61*, 48-60 (1986).
7. Jiles D., Gao Z., *Modeling of Hysteresis in Magnetic Materials.* Internat. Symp. of Comp. on Magnetism, ICSM, Wien, 1995.
8. Prigrozy S., *PSPICE Computer Modeling of Hysteresis Effects.* IEEE Trans. on Education, **36**, ISS *1*, 2-5 (1993).
9. . . *SABER 3.1 a User's Guide.* Analogy Inc., Oct. 1990.
10. Spataro V., *Design High Performance Pulse Transformers in Easy Stages.* EDN, March, 77-82 (1995).
11. . . *Amorphous Magnetic Materials Data Sheets.* Magnetics Inc., 1995.

MACROMODELAREA SPICE ANALOG-COMPORTAMENTALĂ A TRANSFORMATOARELOR

(Rezumat)

Se prezintă o nouă metodă de macromodelare SPICE a transformatoarelor cu miez saturabil, care utilizează descrierea directă a fenomenelor neliniare ce apar în miezul magnetic, cu ajutorul unor surse de tensiune şi curent comportamentale (ABM – Analog Behavioural Modeling), de tipul «ecuaţie matematică» şi «tablou».

Modelul SPICE al ciclului de histerezis este obţinut pe baza realizării unui echivalent electric al câmpului magnetic şi al inducţiei magnetice.

Curba anhisteretică $B(H)$ este aproximată liniar pe porţiuni de o sursă ABM de tip «tablou», în cadrul căreia se specifică direct perechile de puncte (B, H) de pe caracteristica experimentală. Ciclul de histerezis este modelat cu ajutorul unui circuit trigger Schmidt, care deplasează curba anhisteretică $B(H)$ cu valoarea curentă a câmpului coercitiv H_c, de o parte şi de alta a axei $Y(\equiv B)$.

Principalul avantaj al metodei propuse de macromodelare a miezurilor magnetice saturabile este reprezentat de înlocuirea aproximării curbei anhisteretice $B(H)$ cu o ecuaţie matematică empirică (ca în cazul modelelor SPICE clasice), cu o aproximare liniară pe porţiuni de înaltă precizie. În consecinţă, macromodelul propus este capabil să descrie orice tip de caracteristică $B(H)$ (inclusiv cicluri practic rectangulare, de tipul celor ale materialelor magnetice amorfe).

Utilizarea surselor ABM neliniare de tipul «ecuaţie matematică» şi «tablou» conduce la posibilitatea specificării directe a datelor de catalog drept parametri de model şi astfel etapa extragerii parametrilor este eliminată.

BULETINUL INSTITUTULUI POLITEHNIC DIN IAŞI
Tomul XLIV (XLVIII), Fasc. 1–2, 1998
Secţia III
ELECTROTEHNICĂ. ENERGETICĂ. ELECTRONICĂ

D.C. 621.3.029.5

ON THE HYBRID PLL/DDS FREQUENCY SYNTHESIZER

BY

VIOREL OLARIU

Some new hybrid PLL/DDS frequency synthesis topics are presented. These approaches allow to build frequency synthesizers that reach very high performances, but having much simpler circuitry than traditional ones.

1. Introduction

Modern communication systems are placing ever-increasing demands on the resolution, bandwidth and switching speed, but also on the power consumption, weight and cost price. In the past, these requirements have been satisfied by the conventional phase-locked loop (PLL) synthesizer [1]. The fundamental advantage of PLL's has been their ability to synthesize an output sine wave of high spectral purity which may be tuned over a wide bandwidth. However, the switching speed and resolution of synthesizers are becoming critically important as frequency agile communications systems such as CDMA digital cellular telephones, spread spectrum wireless LANs, and military frequency-hopped communications systems become widespread. Conventional PLLs are ill-suited to these applications because they suffer from an inherent inability to simultaneously provide fast frequency switching and high resolution without substantial design complexity. This is evident in the simplified block diagram of the PLL in Fig. 1. The resolution of the PLL is determined primarily by the frequency at the input to the phase detector. Lower reference frequencies result in closer spacing between the output frequencies of the synthesizer, but also require reduction in the loop filter bandwidth. This reduced loop filter bandwidth increases the time constant of the loop transient response and therefore degrades the switching speed of the synthesizer. Multiple-loop techniques have been employed in an attempt to improve frequency resolution without prohibitive increases in switching speed. However, these techniques substantially increase hardware complexity and usually require many precision analog components.

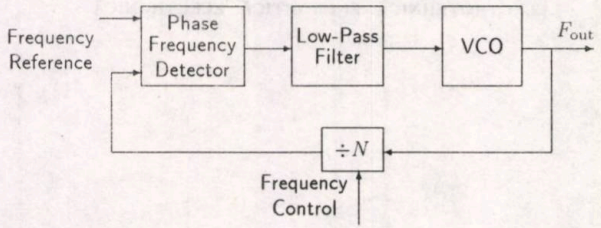

Fig. 1.– Simple PLL frequency synthesizer.

In the last several years Direct Digital Synthesis (DDS) techniques have become an increasingly popular method of frequency synthesis. This has occurred in response to the stringent performance requirements of applications such as frequency hopping spread spectrum, Doppler and chirp radar, magnetic resonance spectroscopy/imaging and test equipment design. Direct Digital Frequency Synthesizers (DDFS) offer many important advantages over PLL-based synthesizers, including ultra-small frequency resolution, fast and phase-continuous frequency switching, exceptional linearity and excellent temperature and aging stability. Of particular importance in applications such as frequency hopping is the frequency switching time, or latency, which determines the maximum hopping rate.

Most DDFSs use the Sine Table Lookup Method, first published by T i e r n e y, R a d e r and G o l d in 1971 [2]. The idea is to generate a sinusoidal output by periodically accessing ROM-stored digital samples of a sine wave, and converting the samples by means of a digital-to-analog converter. The ROM addresses are computed using a digital Phase Accumulator.

The method can be stated mathematically as follows. Equally-spaced samples S_m of one period of the cosine function are stored in a ROM of size 2^L. At address m, the stored value is

$$S_m = \cos\left(\frac{2\pi}{2^L}m\right), \quad 0 \le m \le 2^L - 1. \tag{1}$$

The samples stored at multiples lk, $(l = 0, 1, \ldots)$, of a "frequency setting word" k, generated by a Phase Accumulator, are converted by means of a D/A converter (DAC). The output of the DAC can be expressed as

$$V_0(l\Delta t) = \cos\left(2\pi\frac{F_c}{2^L}kl\Delta t\right), \tag{2}$$

where the rate at which the samples are computed is $F_c = 1/\Delta t$. From this expression it is clear that the frequency of the output is

$$F_{out} = \frac{F_c}{2^L}k. \tag{3}$$

A widely used VLSI architecture for DDS, henceforth called the "traditional" design, is shown in Fig. 2. The Phase Accumulator consists of the pipelined adder with feedback. The L-bit samples at its output are truncated to W bits in order to yield a reasonably sized ROM.

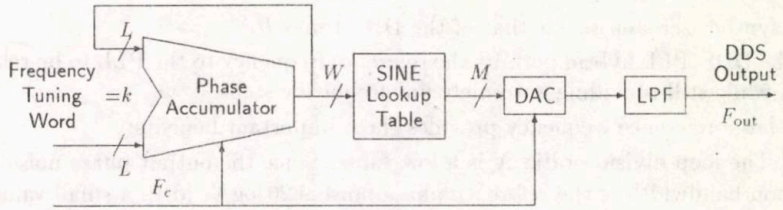

Fig. 2.- Traditional Direct Digital Frequency Synthesizer Architecture.

Three figures of merit are of particular interest: frequency, phase and amplitude resolution. Frequency resolution is the smallest change that can be generated in the output frequency, and is given by $F_c/2^L$. Alternatively, it is specified in bits as the width of the Phase Accumulator. Phase resolution expresses the phase difference between neighbouring samples and can be expressed as the bit width of the ROM addresses. Amplitude resolution is expressed by the number of bits used to represent the samples.

Spread spectrum applications impose an extremely stringent set of specifications on a frequency synthesizer which include the achievement of high resolution and very fast switching times over a wide bandwidth in a design that is compact, reliable and easy reproducible. These requirements cannot be satisfied by either PLL or DDS method. Combining the advantages of both techniques can produce specifications that are impossible to achieve neither by PLL nor by DDS. One can build frequency synthesizers that can meet simultaneously the most severe demands on the resolution, bandwidth, switching speed and spectral purity.

In what follows some hybrid PLL/DDS frequency synthesis approaches are presented.

2. PLL with DDS-Generated Frequency Offset Synthesizer

The PLL with frequency offset approach is typical of multi-loop synthesizer designs, but this hybrid replaces fine frequency step PPLs with a single DDS (Fig. 3). Due to the fine resolution of the DDS, this synthesizer can provide better frequency resolution than a PLL approach containing many loops. If the design does not include the optional fixed P divider, then the synthesizer output frequency is given by:

$$F_{\text{out}} = NF_{\text{Ref}} + F_{\text{DDS}}. \tag{4}$$

The PLL provides the coarse steps in units of F_{Ref}. The DDS provides the fine resolution to fill the gaps between the coarse steps. For continuous frequency coverage, the DDS output bandwidth must be greater than or equal to the reference frequency:

$$\text{BW}_{\text{DDS}} \geq F_{\text{Ref}}. \tag{5}$$

The synthesizer step size is that of the DDS, usually $\ll 1$ Hz.

If the design includes the optional fixed P divider between the synthesizer output and the mixer, then the output frequency is given by:

$$F_{\text{out}} = NPF_{\text{Ref}} + PF_{\text{DDS}}. \tag{6}$$

The synthesizer step size is that of the DDS times P.

The DDS/PLL hybrid permits the reference frequency to the PLL to be relatively large, while still providing extremely fine frequency steps.

A large reference frequency provides three important benefits:

1° The loop division ratio N is a low value. Since the output phase noise within the loop bandwidth is the reference phase noise $+20\log N$, [dB], a small value of N minimizes this noise.

2° The loop bandwidth is typically $\leq 10\%$ of the reference frequency (this is a rule of thumb). Therefore, a large reference frequency permits a wide loop bandwidth. Since the VCO noise is suppressed by 12 dB/octave beginning at ω_{3dB} and headed toward DC, a wide loop bandwidth yields a low phase noise output despite a noisy VCO.

3° The wide loop bandwidth made possible by this synthesizer provides a loop with proportionally faster settling time.

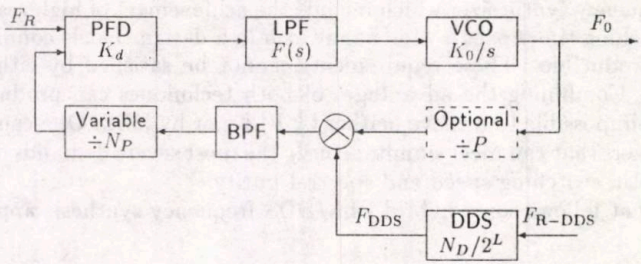

Fig. 3.– PLL with DDS-generated frequency offset synthesizer.

This topology also has some performances and design advantages: a) broad output bandwidth (because the reference frequency can be made relatively large); b) extremely fine frequency resolution with constant steps (because of the fine frequency resolution of the DDS); c) fast settling time (because of the wide loop bandwidth made possible by the large reference frequency); d) low phase noise (because of the small loop division ratio); e) low spurious noise; f) minimal power; g) performance analysis is the same as a conventional PLL synthesizer.

3. DDS-Driven PLL Frequency Synthesizer

Fig. 4 shows a phase locked loop frequency synthesizer with the reference frequency generated by a DDS. A filtered, limited DDS output serves as reference for the PLL. An optional divider may be used to provide an appropriate centre frequency for a particular filter technology (such as a crystal filter, where the range of centre frequencies may be limited), or simply to improve its noise and spurious characteristics.

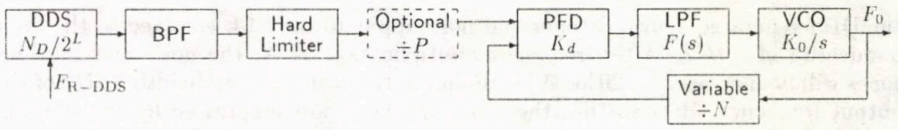

Fig. 4. DDS-driven PLL Frequency Synthesizer.

The DDS-driven PLL output frequency has the same resolution as the input reference frequency. For example, if the PLL output range is 800 to 1.000 MHz and if the reference frequency applied to the PLL is 10 MHz, the PLL can output 800, 810, 820,....990, 1.000 MHz. Each PLL output is the division ratio of the loop (N – Fig. 4) times the reference frequency. Using a DDS as the loop reference lets the designer vary the reference frequency in extremely small steps. Appropriate selection of the DDS output bandwidth gives the synthesizer continuous frequency coverage with a resolution of N times the DDS frequency resolution. So, for continuous coverage, the DDS bandwidth must be

$$BW_{DDS} \geq \frac{DDS_{Centre\ Frequency}}{N_{min}}, \tag{7}$$

where N_{min} is the minimum PLL division ratio. Note that the step size of the DDS-driven PLL varies with N and therefore is not constant throughout the range of output frequencies.

The performance of this approach is a function of the DDS characteristics, the BPF bandwidth and the PLL parameters. If the switching speed is unimportant, the PLL loop bandwidth can be extremely narrow. In this case, the phase noise and spurious performance of the output is essentially that of the VCO. The band-pass filter in Fig. 4 can be replaced with a low-pass filter since the reference will have a minimal effect on the output spectrum. If the VCO is clean, this may be the simplest approach to a synthesizer with broad bandwidth, fine resolution, good spurious and phase noise performance, small size and low power, but with slow switching between output frequencies.

For a fast switching speed, the PLL loop bandwidth must be made correspondingly larger. In this case the band pass filter, hard limiter, and optional divider in Fig. 4 become important. In the absence of these three functions, the unmodified DDS output (with anti-aliasing filter) is multiplied by N in frequency by the PLL. Within the loop bandwidth, noise and spurs are affected as follows at the DDS output.

In the DDS-driven PLL, the DDS supplies the reference frequency for the PLL. Ideally, the reference frequency would have low phase noise and spurious content. Although the DDS output does have low phase noise, its spurious content exceeds that of a high-grade reference oscillator. These spurious occur mainly by phase truncation and amplitude quantization of the signal generated by the DDS [3]. The PLL acts as frequency multiplier relative to reference frequency [1]. Frequency multiplication by N increases the amplitude of each spurious tone by N, with no effect on the offset frequency. Therefore, frequency multiplication by N increases the power of DDS phase truncation spurs by N^2 (or $20 \log N$, [dB]), but does not change the frequency offset of these spurs from the carrier. The band-pass filter in Fig. 4 keeps

the DDS-generated spurious tones and noise input to the PLL confined to the filter bandwidth of $\pm B/2$. After frequency multiplication by N, the noise and spurious tones will be increased by $20 \log N$, [dB], but only within the bandwidth $\pm B/2$ of the output frequency. Beyond this, the spurs and noise are suppressed by the skirts of the BPF. In essence, the BPF serves as a tunable high-frequency trancking filter, but it is actually a fixed, low frequency design. The output spectrum is a clean tone surrounded by a pedestal of noise and spurs fall off rapidly beyond this point due to the BPF and the 1st order response loop. If a narrow bandwidth crystal filter is used, the pedestal can be made extremely narrow. The selection of the BPF bandwidth and center frequency is a tradeoff between switching speed, noise performance, and the need for continuous frequency coverage. Good phase noise and anti-microphonic design practice dictate that N be small, and consequently that the reference frequency be high. A small N requires a relatively large BPF bandwidth to provide continuous coverage (s. Eq. (7)). Certain filter technologies may not be available at the desired reference frequency. Also note that a narrow BPF bandwidth also adversely affects switching speed. Therefore, the selection of the BPF center frequency and bandwidth is a balancing act between these issues. The resulting spectrum can be made nearly spur-free when observed over large frequency spans, but has the noise pedestal when observed close-in. This may not be acceptable for instrument-grade applications. For these applications an extremely narrow BW can be used to eliminate the pedestal (at the expense of switching speed), or another synthesizer topology can be used. This topology may be ideal, however, in a communications application where the transmitted spectrum is wider than the synthesizer noise pedestal.

The hard limiter in Fig. 4 suppresses the AM spurious components from the DDS. These components are the AM amplitude quantization process, as well as AM portion of the DDS thermal noise. As AM spurs have an unpredictable effect on PLL output performance, it is best to eliminate them. In practice, the hard limiter provides a noticeable improvement in synthesizer performance.

The optional divider in Fig. 4 performs two functions. First, it improves the spurious and noise performance of the DDS, in general by $20 \log P$, [dB]. Second, it provides flexibility in selecting the reference frequency to the PLL and the center frequency of the crystal filter. This is because the DDS output and PLL reference input are at different frequencies. The resulting extra degree of freedom may help in the specification of the BPF response.

4. PLL Frequency Synthesizer with a DDS as a Fractional-N Divider

In Fig. 5 it is assumed that the DDS includes the numerical controlled oscillator and the DAC. The PLL output, divided by P, is feeding the clock input of the DDS. Since the DDS output frequency is

$$F_{\mathrm{DDS}} = \frac{N_D}{2^L} F_C, \tag{8}$$

a simple calculation of the output frequency of the locked PLL leads to

$$F_0 = \frac{2^L}{N_D} N_P P F_R = M F_R, \quad \text{with} \quad M = \frac{2^L}{N_D} N_p P, \tag{9}$$

where L is the phase accumulator length of the DDS [2], [3]. It comes out that the loop behaves like a frequency multiplier where the global multiplication factor, M, is a fractional number. The output frequency change is proportional to N_P but in inverse proportion to N_D (the number which is loaded in the phase register of the DDS). A typical value for L is 32; N_D can be taken $2^L/3$ (theoretically $2^L/2$). The resolution of the frequency synthesizer is

$$\Delta F_0 = \frac{2^L}{N_D(N_D+1)} N_P P F_R. \tag{10}$$

It is noticeable that, although the resolution is not a constant, this is not a major drawback since it has a very small value (typically less than $10^{-9}F_0$).

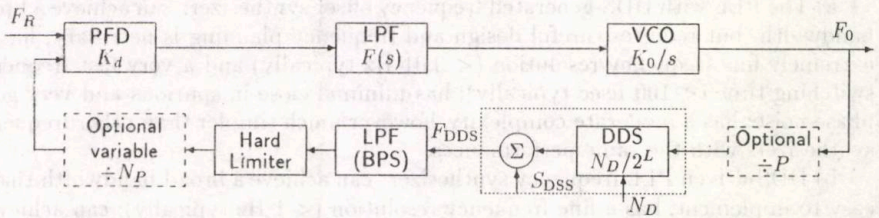

Fig. 5. – PLL frequency synthesizer with a DDS as a fractional-N divider.

The real problem concerning this approach is the appearance at the synthesizer output of the quantization and phase truncation spurious of the DDS. The output spurious of the DDS, S_{DDS}, can be assumed, with a good approximation, as a linear additive noise. Using the theory of the feedback circuits and the general theory of the PLL [1], [3], one can find the spurious contribution from the DDS output to the frequency synthesizer output:

$$\frac{S_{OUT}(s)}{S_{DDS}(s)} = \frac{K_d \frac{K_0}{s} F(s) \frac{1}{N_P}}{1 + K_d \frac{K_0}{s} F(s) \frac{1}{M}}, \tag{11}$$

where $S_{OUT}(s)$ is the DDS spurious contribution to the output of the frequency synthesizer. So, the loop acts as a low-pass filter with respect to the DDS spurious and therefore they are multiplied by $M/N_P = (2^L/N_D)P$ inside the 3 dB loop bandwidth. From this point of view the performances of this approach are nearly similar to DDS Driving PLL approach [4]. Since F_R can be chosen much larger (hundreds of kHz...tens of MHz) than the one used for a typical PLL synthesizer, the loop bandwidth can be increased proportionally allowing a much faster frequency switching speed. However, the larger loop bandwidth, the larger is the DDS output spurious contribution to the frequency synthesizer output. A technique that can meet decreasing settling time while keeping the spectral purity to the designer's specifications can be a non-linear filter having two time constants [3]: a lower one (that means a wide loop bandwidth), when the loop is far from the lock state and a larger one (that means a narrow loop bandwidth), when the loop is near lock state. The existence on the loop feedback path of N_P, N_D and P factors results in some extra degree of freedom which may help in frequency synthesizer designing. So, an adequate choice

of V_P and P coefficients allows a wider bandwidth of the frequency synthesizer while maintaining a minimum $N_{D_{max}}/N_{D_{min}}$ ratio (1...2%) and the placing of the N_D in an optimal zone for minimal spurious level generated by the DDS [5].

The presented approach is extremely simple and the main advantage is that it has no need for a high frequency reference generator (with good stability and low phase noise) at high costs as in other direct digital frequency synthesizers.

5. Conclusions

Some hybrid PLL/DDS frequency synthesizers are presented. Making a comparison between these approaches it comes out that:

a) The PLL with DDS-generated frequency offset synthesizer: can achieve a broad bandwidth, but requires careful design and frequency planning is necessary; has an extremely fine frequency resolution (< 0.01 Hz typically) and a very fast frequency switching time (< 100 μsec typically); has minimal close-in spurious and very good phase noise; has a moderate complexity, however much simpler than other frequency synthesizers with the same performances.

b) DDS-driven PLL frequency synthesizer: can achieve a broad bandwidth that is easy to implement; has a fine frequency resolution (< 1 Hz typically); can achieve a fast frequency switching time (< 10 msec typically), but this is tradeoff versus close-in spurious noise; has good phase noise and excellent spurs over broad bandwidth; has a simple circuitry.

c) PLL frequency synthesizer with a DDS as a fractional-N divider has mainly the same performances as the DDS-driven PLL frequency synthesizer, but its variation with N_D (the control number of the DDS) is non-linear. On the other hand, this approach has the simplest circuitry.

Received, May 5, 1997

Electronic Research Institute, Jassy Branch

REFERENCES

1. Manassewitsch V., *Frequency Synthesizers. Theory and Design.* J. Willey a. Sons, New York, 1976.
2. Tierney J., Rader C.M., Gold B., *A Digital Frequency Synthesizer.* IEEE Trans. Audio Electroacustics, **AU-19**, *3* (1971).
3. Rohde U., *Digital PLL Frequency Synthesizers. Theory and Design.* Prentice Hall, New York, 1983.
4. *** Qualcomm, Inc., *Hybrid PPL/DDS Frequency Synthesizers.* Application Note AN2334-4.
5. Nicholas III H.T., Samueli H., *A 150-MHz Direct Digital Frequency Synthesizer in 1.25-μm CMOS with 90-dBc Spurious Performance.* IEEE J. Solid-State Circuits, **26**, *12* (1991).

ASUPRA SINTETIZOARELOR DE FRECVENŢĂ HIBRIDE PLL/DDS

(Rezumat)

Se prezintă şi se analizează cateva topologii noi de sinteză a frecvenţei realizate în manieră hibridă PLL/DDS (sinteză indirectă - bazată pe bucla cu calare de fază/sinteză digitală directă). Aceste metode permit realizarea unor sintetizoare de frecvenţă cu scheme electrice mult mai simple decat cele cu performanţe similare realizate prin metodele tradiţionale.

BULETINUL INSTITUTULUI POLITEHNIC DIN IAŞI
Tomul XLIV (XLVIII), Fasc. 1–2, 1998
Secţia III
ELECTROTEHNICĂ. ENERGETICĂ. ELECTRONICĂ

D.C. 621.317.761

FREQUENCY-METER WITH MICROPROCESSOR. SOFTWARE ASPECTS. FREQUENCY-MEASURING WORKING

BY

LAURENŢIU DIMITRIU and LILIANA VORNICU

A frequency-meter with a large range of measuring (0.01 Hz ... 1 MHz) based on the programmable counters utilization is presented. The main software problems for the frequency-meter working (100 Hz ... 1 MHz) are shown. The used principle allows the substantially reducing of the measuring circuit's working time with the microprocessor, a useful feature in real time applications.

1. Introduction

In some real time applications of microprocessors it has be solved the optimal working time problems. This working time can be increased in measurement circuits of process parameters and it could appear the risk of loosing control by the microprocessor. This kind of situation is presented in what follows.

It is considered a microsystems in a specific application, also used to measure and to display the frequency of some signals in a large range of values (0.01 Hz ... 1 MHz). The utilization of standard hardware resources allows solving the problem of measuring and frequency display in such a range, but it needs a complex software, increasing significantly microprocessor's working time. For very low frequencies (0.01 Hz ... 100 Hz) the signal's period is measured and the frequency is obtained using a dividing operation [1]. For the range of 100 Hz ... 1 MHz a direct frequency measurement method was used. To reduce the working time with the microprocessor it is used a specific hardware structure, based on the 8253 type programmable counters resources [2]. Finally, a simplified software is obtained.

Some specific software for frequency-measuring working are also presented.

2. Working Algorithm with Direct Frequency Measurement

In the Fig. 1 the schematic diagram of the frequency-meter with microprocessor is presented. There are shown all specific circuits and the modality of interconnection with the microsystems is indicated.

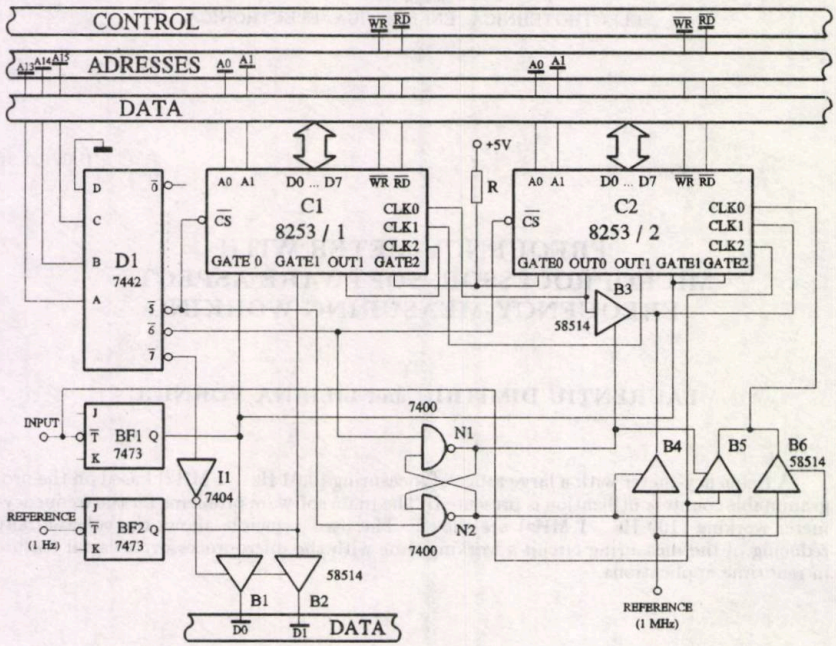

Fig. 1

Frequency measurement working uses the sections of C2 (8253 type) programmable counter. The direct frequency measurement is done in two ranges, noted range *3* and range *4* (ranges *1* and *2* are used in period-measuring mode). The differences between the ranges *3* and *4* are marked using b_7 bit of PORT *P* memory location. The bit b_7 has the value "1" for the range *3* and "0" for the range *4*. The assignation of this value is done during the initialization programme of the system.

The commands for the circuits are done when a transition from "HIGH" to "LOW" of 0.5 Hz reference signal is detected. This detection is achieved comparing the logic level of reference signal from the moment when the frequency-measuring programme starts with that one from the precedent test. The present value is delivered by the bit b_1 of PORT *A* and the previous one by bit B_1 of PORT *P*.

The logic diagram of the programme is presented in Fig. 2.

The programme begins with section COUNTER *1* of C*2* address loading (C001H) into BC register. Then the address of PORT *P* is loaded into HL register.

Then, the programme is continued with the detection of "HIGH" to "LOW" transition of 0.5 Hz reference signal. The present value is transferred into accumulator and the bit b_1 is tested. If $b_1 = 1$, it means that the counter has not finished the counting. In this situation, after a value assignation for b_1, a jump to the main programme is effected. If $b_1 = 0$, the transfer of data could be done. But first it is necessary to know if for the previous test the bit value was not "0" too, respectively a previous command of the counter was effected. To avoid this situation, the bit b_1

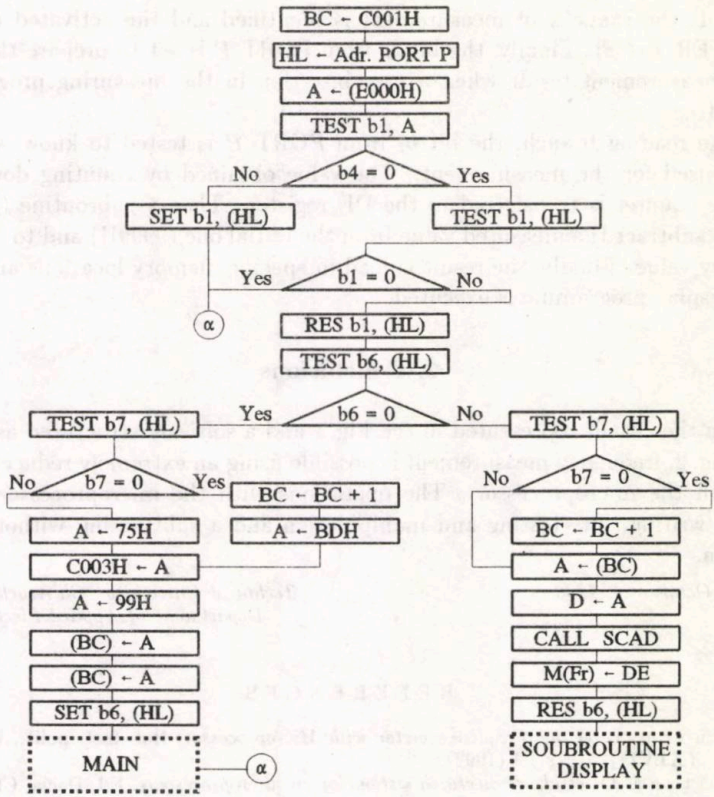

Fig. 2

of PORT P (containing the previous value of reference signal) is tested. If $b_1 = 0$, the previous value of reference signal was "0" and a jump to the main programme is effected. If in PORT P $b_1 = 1$, the useful transition of reference signal is detected. Now the transfers of data could be done.

The transfers of data are effected in two distinct stages. In the first stage the control words and initial values for the counters are written. In the second one, the content of adequate counter is read. Between the two stages, the measurement of signal frequency is effected.

The start of the programme's branches corresponding to the two stages is decided by the value of the bit b_6 from PORT P. If $b_6 = 0$, the counters are loaded with adequate values. For $b_6 = 1$ reading operation are executed.

In the writing branch, the system must decide the counter which works. So, for the range *3* of measurement (100 Hz ... 10 kHz) the COUNTER *2* (C*2*) is used, respectively COUNTER *1* (C*2*) for the range *4* (10 kHz ... 1 MHz). The decision is taken depending of the value of the bit b_7 from PORT P. If $b_7 = 0$, the range *3* of measurement is identified and the activated counter is COUNTER *2* (C*2*).

If $b_7 = 1$, the range *4* of measurement is identified and the activated counter is COUNTER *1* (C2). Finally, the bit b_6 from PORT *P* is set to prepare the reading of the measurement result when a new insertion in the measuring programme is executed.

In the reading branch, the bit b_7 from PORT *P* is tested to know who is the counter used for the measurement. The value obtained by counting down in the adequate counter is transferred in the DE register. Then a subroutine (SCAD) is called to subtract the measured value from the initial one (9999H) and to obtain the frequency value. Finally, the result is load in specific memory locations and a jump to the display programme is executed.

3. Conclusions

Using the circuit represented in the Fig. 1 and a software structured as is shown in the Fig. 2, frequency measurement is possible using an extremely reduced working time with the microprocessor. The operations with the microprocessor are only reading, writing, bits testing and manipulation and a subtracting without borrow operation.

Received, October 21, 1996

Technical University "Gh.Asachi", Jassy,
Department of Applied Electronics

REFERENCES

1. V o r n i c u L. *et al.*, *Frequency-meter with Microprocessor.* Bul. Inst. polit., Iaşi, **XLIII (XLVII)**, *1-2*, s. III (1997).
2. C ă p ă ţ î n ă O. *et al.*, *Proiectarea sistemelor cu microprocesoare.* Ed. Dacia, Cluj-Napoca, 1983.

FRECVENŢMETRU CU MICROPROCESOR. ASPECTE SOFTWARE. FUNCŢIONAREA CU MĂSURAREA FRECVENŢEI

(Rezumat)

Se prezintă un frecvenţmetru cu gamă extinsă de măsurare (0,01 Hz ... 1 MHz) utilizand numărătoare programabile (8253). Măsurarea se efectuează în patru subgame, pentru două (la capătul superior al domeniului) măsurand direct frecvenţa. Se prezintă modul specific de utilizare a numărătoarelor programabile pentru efectuarea măsurării. Programul de lucru face apel la operaţiuni simple, cu durată redusă de execuţie: scrieri, citiri, testări şi manipulări la nivel de bit şi o scădere fără împrumut. Timpul de lucru cu microprocesorul, a circuitului de măsurare, se reduce substanţial, asigurand avantaje însemnate pentru aplicaţii de timp real.

BULETINUL INSTITUTULUI POLITEHNIC DIN IAŞI
Tomul XLIV (XLVIII), Fasc. 1-2, 1998
Secţia III
ELECTROTEHNICĂ. ENERGETICĂ. ELECTRONICĂ

D.C. 621.395.34

INTEGRATION OF THE FUNCTION OF RECEIVING PULSE AND TONE SELECTION INFORMATION IN A LOW CAPACITY ELECTRONIC TELEPHONE EXCHANGE

BY
PETRUŢ DUMA, LUMINIŢA SCRIPCARIU and CLARISSA GÂTLAN

The hardware structure of the individual subscriber circuit of a low capacity electronic telephone exchange for which the function of receiving tone and pulse selection information is integrated using TELTONE M957-01 and M959 receivers is presented. There are also described the graph of states and the command programme for software receiving the selection information.

1. Introduction

The general structure of a low capacity electronic telephone exchange is presented in Fig. 1, where the symbols have the following meanings: I – interface to the external medium; RC – connection network; MT – tones machine; UC – command unit.

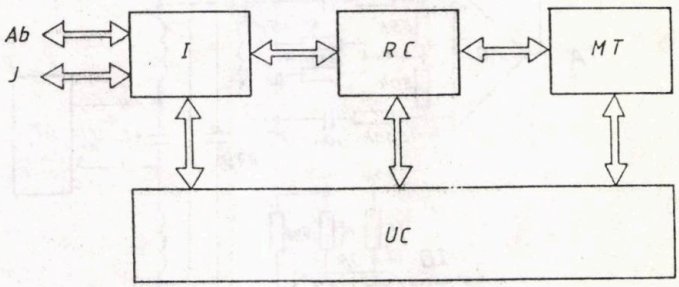

Fig. 1

The external medium includes the subscribers' lines (LAb) through which the subscribers' telephone sets are connected to the exchange, and the junction lines (LJ) through which the exchanges themselves are connected. The interface to the external medium consists of the individual subscriber circuits (CIA) and the junction circuits (CJ).

The connection network has the role to establish the telephone links between subscribers and consists of a switch through which the conversation signals are transported.

The tones machine transmits to the subscribers all the tones required by the exchange's operation and the calling signal. Vocal messages can also be sent from this machine towards the subscribers, during the conversation, the tones transmission or during vocal telephone services.

The command unit is based on a microprocessor system or a microcontroller and is designed to manage the resources of exchange.

2. Hardware Structure of the Individual Subscriber Circuit

The individual subscriber circuit performs the following functions:

a) supplies with DC power, through the line, the subscriber's telephone set;

b) monitors the status of the subscriber's lines for setting, maintaining and releasing a telephone link;

c) receives the pulse/tone selection information;

d) transmits the calling signal to the called subscriber;

e) adapts the *LAb* to the external medium interface;

f) performs the galvanic separation between the exchange and the external medium;

g) insures the protection against the voltages induced in the subscribers' lines by the high-voltage power transporter lines or the atmosphere electric charges;

h) transmits the tones and certain vocal messages;

i) performs the bidirectional transmission of the conversation signal.

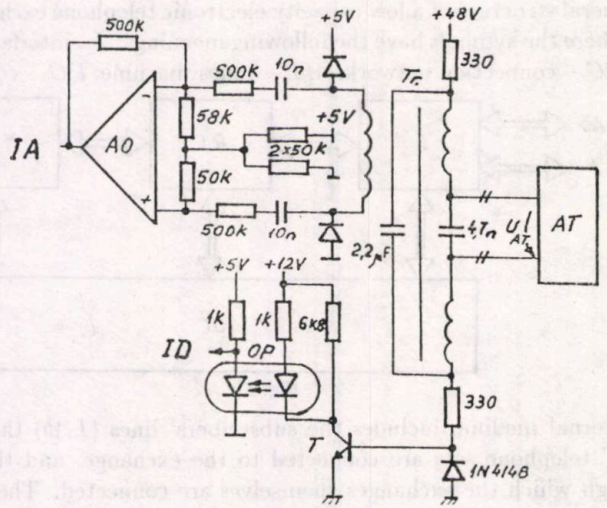

Fig. 2

The individual subscriber circuit has the hardware structure shown in Fig. 2 (only the elements related to the matter of receiving the selection information are depicted). Monitoring the state of the subscriber line and reception of the pulse

selection information are performed using transistor T and octocoupler OP. This structure transforms the pulses from the subscriber's DC loop in TTL level pulses (ID). Receiving the pulse selection information is made using the M959 circuit, connected as in Fig. 3. The reception of a digit of the telephone number is signalised by the STROBE (ST) output, while picking up the phone is signalised by output OFF HOOK (OH).

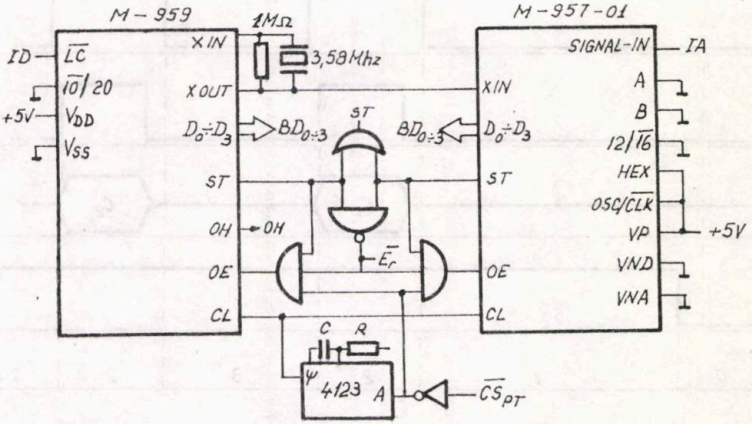

Fig. 3

For the reception of the tone selection information, M957-01 DTMF receiver is used, which is connected to the telephone line through a transformer TR and a operational amplifier AO (IA). The reception of a tone pair is signalised at STROBE (ST) output of the circuit.

The two receivers are controlled through a logical structure, by a command unit. After receiving a digit of the selection information, output ST is logical 1. The command unit considers the two receivers as an input port addressed at PT. From data bus lines BD_{0-3} of this port, the binary code of the received digit is read when activating OUTPUT ENABLE (OE). Monostable 4123 has the role of disabling the strobe output of the receivers after the received digit is read. The waveforms of receiving the selection information are shown in Figs. 4 (pulse) and 5 (tone).

3. Graph of Stages Depicting the Process of Receiving the Selection Information from One Subscriber

The process of receiving the selection information from one subscriber is a complex sequential process. A graph of states must be used for its description. The transitions between states are induced by events which are a generalization of the input signal meaning that they can be input signals and/or the result of certain internal syster rocessings.

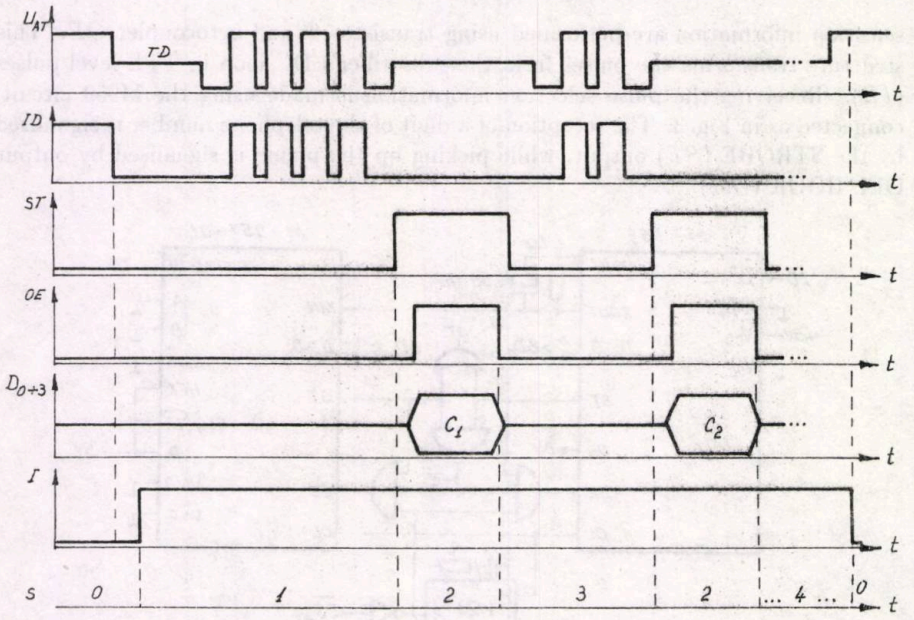
UAT
TD
ID
ST
OE
D0÷3
C1
C2
I
S
0
1
2
3
2
4
0
t

Fig. 4

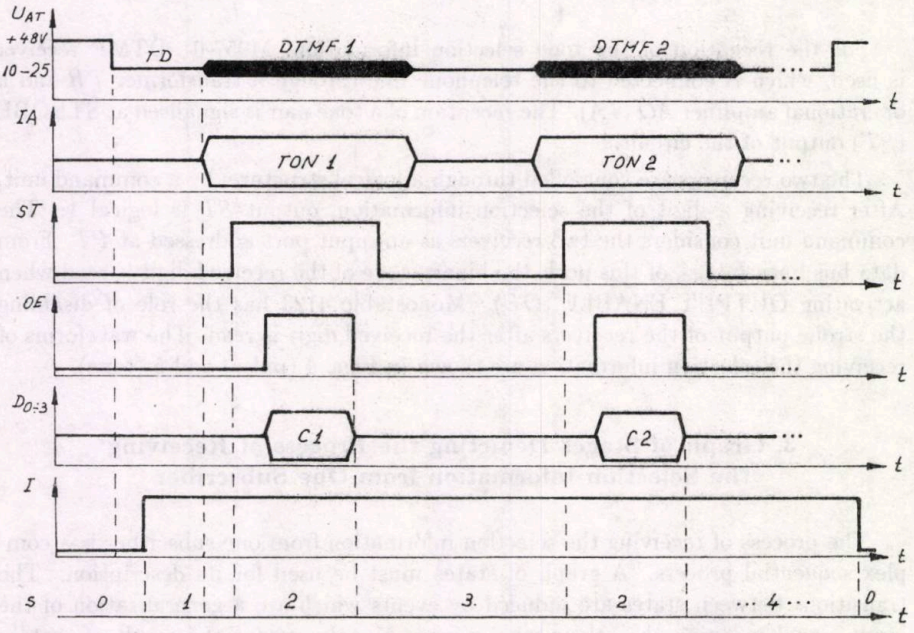
UAT
+48V
10-25
TD
DTMF 1
DTMF 2
IA
TON 1
TON 2
ST
OE
D0÷3
C1
C2
I
S
0
1
2
3
2
4
0
t

Fig. 5

Taking into account the shape of the input signals (Figs. 4 and 5), resulted after the reception of the tone and pulse selection information, and the internal processings which the system must perform, the next states have been defined for the process of receiving the selection information from one subscriber:

a) State 0 – subscriber in stand-by position; when he picks up the receiver, the exchange sends the dialling tone which constitutes an invitation for the transmission of the selection information.

b) State 1 – a waiting state during which the dialling tone is received; the interruption of the dialling tone transmission is made when selection information starts to be transmitted.

c) State 2 – reception of a digit from selection information.

d) State 3 – reception of a pause between two digits from selection information.

e) State 4 – selection information processing.

f) State 5 – false call state – the time assigned to selection information reception was exceeded.

The graph of states describing this process is presented in Fig. 6.

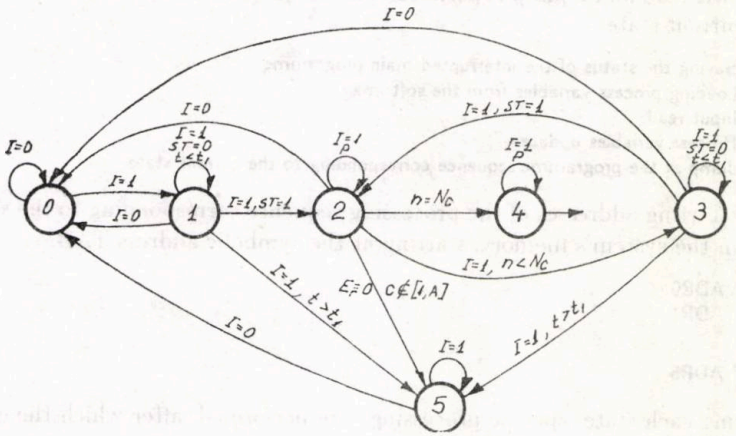

Fig. 6

The variables used in the process description have the following significations: S – state; OH – off hook; ST – valid data; Er – error; t – time counter (t_1 – maximum duration of the admissible reception duration for a digit of the selection information); n – digit counter (N_c – maximum number of receivable digits); C – received digit.

4. Command Software for the Reception of Selection Information from One Subscriber

The command unit solves the process of receiving selection information using time sharing in successive basic cycles. Each cycle loads the input and performs the current state specific processings. The system works in real time using periodic interrupt operation. The command software consists of two distinctive parts:

1° A starting part – called the initialisation sequence (INIT) – during which the peripheral circuits and the periodic interrupt operation are programmed, the process variables and the main programme variables are initialised, etc. This sequence is executed once by the command unit and it is followed by a basic programme during which various processings are executed.

```
INIT: Peripheral circuits programming.
      Interrupt operation programming.
      Initialisation of process variables.
      Initialisation main programme variables.
      Other initialisation.
      Enable interrupt.
      . . . . . .
      Main programme.
      . . . . . .
```

2° The second part is the sequence of treating interrupt requests, during which the input is read and a jump is performed at the programme sequence corresponding to the current state.

```
SCI: Saving the status of the interrupted main programme.
     Loading process variables from the soft image.
     Input read.
     Process variables update.
     Jump at the programme sequence corresponding to the current state.
```

The starting addresses of the processing sequence corresponding to the states are placed in the system's memory, starting at the symbolic address TAB.

```
TAB: ADR0
     ADR1
     . . . . . .
     ADR5
```

During each state, specific processings are performed, after which the execution of the main programme is resumed.

```
ADRi: . . . . . .
      Current state specific processings.
      . . . . . .
Cont: Saving process variables.
      Restoring main programme state.
      Enable interrupt.
      Return to main programme.
```

4.1. State Description

S t a t e 0: test if the calling subscriber has picked up the phone.

If $OH = 0$, then the subscriber did not pick up the phone and state 0 is preserved.

If $OH = 1$, then the subscriber has picked up the receiver. The dialling tone is transmitted and the transition to state 1 is performed.

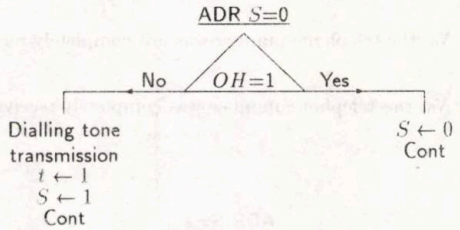

S t a t e 1: the subscriber is transmitted the dialling tone until he starts the transmission of the selection information or he hangs up. Test on input OH.

If $OH = 0$, the subscriber hung up. The dialling tone transmission is cancelled and the transition to state 0 is performed.

If $OH = 1$ off hook status - test on input ST.

If $ST = 1$, reception of a digit from the selection information. The dialling tone transmission is cancelled and the transition to state 2 is performed.

If $ST = 0$, the selection information transmission did not start. Time is counted and the duration of dialling tone transmission is tested.

If $t < t_1$, wait for the transmission of the selection information. State 1 is preserved.

If $t \geq t_1$, false call tone is transmitted to the subscriber due to the fact that the selection information transmission did not start during the adequate time interval. Transition to state 5.

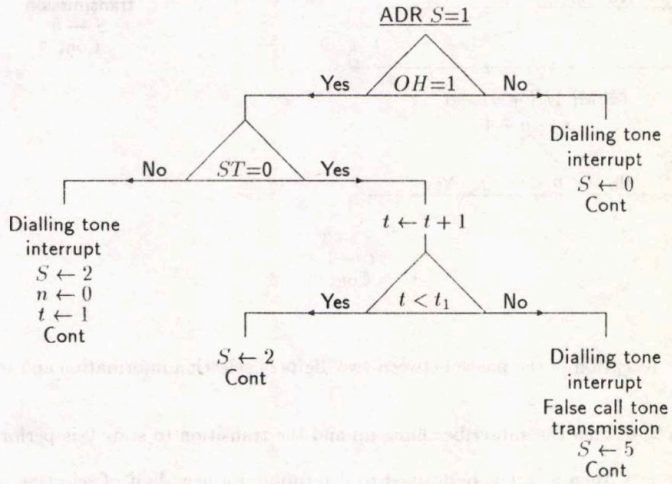

S t a t e 2: the received digit is read from the tone or pulse receiver and then it is processed. Test on input OH.

If $OH = 0$, the subscriber hung up. Transition to state 0.

If $OH = 1$, off hook status. Test on input Er.

If $Er = 0$, the hardware structure detected a reception error. The subscriber is sent the warning tone and a transition to state 5 is performed.

If $Er = 1$, a digit was correctly received. The received digit is read from the input port. Test if it is a valid digit (from 0 to 9).

If $C \notin [1, A]$ - invalid digit. Warning tone. Transition to state 5.

If $C \in [1, A]$ - valid digit. If 0, the digit is converted. The received digit is saved in the process software image, counted and the number of the received digits is tested.

If $n < N_0$, the telephone number was not completely received and the transition to state 3 is performed.

If $n = N_0$, the telephone number was completely received and the transition to state 4 is performed.

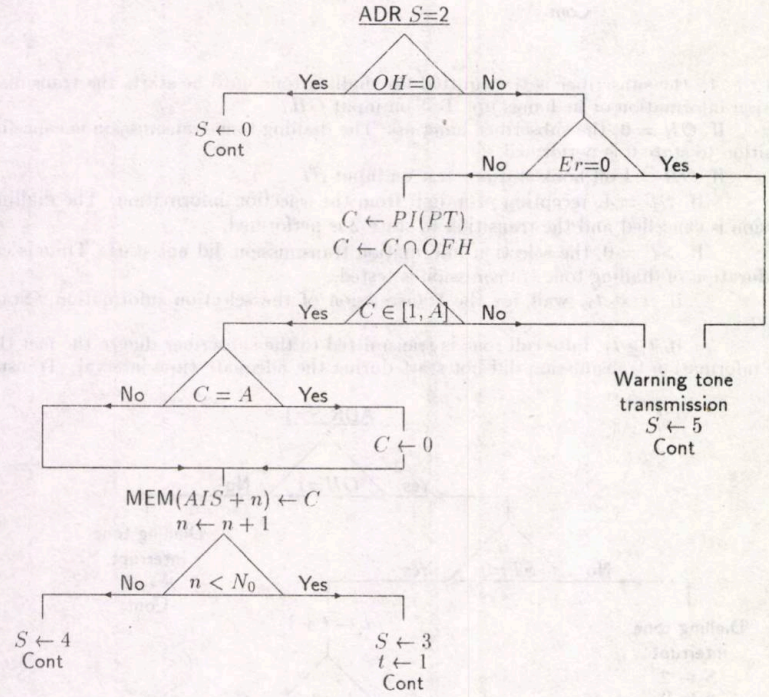

S t a t e 3: reception of the pause between two digits of selection information and test of input OH.

If $OH = 0$, then the subscriber hung up and the transition to state 0 is performed.

If $OH = 1$, then a test is performed to determine if a new digit of selection information was received.

If $ST = 1$, a new digit of the selection information was received and the transition to state 2 is performed.

If $ST = 0$, the pause between the two digits continues. Its duration is counted and tested:

if $t < t_1$, state 3 is preserved;

if $t \geq t_1$, the maximal admissible duration of a pause between two digits is exceeded: the subscriber is sent the false call tone and the transition to state 5 is performed.

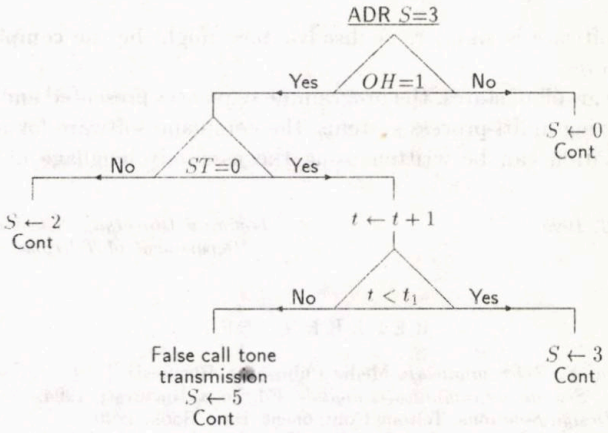

S t a t e 4: processing of the selection information. This state continues the process of establishing a telephone link through the exchange. Test on input OH.

If $OH = 0$, then the subscriber hung up and the transition to state 0 is performed.

If $OH = 1$, the process continues.

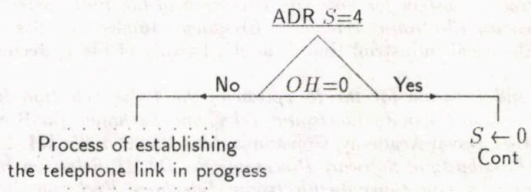

S t a t e 5: false call or warning tone is transmitted to the subscriber until it hangs up.

If $OH = 1$, state 5 is preserved.

If $OH = 0$, false call tone transmission is cancelled and the transition to state 0 is performed.

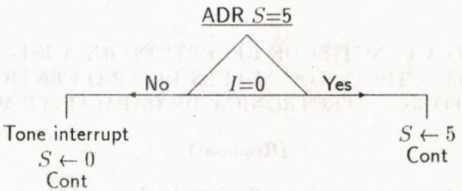

5. Conclusions

The use of tone and pulse selection information receivers in the hardware structure of the individual subscriber circuits allows to increase the number of the exchange's subscribers, since the command software, working in real time, may have the duration of the interruption period of 100 ... 200 ms (compared to 2 ... 5 ms). Moreover,

the command software is simpler. A disadvantage might be the complexity of the hardware structure.

Based on the graph of states, the programme sequences presented and the method of software realizing multi-process systems, the command software for receiving the selection information can be written using the assembly language of the specific command unit.

Received, October 1, 1996

Technical University "Gh. Asachi", Jassy, Department of Telecommunications

REFERENCES

1. R ă d u l e s c u T., *Telecomunicaţii*. Media Publishing, Bucureşti, 1994.
2. B o r c o c i E., *Sisteme de comunicaţie digitale*. Ed. Vega, Bucureşti, 1994.
3. . . . *Telecom Design Solutions*. Teltone Component. Data Book, 1990.
4. . . . INTEL 8051 Family Microcontroller, Data Book, 1990.
5. R o n y P.R., D.G.L., J.A.T., *Microcomputer Interfacing and Programming*. Howard W. Sams & Co.Inc., 1987.
6. D u m a P., *Graph of Stages Depicting the Process of Establishing a Telephone Connection*. Proc. of the Internat. Symp. on Signals, Circuits and Systems, Faculty of Electronics and Telecommunications, Jassy, IEEE Romania, Section CAS Ch., Nov. 4-5, 1993, 181-184.
7. D u m a P., *Multi-Process System for Software Reception of the Pulse Selection Information in a Low Capacity Electronic Telephone Exchange*. Jubilee Sci. Ses. "85 Years from Founding of Electrical Industrial High School", Faculty of Electrotechnics, Jassy, Nov. 2-4, 1995.
8. D u m a P., *Command Program for the Reception of the Pulse Selection Information One Subscriber in a Low Capacity Electronic Telephone Exchange* (in Romanian). XIVth Sci. Ses., Military Naval Academy, Constanţa, May 25-26, 1995, **III**, 277-282.
9. D u m a P., *About a Possibility of Software Processing the DTMF Selection Information from One Subscriber in a Low Capacity Electronic Telephone Exchange*. The 5th Internat. Conf. on Optimization of Electric and Electronic Equipments, "Transilvania" University, Brashov, May 15-17, 1996, 513-520.
10. D u m a P., *Multi-Process System for Software Reception of DTMF Selection Information in a Low Capacity Electronic Telephone Exchange*. National Symp. on Autom. a. Testing, A&T'96-THETA 10, May 23-24, 1996, Cluj-Napoca, 361-366.

INTEGRAREA FUNCŢIEI DE RECEPŢIONARE A INFORMAŢIEI DE SELECŢIE IN TON ŞI PULS DINTR-O CENTRALĂ TELEFONICĂ ELECTRONICĂ DE CAPACITATE MICĂ

(Rezumat)

Se prezintă structura hard a circuitului individual de abonat dintr-o centrală telefonică de capacitate mică pentru care funcţia de recepţionare a informaţiei de selecţie în ton/puls este integrată cu receptoarele TELTONE: M 957-01/M 959. De asemenea sunt descrise graful de stări şi programul de comandă pentru recepţionarea informaţiei de selecţie prin soft.

BULETINUL INSTITUTULUI POLITEHNIC DIN IAŞI
Tomul XLIV (XLVIII), Fasc. 1-2, 1998
Secţia III
ELECTROTEHNICĂ. ENERGETICĂ. ELECTRONICĂ

C.D. 621.316.722

MÉTHODE DE PROGRAMMATION QUADRATIQUE SUCCESSIVE

PAR
GH. CÂRŢINĂ et GH. HAZI

En partant d'un modèle mathématique plus précis pour l'optimisation du réglage tension/puissance réactive et en s'appuyant sur l'algorithme du gradient réduit conjugué, on propose une méthode de programmation quadratique successive en deux phases, qui s'avère très efficace meme pour les réseaux électriques de grande taille.

1. Introduction

Le réglage tension/puissance réactive, (VQ), dans les réseaux électriques, représente un problème très important et complexe, demandant un grand effort et temps de la part des ingénieurs de système, qui doivent définir les stratégies correspondantes et réaliser la mise en oeuvre des algorithmes de conduite.

Le problème du réglage VQ a deux aspects différents [1]:

a) l'optimisation des régimes (prévisibles);

b) la correction des tensions qui ont franchi leurs frontières, pour certaines contingences.

Dans le cas du premier aspect, on peut déceler deux objectifs:

a_1) l'optimisation du plan de tension;

a_2) la minimisation des pertes de puissance active.

La réalisation du plan optimal de tension est conditionnée par l'exactitude de la prévision des puissances. Dans le cas d'une faible prévision il est nécessaire une autre prévision, à très court terme ($15' \dots 30'$), partant de l'estimation de l'état actuel, suivie de l'optimisation correspodante [5].

L'optimisation du réglage VQ dans les réseaux électriques consiste à minimiser une fonction des variables $[\theta]$, $[U]$, $[W]$, tout en respectant les équations algébriques du réseau et les contraintes d'inégalité, qui traduisent les limites de fonctionnement des composants du réseau. Un tel problème se pose sous la forme d'un programme nonlinéaire:

$$F([\theta],[U],[W]) = \Delta P([\theta],[U],[W]) + \tag{1}$$
$$+\sum_{i\in q} CP_i(QP_i) + \frac{1}{T}\sum_{i,j\in r} C\mathrm{PLOT}_{i,j\in r}(\Delta W_{i,j}) = \min!,$$

$$P_i([\theta],[U],[W]) - P_i^{\text{imp}} = 0, \quad i \in n \setminus e, \text{ dimension } N-1, \tag{2}$$

$$Q_i([\theta],[U],[W]) - Q_i^{\text{imp}} = 0, \quad i \in C, \text{ dimension } C, \tag{3}$$

$$U_i^{\min} \le U_i \le U_i^{\text{Max}}, \quad i \in n, \text{ dimension } N, \tag{4}$$

$$Q_i^{\min} \le Q_i([\theta],[U],[W]) \le Q_i^{\text{Max}}, \quad i \in q, \text{ dimension } Q, \tag{5}$$

$$W_{i,j}^{\min} \le W_{i,j} \le W_{i,j}^{\text{Max}}, \quad i,j \in r, \text{ dimension } R, \tag{6}$$

$$0 \le I_{i,j}^2([\theta],[U],[W]) \le I_{i,j}^{\text{Max}\,2}, \quad i,j \in l, \text{ dimension } L, \tag{7}$$

où: $F([\theta],[U],[W])$ représente la fonction objectif du modèle, [MW]; $\Delta P([\theta],[U],[W])$ – les pertes de puissance active, [MW]; $CP_i(QP_i)$ – le coût de la production de la puissance réactive QP_i, dans la source réactive du noeud i, [MW]; $C\text{PLOT}_{i,j}(\Delta W_{i,j})$ – le coût du changement des plots au transformateur (i,j), [MW]; T – la période pour laquelle on réalise l'optimisation, [h]; $[U]$ – la matrice des tensions aux noeuds, dimension N; $[\theta]$ – la matrice des angles des tensions aux noeuds, par rapport à la tension du noeud d'équilibre, dimension $N-1$; $[W]$ – la matrice des plots des transformateurs, dimension R; e – le noeud d'équilibre du réseau; c, q, r – les ensembles des noeuds consommateurs, avec réglage de la puissance réactive, respectivement, avec des transformateurs ayant le réglage des plots.

Les variables du modèle d'optimisation sont:

$$[Z] = [[X] \;\; [Y]]_t; \quad [X] = [[U_q] \;\; [W]]_t; \quad [Y] = [[\theta] \;\; [U_c]]_t, \tag{8}$$

où: $[X]$ sont les variables de réglage (indépendantes), $[Y]$ – les variables d'état (dépendantes).

2. Les méthodes de programmation quadratique successive

Ces méthodes sont considérées aujourd'hui comme les plus efficaces. Elles possèdent une vitesse de convergence superlinéaire et même quadratique, dans le cas des méthodes Newton, ce qui les rend supérieures aux autres méthodes [7].

D'abord on va mettre le modèle d'optimisation du réglage VQ sous la forme quadratique. On peut formuler le problème (1),...,(7) sous une forme synthétique à savoir:

$$F(Z_1, Z_2, ..., Z_M) = \min!, \quad M = I + D, \tag{9}$$

$$f_{a_i}(Z_1, Z_2, ..., Z_M) = 0, \quad i = 1, 2, ..., D, \tag{10}$$

$$f_{i_c}(Z_1, Z_2, ..., Z_M) \leq 0, \quad i = 1, 2, ..., M_c, \tag{11}$$

où: I, D et M_c sont le nombre des variables indépendantes, dépendantes, respectivement le nombre des contraintes d'inégalité.

En considérant un point de départ, $[Z^0]$, et en gardant du développement en série Taylor de la fonction objectif, $F([Z])$, les termes du deuxième degré et des contraintes, les termes du premier degré y compris, on obtient le modèle quadratique:

$$FQ([Z]) = F^0 + [\nabla F]_t[\Delta Z] + \tfrac{1}{2}[\Delta Z]_t[H][\Delta Z] = \min!, \tag{12}$$

$$[f_a^0] + [Jf_a][\Delta Z] = 0, \tag{13}$$

$$[f_i^0] + [Jf_i][\Delta Z] \leq 0, \tag{14}$$

où: $[\Delta Z]$ représente la matrice colonne des nouvelles variables, $[H]$ – le hessien de la fonction objectif, $[f_a]$, $[f_i]$, $[Jf_a]$, $[Jf_i]$ – les matrices colonne et les jacobiens des contraintes actives (d'égalité), respectivement, libres (d'inégalité).

De cette façon l'optimisation du réglage VQ peut être considérée un problème de programmation quadratique successive, en deux phases:

1° *La phase I*: la détermination d'une solution réalisable du modèle nonlinéaire (9),...,(11).

2° *La phase II*: la solution du modèle quadratique (12),...,(14).

Si la solution de la première phase n'est pas difficile, celle de la deuxième est plus compliquée. Pour aboutir à un algorithme efficace on effectue plusieurs transformations. Ainsi, en utilisant la relation (8), le modèle quadratique (12),...,(14) peut être mis sous la forme:

$$\begin{aligned} FQ([\Delta X], [\Delta Y]) &= F^0 + [\nabla F_x][\Delta X] + [\nabla F_y][\Delta Y] + \\ &+ \tfrac{1}{2}[\Delta X]_t[H_{xx}][\Delta X] + \tfrac{1}{2}[\Delta Y]_t[H_{yy}][\Delta Y] + [\Delta X]_t[H_{xy}][\Delta Y] = \min!, \end{aligned} \tag{15}$$

$$[f_a^0] + [Jf_{a_x}][\Delta X] + [Jf_{a_y}][\Delta Y] = 0, \tag{16}$$

$$[f_i^0] + [Jf_{i_x}][\Delta X] + [Jf_{i_y}][\Delta Y] \leq 0. \tag{17}$$

Le gradient réduit de la fonction quadratique, $FQ([\Delta X], [\Delta Y])$, (v. rel. (15)), a pour expression:

$$[\nabla FQ_r] = [\nabla FQ_x] - [Jf_{a_x}]_t[Jf_{a_y}]_t^{-1}[\nabla FQ_y], \tag{18}$$

où

$$[\nabla FQ_x] = [\nabla F_x] + [H_{xx}][\Delta X] + [H_{xy}][\Delta Y], \tag{19}$$

$$[\nabla FQ_y] = [\nabla F_y] + [H_{yy}][\Delta Y] + [H_{xy}]_t[\Delta X]. \tag{20}$$

Après l'élimination des variables $[\Delta Y]$, des relations (15),...,(20), on obtient la nouvelle forme du modèle quadratique:

$$FQR([\Delta X]) = FQR^0 + [G][\Delta X] + \tfrac{1}{2}[\Delta X]_t[H_r][\Delta X], \tag{21}$$

$$[\Delta Y] = [T_y][\Delta X] + T \tag{22}$$

et l'expressions du gradient (réduit):

$$[G] = [\nabla FQR] = [G_0] + [H_r][\Delta X] \tag{23}$$

où on a utilisé les notations:

$$[G_0] = [\nabla F_x] + [T_y]_t[\nabla F_y] + [[H_{xy}] + [T_y]_t[H_{yy}]][T], \tag{24}$$

$$[H_r] = [H_{xx}] + [H_{xy}][T_y] + [T_y]_t[H_{xy}]_t + [T_y]_t[H_{yy}][T_y], \tag{25}$$

$$[T_y] = -[Jf_{a_y}]^{-1}[Jf_{a_x}]; \quad [T] = -[Jf_{a_y}]^{-1}[f_a^0]. \tag{26}$$

Avec les expressions ci-dessus on peut démarrer le processus itératif d'optimisation du modèle quadratique (21), (22):

$$[\Delta X_k] = [\Delta X_{k-1}] + \alpha_k[D_k^0]; \quad [D_k^0] = \frac{[D_k]}{|[D_k]|}; \quad k = 1, 2, ..., \tag{27}$$

où $[D_k]$ et α_k représentent la direction, respectivement le pas de déplacement du point $[\Delta X]$ dans l'itération k. Si l'on utilise l'algorithme du gradient conjugué, le point $[\Delta X_k]$ est déterminé comme minimum de la fonction quadratique $FQR([\Delta X])$, dans la direction $[D_k]$:

$$[D_k] = -[G_k] + \frac{[G_k]_t[G_k]}{[G_{k-1}]_t[G_{k-1}]}[D_{k-1}], \quad k > 1; \tag{28}$$

$$[D_k] = -[G_k], \quad k = 1; \tag{29}$$

$$\alpha_{\text{opt}} = -\frac{[G_k]_t[D_k^0]}{[D_k^0]_t[H_r][D_k^0]}. \tag{30}$$

Afin d'observer les contraintes d'inégalité, (v. rel.(17)), le pas de déplacement doit être inférieur à la valeur admissible:

$$\alpha_{\text{ad}} = \min_j(\alpha_j); \quad \alpha_j = \frac{f_{l_j}(\Delta X_{k-1})}{[\nabla f_{l_{x_j}}]_t[D_k^0]}; \quad \alpha_k = \min(\alpha_{\text{opt}}, \alpha_{\text{ad}}). \tag{31}$$

Les deux algorithmes de l'optimisation du réglage VQ sont:

A. *La première phase*: la détermination d'une solution réalisable du modèle non-linéaire (9),...,(11):

1° Initialisation de $[Z]$, $[Z] = [Z^0]$.

2° On calcule les valeurs: $[H]$, $[\nabla F]$, $[J_a]$, $[J_l]$, $[F^0]$, $[f_a]$, $[f_l]$.

3° On calcule les variables $[\Delta Z]$, comme solutions du modèle quadratique.

4° $[Z] = [Z] + [\Delta Z]$.

5° Si $|[\Delta Z]| >$eps, on revient à 2°.

6° STOP.

B. *La deuxième phase*: la solution du modèle quadratique (21).....(23):

1° Initialisation: $k = 0$, $[\Delta Z] = 0$.

2° On calcule le gradient réduit (G), la direction d'optimisation (D_k), le pas de déplacement (α_k) (v. rel.(23), (28) et (31)).

3° On calcule les variables $[\Delta X]$, (v. rel.(27)).

4° On calcule les variables $[\Delta Y]$, (v. rel.(22)).

5° Si toutes les directions sont bloquées, SAUT à 7°.

6° Si une contrainte d'inégalité devient active, on change la base et on revient à 2°.

7° STOP.

Tableau 1

Variable	U_{46}	$W_{1,6}$	$W_{4,31}$	$W_{5,46}$	$W_{2,12}$
ΔFQR, [MW]	0,0358	-0,0243	-0,0251	-0,0485	-0,148
ΔFQR, [%]	-12,71	-8,63	-8,90	-17,22	-52,54

La méthode proposée a été testée pour plusieurs réseaux à HT. Dans tous les cas le minimum a été atteint pratiquement après trois itérations. Le Tableau 1 présente, pour un réseau à HT avec 50 noeuds, la contribution de chaque variable de réglage au processus d'optimisation. Bien que l'importance du réglage *on-line* VQ est généralement acceptée, il faut souligner l'existance de nombreux obstacles dans la réalisation pratique de cet objectif. Les obstacles concernent les exigences de la transmission des données, la complexité des algorithmes, le temps de calcul, etc. et ils limitent l'utilisation *on-line* du réglage VQ.

Pour franchir ces difficultés on propose à introduire un coefficient d'efficience, „Efficiency Coefficient" (EC), pour mesurer l'effet des différentes variables de réglage:

$$EC_{k,u} = S_{k,u}\Delta u^{\mathrm{Max}}, \tag{32}$$

où $S_{k,u}$ est la sensibilité de réglage, Δu^{Max} – la réserve de réglage de la variable u.

Dans les problèmes pratiques on constate qu'on obtient de très bons résultats avec cet algorithme pseudo-optimal qui „sacrifie" l'optimisation mathématique en faveur de l'efficience et de la rapidité. Dans le cas du réseau considéré (Tableau 1) la solution pseudo-optimale obtenue avec la relation (32) – un réglage successif – (W_{2-12}, U_{46}, W_{1-6}) – peut remplacer la solution optimale exacte, ce qui simplifie le réglage *on-line*.

3. Conclusions

Du point de vue pratique la méthode d'optimisation proposée est très précise et fournit la solution dès les premières itérations. Cette efficacité est due à la grande vitesse de convergence de la programmation quadratique.

Reçue le 26 mars 1997

Université Technique „Gh. Asachi", Jassy,
Chaire d'Energetique

BIBLIOGRAPHIE

1. Florez J., Tapia A., Criado R., Grijalba J.M., *Secondary Voltage Control Based on a Robust Multivariable PI Controller*. 11th PSCC, Avignon, Aug. 30 - Sept. 9, 1993, vol. **II**, 1011-1016.
2. Liu X., Vialas C., Ilic M., Athans M., Heilbronn B., *A New Concept for Tertiary Coordination of Secondary Voltage Control on a Large Power Network*. 11th PSCC, Avignon, Aug. 30 - Sept. 9, 1993, vol. **II**, 995-1002.
3. Abdul-Rahman K.H., Shahidehpour S.M., Daneshdoost M., *An Approach to Optimal VAR Control with Fuzzy Reactive Loads*. IEEE Trans. on Power Systems, **10**, *1*, 88-94 (1995).
4. Ying-Tung Hsiao, Hsiao-Dong Chiang, Chun-Chang Liu, Yuan-Lin Chen, *A Computer Package for Optimal Multi-objective VAR Planning in Large Scale Power Systems*. IEEE Trans. on Power Systems, **9**, *2*, 668-675 (1994).
5. Corsi S., Marannino P., Losignore N., Moreschini G., Piccini G., *Coordination between the Reactive Power Scheduling Function and the Hierarchical Voltage Control of EHV ENEL System*. IEEE Trans. on Power Systems, **10**, *2*, 686-694 (1995).
6. Castro C.A., Bose A., *Correctability of Voltage Violations on-line Contingency Analysis*. IEEE Trans. on Power Systems, **9**, *3*, 1651-1657 (1994).
7. Blanchon G., Bonnans J.F., Dodu J.C., *Application d'une méthode de programmation quadratique successive à l'optimisation des puissances dans les réseaux électriques de grande taille*. EdF, Bull. DER, Série C, *2*, 68-101 (1991).
8. Carţină Gh., Georgescu Gh., Gavrilaş M., Bonciu C., *Reţele neuronale artificiale şi sisteme expert în energetică*. Ed. „Gh.Asachi", Iaşi, 1994.

METODĂ DE PROGRAMARE PĂTRATICĂ SUCCESIVĂ

(Rezumat)

Se prezintă o metodă de programare pătratică succesivă, bazată pe gradientul redus conjugat, care se dovedeşte foarte eficientă în problemele de optimizare.

BULETINUL INSTITUTULUI POLITEHNIC DIN IAŞI
Tomul XLIV (XLVIII), Fasc. 1–2, 1998
Secţia III
ELECTROTEHNICĂ. ENERGETICĂ. ELECTRONICĂ

D.C. 621.315.052

SOME ASPECTS REGARDING THE POWER FLOW ANALYSIS USING A FUZZY LOAD DESCRIPTION

BY

EUGEN BÂRLĂDEANU, AL. POEATĂ and MONICA MUŞAT

Some aspects related to the optimal operation states of the power system using a fuzzy load description are presented. For finding the optimal power flow, from the economical point of view (the cost of energy generation), there can be used the fuzzy linear programming methods. A problem that must be considered is taking into account those constraints that did not appeared in the linear programming model. The paper presents a method for finding the optimal variations of the generated powers such as the weak constraints related by the powers flow be satisfied as good as possible.

1. Introduction

Lately new mathematical models which can take into account the uncertainties about the loads appeared. These uncertainties are due, mainly, to the loads forecasting which depends on a series of economic and political scenarios. The uncertainty of the loads, given sometimes by linguistic declarations, can be modelled using the Fuzzy Set Theory. In essence, the Fuzzy Set Theory replaced the concept of "probability" with that of "possibility". Thus, the linguistic declaration "the load is between $P^{(1)}$ and $P^{(4)}$, but the best estimation is between $P^{(2)}$ and $P^{(3)}$" is transformed into a fuzzy number (FN) with a trapezoidal membership function like the one in the Fig. 1.

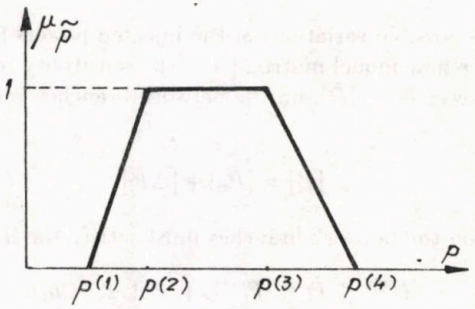

Fig. 1.– Trapezoidal fuzzy load.

The problem of finding the optimal power flow for an electric network considering the loads as FNs is reduced now to a fuzzy linear programming problem, where the objective function is represented by the generation costs for the electric power [1]:

$$\tilde{Z} = \sum_{i=1}^{N_g} a_i \tilde{P}_i, \tag{1}$$

where: $\tilde{Z}$ is the total generation cost (FN); a_i – the specific generation cost of generator i; $\tilde{P}_i$ – the fuzzy power of generator i; N_g – the number of generators.

The equality constraints come from the powers flow equations and the inequality ones from ordering the values corresponding to the trapezoidal membership functions and, also, from the limits imposed to the generators. The objective function is a sum of FNs and the minimisation problem is reduced to the minimisation of the removal (the mean value), $\mathrm{Rem}(\tilde{Z}, 0)$ gives by the relation [1], [5]:

$$\mathrm{Min}\,\mathrm{Rem}(\tilde{Z}, 0) = \frac{\mathrm{Min}(Z^{(1)} + Z^{(2)} + Z^{(3)} + Z^{(4)})}{4}, \tag{2}$$

where $Z^{(1)}, \ldots, Z^{(4)}$ are the breaking points for the trapezoidal membership function for the FN $\tilde{Z}$.

If for finding the powers flow is used a DC power flow model, then the relation (2) and the equality and inequality constraints allow to be determined the optimal (fuzzy) powers produced by the generators. But, besides the inequality constraints related by the powers of the generators (hard constraints), there are also some constraints for the powers flow on the branches of the electric network. The fuzzy power flows, using a DC fuzzy model flow, can be obtained considering the next steps:

a) The voltage angles, $[\theta_d]$, and the branches powers, $[P_{dl}]$, will be determined using the mean values for the powers of the generators and loads.

b) The possible variations for the voltage angles, $[\Delta\tilde{\theta}]$, and for the powers flow in the branches, $[\Delta\tilde{P}_l]$, will be calculated taking into account the previous calculated values:

$$[\Delta\tilde{\theta}] = [B]^{-1}[\Delta\tilde{P}], \tag{3}$$

$$[\Delta\tilde{P}_l] = [A][\Delta\tilde{P}], \tag{4}$$

where: $[\Delta\tilde{P}]$ is the possible variations of the injected powers from the mean values; $[B]$ – the DC power flow model matrix; $[A]$ – the sensitivity coefficient matrix.

c) The fuzzy power flow, $[\tilde{P}_l]$, on the network branches will be determined with the relation:

$$[\tilde{P}_l] = [P_{dl}] + [\Delta\tilde{P}_l]. \tag{5}$$

The fuzzy powers on the network branches must satisfy the inequalities:

$$P_{l_i}^{\min} \leq \tilde{P}_{l_i} \leq P_{l_i}^{\max}, \ (i = 1, 2, \ldots, n_l), \tag{6}$$

where n_l is the number of network branches.

These constraints are weak ones, in contrast with those that refer to the generators powers, because there are accepted little oversteps.

If it is wanted to find the best solution for the these inequalities, it is necessary to correct the operational state by modifying the nodes injected powers.

There are known several methods [1], [3] for correcting the state of the electric system, but, those methods give the membership functions with special formes for the fuzzy generated powers. Many of these functions have not a clear physical meaning.

2. The Correction of the Fuzzy Power Flow

The problem of finding a new distribution for the powers between the generator units, for not overstep the inequalities (6), is difficult (modifying the power for one generator, the power flow in many branches change and not always in a desired way). The direction and the value of these changes, in DC fuzzy model flow, are given by the sensitivity coefficients, a_{ij}, from the matrix $[A]$. The importance of modifying the power for generator j, to decrease the load on the line i, depends on the line load, on the corresponding sensitivity coefficient and, also, on the effects on the others branches. This importance may be expressed by a coefficient (factor) given by the relation:

$$W_{ij} = \mu_{H_i} |a^*_{ij}| \mu_{N_{ij}}, \tag{7}$$

where: μ_{H_i} is the load factor for the branch i given by Fig. 2 ($\tilde{P}_{H_i}$ is the fuzzy power corresponding to a "heavy" load and $\tilde{P}_i$ - the fuzzy load flows on this branch); a^*_{ij} - the normalised sensitivity coefficient; $\mu_{N_{ij}}$ - the non-influence degree of others branches when the generator's j power varies in the way of decreasing the load on line i:

$$\mu_{N_{ij}} = \frac{\sum\limits_{\substack{k=1 \\ (k \neq i)}}^{n_l} (1 - \mu_{H_k}) |a^*_{kj}|}{\sum\limits_{\substack{k=1 \\ (k \neq i)}}^{n_l} |a^*_{kj}|}. \tag{8}$$

To calculate the degree $\mu_{N_{ij}}$ one must consider only the branches for which the load increases when the load on the line i decreases because of the power variation (increase or decrease) of the generator j. The form (8) of these degree is the consequence of the following reasoning: "the lower the line k is loaded, unload given by $(1 - \mu_{H_k})$, the less the negative influence of the power variation for the generator j is". When the influence is very weak (for low loaded branches) the degree is almost one and when the influence is strong (many loaded branches) this degree is zero.

If there are many overloaded branches, the optimal variation ΔP_j for the power of generator j may be determined with the relation:

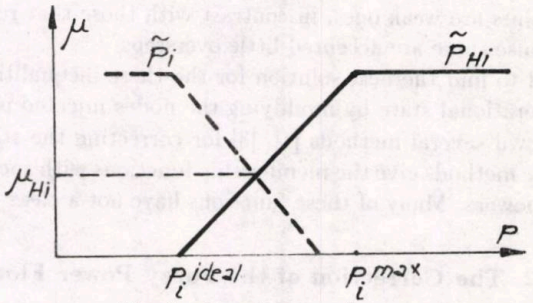

Fig. 2.– Branch power flow.

$$\Delta P_j = \frac{\sum_{i=1}^{n'} W_{ij} \Delta P_{ij}}{\sum_{i=1}^{n'} W_{ij}}, \tag{9}$$

where: n' is the number of the overloaded branches; ΔP_{ij} – the maximum variation rate for the power of generator j (depending on line i, this rate may be more or less than zero).

Thus, if overloaded branches appear after knowing the optimal power flow or in the operation time, then may be determined the optimal variation for the generators' powers having fuzzy information about the consumers loads.

The problem is simplified if a lot of the loads and generators' powers are considered modifying together (increasing or decreasing simultaneously), in contrast with the general case, which is taking into account in this paper, when there are possible combination of these variables.

3. Numerical Example

For illustrating the proposed method, an electric system with 3 nodes and 3 branches is considered (Fig. 3).

The loads and lines characteristics are given in Tables 1 and 2.

Table 1
Fuzzy Load Characteristics

Node	$\tilde{P}_c$, [MW]				Central value
	$P_c^{(1)}$	$P_c^{(2)}$	$P_c^{(3)}$	$P_c^{(4)}$	MW
1	50	55	60	65	57.5
2	100	110	120	130	115.0

If we presume the fuzzy optimal generations are those in Table 3, we obtain the fuzzy power flow given in Table 4.

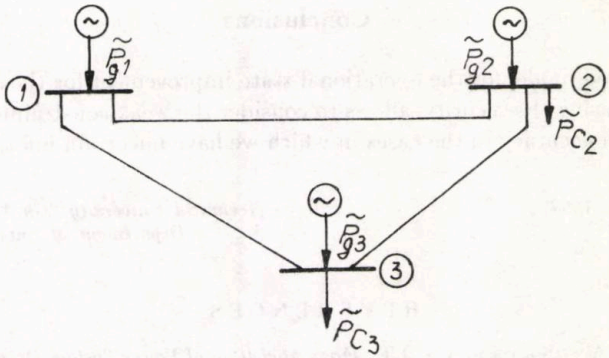

Fig. 3.– System configuration.

Table 2
Lines Data

Branch number	Sending bus	Receiving bus	X Ω	P^{ideal} MW	P^{max} MW
1	1	2	24	30	40
2	1	3	20	70	90
3	2	3	28	25	30

Table 3
Fuzzy Generation

Node	$\tilde{P}_{g_i}$ [MW]				Central value
	$P_g^{(1)}$	$P_g^{(2)}$	$P_g^{(3)}$	$P_g^{(4)}$	MW
1	80	80	85	95	85.0
2	40	50	50	50	47.5
3	30	35	45	50	40.0

Table 4
Fuzzy Power Flow

Branch number	$\tilde{P}_l$, [MW]				Central value
	$P_l^{(1)}$	$P_l^{(2)}$	$P_l^{(3)}$	$P_l^{(4)}$	MW
1	13.720	21.152	29.963	40.045	27.220
2	36.300	48.860	65.050	80.950	57.790
3	5.350	14.470	21.420	27.400	17.210

We can see that the line *2* is "possible" to be overloaded. For knowing what generators (the node *2* or *3*) are more appropriate to be used for unloading the line *2*, the degrees W_{22} and W_{23} will be determined considering that the normalised sensitivity coefficient matrix is:

$$[A^*] = \begin{bmatrix} -0.915 & -0.378 \\ -0.460 & -1.000 \\ 0.460 & -0.377 \end{bmatrix}. \tag{10}$$

It results:

$$W_{22} = 0.28 \cdot 0.46 \cdot (1 - 0.06) = 0.121, \qquad W_{23} = 0.28 \cdot 0.377 \cdot 1 = 0.105. \tag{11}$$

Thus, with the constant fuzzy load presumption is more useful to increase the generated power of the node *2*. In this way a little overload on line *3* being produced.

4. Conclusions

The proposed model for the operational state improvement for the electrical systems, for increasing the security, allows to consider the weak constraints for the load flow with much accuracy in the cases in which we have uncertain information about the loads.

Received May 14, 1997

Technical University "Gh.Asachi", Jassy, Department of Energetics

REFERENCES

1. Miranda V., Saraiava J.T., *Fuzzy Modelling of Power System Optimal Load Flow.* IEEE Trans. on Power Systems, **7**, *2*, 843-849 (1992).
2. Saraiava J.T., Duarte F.O., *Enhanced Fuzzy Power Flow Models Integrating Correlation Between Nodal Injections.* Computer Sci. a. Telecom. Proc., **2**, 8th Mediteranian Electrot. Conf., May 1996, Italy, 885-888.
3. Saraiava J.T., Miranda V., *Impact on Some Planning Decisions from a Fuzzy Modelling of Power Systems.* IEEE Trans. on Power Systems, **9**, *2*, 819-825 (1994).
4. Nümuro T., Yokoyama R., *Post-processing of Economic Despatch Solutions for Security Enhancement Based on Approximate Reasoning.* IEEE Trans. on Power Systems, **2**, *2*, 982-988 (1996).
5. Barlădeanu E., *Contribuţii la ameliorarea metodelor de studiu privind regimurile şi dezvoltarea sistemelor electroenergetice.* Ph.D. Diss., Techn. Univ. "Gh.Asachi", Jassy, 1996.

CONSIDERAŢII PRIVIND STUDIUL REGIMURILOR REŢELELOR ELECTRICE UTILIZAND DESCRIEREA FUZZY A SARCINILOR

(Rezumat)

Se prezintă unele aspecte ale exploatării optimale a sistemelor electroenergetice utilizand reprezentarea fuzzy a sarcinilor. Determinarea regimului optim, din punct de vedere al costului producerii energiei, se poate efectua prin metode specifice programării liniare fuzzy. Se pune problema respectării şi a restricţiilor care nu au intrat în modelul de programare liniară. Se propune o metodă de determinare a modificărilor optimale ale puterilor centralelor astfel încat „restricţiile slabe" legate de circulaţia puterilor să fie cat mai bine îndeplinite.

BULETINUL INSTITUTULUI POLITEHNIC DIN IAŞI
Tomul XLIV (XLVIII), Fasc. 1–2, 1998
Secţia III
ELECTROTEHNICĂ. ENERGETICĂ. ELECTRONICĂ

D.C. 621.3.016.45

OPTIMAL SELECTION OF CAPACITORS FOR REACTIVE POWER COMPENSATION IN DISTRIBUTION SYSTEMS USING GENETIC ALGORITHMS

BY

M. GAVRILAŞ, GH. GEORGESCU and DANIELA RĂDĂŞANU

A Genetic Algorithm based approach to the optimal selection of capacitors in power distribution systems is presented. The main advantage of the Genetic Algorithm formulation is that fairly accurate results can be obtained with a very simple problem representation.

1. Introduction

The last decade reveals studies in the field of artificial intelligence, which emphasize initially unexpected abilities of parallel computation techniques to solve optimization problems. Among these techniques, the Genetic Algorithms (GAs) seem to be the best answer to complex problems, especially those dealing with integer optimization.

There is a reach literature which quotes many studies that suggest the use of GAs to solve problems specific to power transmission and distribution, such as: unit commitment, optimal reconfiguration of distribution systems, optimal VAR control or optimal compensation of reactive power [1],...,[3]. This paper presents an application of a GA to the optimal selection of capacitors in reactive power compensation for distribution systems.

2. Genetic Algorithms

GAs are adaptive techniques that determines an optimal or near-optimal solution for an optimization problem using mechanisms specific to genetics and natural evolution. GAs represent the admissible solutions as "strings", which change their structure from the actual to the next generation, directing themselves to the optimal solution. The initial population has a random composition and generations give birth one to another following the "fittest survive" principle. GAs use five major components.

1° *Admissible Solutions* – are represented as strings of a fixed length, which inherently is imposed by the problem itself. The elements of the strings frequently use a binary representation (e.g., 0–1; on–off; present–absent), but recent studies propose strings with real or integer elements.

2° *The Solution Representation* – uses the optimization problem's objective function. This function determines how well the solution fits to the problem, hence its name of "fitness function". By their intimate mechanisms GAs move towards that point in the problem space which maximizes the fitness function. Therefore, if the optimization problem aims to minimizing the objective function, F, the fitness function, f, must be computed as the reciprocal of F ($f = 1/F$).

3° *Reproduction* – using the values of the fitness functions computed in the previous step, a crossover pool is created copying in strings from the actual generation. Those strings with a higher value of the fitness function have a higher probability to produce more offsprings to the next generation. Therefore, more copies of these strings will succeed to reach the crossover pool.

4° *Crossover* – each string in the actual generation contains a part of the information that forms the optimal solution. One way to assemble this information into a single string is to recombine the strings in the crossover pool. The most efficient implementations of the GAs apply a stochastic crossover operator using a probabilistic crossover rate. At the end of this step the population is totaly renewed. The parent strings are replaced by their offsprings, which form a new generation.

5° *Mutation* – it is highly probable to start from an initial population which contains poor information with respect to the optimal solution. In this case there will be no possible crossover operation between the strings in the actual or the ever next generation to drive the GA towards the optimal solution. The population diversification from one generation to another may be encouraged using a mutation operator. Mutations modify at random one or more elements in the string with a probabilistic mutation rate.

3. Optimal Capacitors Selection

The reactive power compensation is known as an efficient way to lower power and energy losses and to maintain the voltage profile within the acceptable limits. Fixed capacitors are widely used as reactive power sources. They may operate on the MV bus of a substation or on the MV or LV buses of the distribution transformers.

For a radial distribution system the problem of optimal capacitor selection consists in the determination of the location, number and type of capacitors, which minimize the daily active energy losses. This problem can be stated as follows:

A. Objective function:

$$F = \sum_{t=1}^{T} \sum_{i=1}^{NF} \sum_{j=S1_i}^{S2_i} I_{jti}^2 r_{ij} = \min!$$

B. Constraints:

a) the available stock of capacitors:

$$\sum_{k=1}^{NT} N_k \leq NC;$$

b) minimum daily reactive power load:

$$q_0 N_k \leq \max_{t=1,\ldots,T}(Q_{kt}),\ k = 1, \ldots, NT;$$

c) voltage limits on the distribution transformer buses:

$$U_k^{\min} \leq U_k \leq U_k^{\max},\ k = 1, \ldots, NT;$$

d) capacity constraint:

$$\sum_{j=S1_i}^{S2_i} I_{jti} \leq I_{\text{admi}},\ i = 1, \ldots, NF,\ t = 1, \ldots, T;$$

e) voltage drop constraint:

$$\sum_{h \in M_i} \sum_{j=S1_h} I_{jth} Z_{jh} \leq \Delta U_{\text{admi}},\ i = 1, \ldots, NF,\ t = 1, \ldots, T,$$

where: T is the period of time considered (for this case $T = 24$ hours); NF – number of feeders; NT – number of distribution transformers; NC – number of capacitors in stock; $S1_i, S2_i$ – the first and the last load section of feeder i; N_k – number of capacitors operating on bus k; I_{jti} – current flow through load section j of the feeder i, at time t; r_{ij} – resistance of load section j of feeder i; q_0 – rated capacity of the capacitors; Q_{kt} – reactive load of the distribution transformer k at time t; $U_k, U_k^{\min}, U_k^{\max}$ – actual, minimum and maximum values of the voltage on bus k; I_{admi} – current limit of feeder i; ΔU_{admi} – voltage drop limit for feeder i; M_i – set of feeders between the power source and feeder i; Z_{jh} – impedance of load on section j of feeder h.

The loads from the secondary of the distribution transformers have been represented using typical active and reactive load curves and direct measurements of currents in the system [4]. Power flows are computed using traditional numerical methods. The GA was implemented for a test system with one feeder and 18 distribution transformers (Fig. 1). For the reactive power compensation we considered a stock of 100 capacitors with rated capacity of 5 kVAr.

4. The Implementation of the GA and Obtained Results

The GA uses strings whose structure may be depicted as follows: a string contains $NT = 18$ elements, one for each distribution transformer. An element memorizes

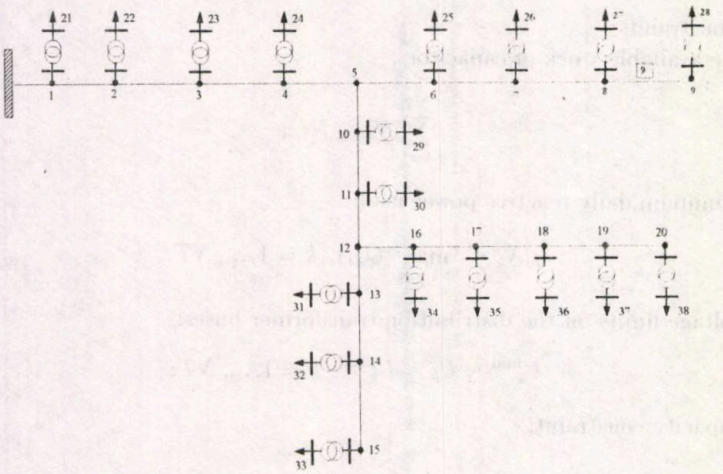

Fig. 1

the number of capacitors operating on the corresponding trnasformer. For the implementation of the GA to the problem of optimal selection of capacitors we have added two new features to the standard implementation, which was described above, namely:

a) The reproduction and crossover stages were assembled into a single step. During this step the parents strings are chosen from the actual population according to the "roulette wheel" selection method described in [2] and submitted to the crossover operation.

b) Mutations act randomly with a prescribed mutation rate, but the number of capacitors from each node modifies between certain prescribed limits Δn (e.g., $\pm 1, \pm 3$).

The implementation of the GA was studied using an initial population of 100 strings and different values for the crossover and mutation rate, with a view to determining the best solution. The crossover rate takes values between 0.6 and 0.9, while the mutation rate ranges from 0.1 to 0.4. For every test we have compared the daily energy losses corresponding to the dominant string with those corresponding to the optimal string. The results are briefly presented and discussed forward.

First we have considered the influence of the parameter Δn. Five pairs of values of this parameter were considered ($\pm 1, \pm 2, \ldots, \pm 5$). The dominant string comes faster close to the optimal one when more capacitors are added or discarded by the mutation operator. Thus, further on we have considered a parameter $\Delta n = \pm 5$.

Then we have studied the influence of the crossover and mutation rate over the performances of the GA. Fig. 2 shows the profile of the energy losses for various mutation rates when the crossover rate is fixed. On the other hand, Fig. 3 shows the same profile for various crossover rates when the mutation rate is fixed. The best solution can be found with a crossover rate of 0.7 and a mutation rate of 0.3.

It is worth to emphasize the way by which the number of capacitors from different

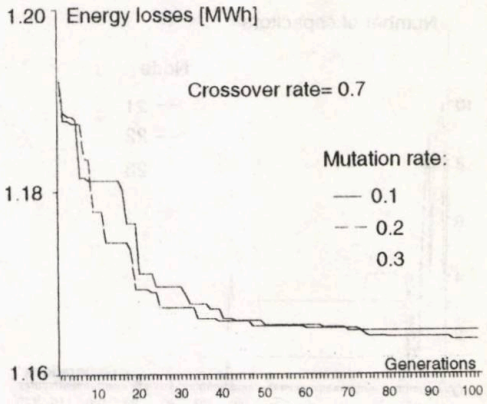

Fig. 2

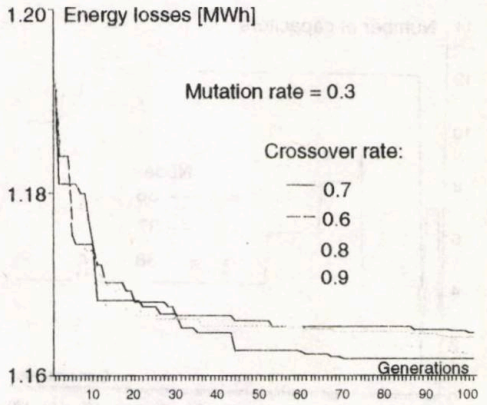

Fig. 3

nodes changes from one generation to another. Figs. 4 and 5 show this evolution for the first and the last three nodes in the system. The trend from these figures describes a normal behaviour, because the reactive power compensation becomes more efficient when applied first to distant loads.

Finally, Fig. 6 shows the variation of the total amount of capacitors installed in the distribution system during the application of the GA. This variable was not controlled during the process. However, Fig. 6 shows that, as a consequence of the intimate mechanisms of the GA, the total amount of installed capacitors tends to the maximum stock. This is a normal behaviour since, if the capacity of the whole stock of capacitors is under the valley load of the system, then the minimum value of energy losses will always be reached only if all the existent capacitors are used. The optimal distribution of the capacitors in the distribution system under analysis is depicted in Table 1.

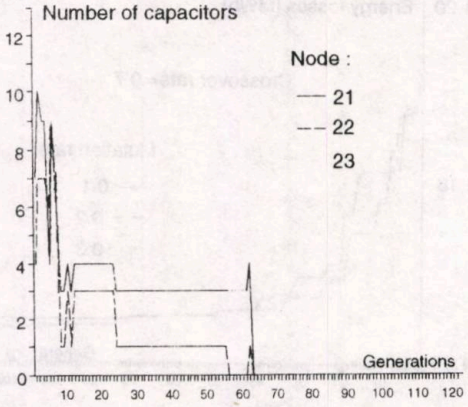

Fig. 4

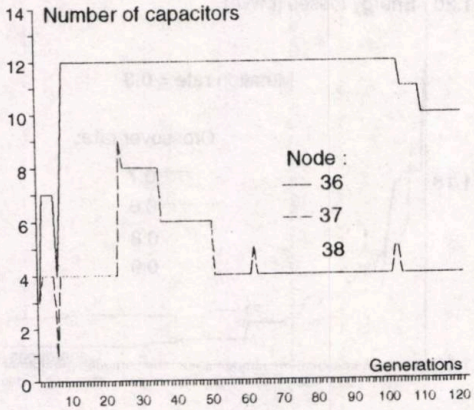

Fig. 5

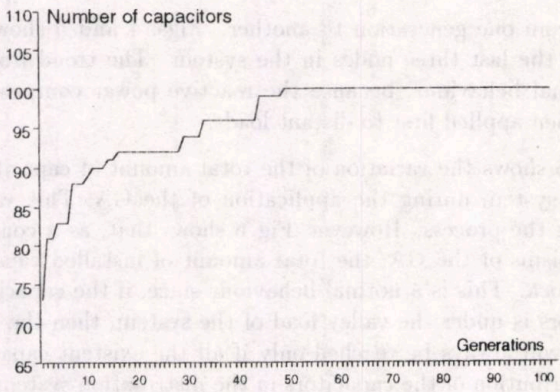

Fig. 6

Table 1

Node	*21*	*22*	*23*	*24*	*25*	*26*	*27*	*28*	*29*	*30*	*31*	*32*	*33*	*34*	*35*	*36*	*37*	*38*
Capacitor	0	0	3	1	6	5	8	11	1	4	9	7	7	5	8	10	4	11
Energy delivered (one day): 127.18 MWh																		
Energy losses before compensation: 1.2660 MWh																		
Energy losses after compensation: 1.1615 MWh										Savings: 104.5 kWh								

5. Conclusions

In comparison with traditional optimization methods, GAs offer two main advantages: a simple and intuitive representation of the admissible solutions; thanks to their parallel mechanisms, GAs can simultaneously analyse more regions in the problem space, thus being less sensitive to local minima.

Received, March 17, 1997

Technical University "Gh.Asachi", Jassy,
Department of Energetics

REFERENCES

1. Nara K., Shicse A., Kitagawa M., Ishihara T., *Implementation of Genetic Algorithms for Distribution Systems Loss Minimum Reconfiguration.* IEEE Trans. on Power Systems, **7**, *3*, 1044-1051 (1992).
2. Wong K.P., Wong Y.W., *Genetic and Genetic/Simulated-Annealing Approaches to Economic Dispatch.* IEE Proc.-Gener. Transm. Distrib., **141**, *5*, 507-512 (1994).
3. Gavrilaş M., Georgescu Gh., *Utilizarea algoritmilor genetici pentru determinarea schemei optime de funcţionare a reţelelor de distribuţie urbană.* Energetica, *6*, s. B, 249-256 (1996).
4. Georgescu Gh., Poeată Al., Gavrilaş M., *Calculul pierderilor de energie în reţelele de distribuţie folosind descompunerea graficelor de sarcină în serii Fourier.* Energetica, *5*, s. B, 223-226 (1995).

SELECTAREA OPTIMALĂ A CONDENSATOARELOR PENTRU COMPENSAREA PUTERII REACTIVE ÎN REŢELELE DE DISTRIBUŢIE UTILIZÂND ALGORITMI GENETICI

(Rezumat)

Se pune în evidenţă posibilitatea utilizării algoritmilor genetici în cazul optimizării repartiţiei surselor de putere reactivă în reţelele de distribuţie. Principalul avantaj oferit de algoritmii genetici îl constituie menţinerea preciziei rezultatelor obţinute în limite foarte bune, asigurând totodată o modelare simplă şi intuitivă a problemei analizate.

BULETINUL INSTITUTULUI POLITEHNIC DIN IAŞI
Tomul XLIV (XLVIII), Fasc. 1–2, 1998
Secţia III
ELECTROTEHNICĂ. ENERGETICĂ. ELECTRONICĂ

MIRCEA-SORIN OPRIŞOR
1936–1997

Pendant l'été 1997 s'est éteint le professeur Mircea O p r i ş o r à la suite d'une maladie incurable.

Né à Jassy, le 20 mars 1936, dans une famille d'intellectuels – le père, ingénieur électricien, professeur à l'Institut Polytechnique, la mère, ingénieur agronome, cadre didactique à l'Institut Agronomique –, il a suivi les cours secondaires au lycée „C. Negruzzi" de sa ville natale, en les terminant en 1954.

Dans la même année il devient étudiant à la faculté d'Electrotechnique de Jassy, obtenant le titre d'ingénieur, dans la spécialité Electromécanique, en 1959.

Il a soutenu sa thèse de doctorat, intitulée „Etudes concernant les possibilités d'utilisation des moteurs asynchrones à double alimentation dans les commandes électriques", en 1974, obtenant le titre scientifique de docteur ingénieur.

M. O p r i ş o r a débuté dans sa profession en travaillant comme ingénieur, d'abord à la Société de Tramways et puis à l'Entreprise Régionale d'Electricité de Jassy. Sa carrière didactique commence en 1965, en qualité d'assistant à la discipline de „Traction électrique", dans le cadre de la faculté d'Electrotechnique de Jassy. Il a déployé toute son activité didactique, de plus de trois décennies, dans cette faculté et dans le même département, celui de l'Utilisation de l'Energie Electrique, montant tous les échelons de l'hiérarchie didactique et obtenant le titre de professeur en 1992. M. O p r i ş o r a conduit des séminaires et des travaux pratiques, a dirigé des projets et a donné des cours aux disciplines de „Traction électrique", „Technologies électriques spéciales", „Utilisation de l'énergie électrique" et „Eclairage électrique".

A côté de l'activité didactique le professeur Mircea O p r i ş o r a déployé une activité scientifique remarquable, concrétisée par 64 articles publiés dans des périodiques scientifiques, dans des volumes des conférences nationales ou internationales ou dans celles des sessions scientifiques. Ses préoccupations scientifiques

ont embrassé une large aire de domaines, commençant par celui des Commandes Electriques et en terminant avec celui de l'Electronique de Puissance.

Il a publié, en collaboration, un manuel de „Traction électrique", à une maison éditrice centrale, ainsi que cinq autres cours et guides de travaux pratiques, dans le cadre de l'Institut Polytechnique de Jassy.

Le professeur Mircea O p r i ş o r a été membre de certaines associations nationales à caractère scientifique (Association Roumaine pour Technologies Nonconventionnelles, Société Professionelle de Commandes Electriques) ainsi que dans la direction de l'Association des Artistes Photographes de Roumanie, en étant un photographe amateur remarcable, avec participations à de nombreuses expositions nationales et internationales.

Le décès prématuré, en pleine activité, du professeur Mircea O p r i ş o r, laisse des regrets unanimes parmi ceux qui l'ont connu.

Université Technique „Gh. Asachi", Jassy,
Chaire d'Utilisation Industrielles,
Commandes Electriques et Automations

BULETINUL INSTITUTULUI POLITEHNIC DIN IAŞI
Tomul XLIV (XLVIII), Fasc. 1–2, 1998
Secţia III
ELECTROTEHNICĂ. ENERGETICĂ. ELECTRONICĂ

RECENZII

BOOK REVIEWS

STROEBE G.H., *Gekonnt telefonieren*. Expert Verlag, Renningen, Germany, 1997, 232 S., ISBN 3-8169-1478-0

Das Telefon ist das private und berufliche Kommunikationsmedium der Gegenwart und vor allem der Zukunft. Es lohnt sich daher, das Verhalten am Telefon zu überprüfen und zu verbessern. Das Buch will den Leser dabei unterstützen. Es bietet nicht Verhaltenstraining mit fertigen Rezepten, sondern: a) behandelt die Vielschichtigkeit der Kommunikation am Telefon; b) zeigt aktuelle, konkrete Probleme auf; c) leitet daraus Methoden und Vorgehensweisen zum besseren Telefonieren ab; d) regt viele praktische Übungen an, die sich allein oder in selbstgebildeten kleinen Arbeitsgruppen mit und ohne externe Unterstützung durchführen lassen; e) enthält Formulare, Fragenkataloge und Prüflisten zur Gesprächsvorbereitung, -durchführung und -auswertung.

Mit einer positiven Einstellung zu sich selbst und zum anderen und mit einem entsprechenden Kommunikationsverhalten (nicht nur am Telefon) können alle Beteiligten nur gewinnen: a) die aktiven Telefonierer durch weniger Streß und mehr Zufriedenheit, weil sie wirksamer und menschlicher miteinander umgehen; b) die Organisationen (Industrie, Verwaltung, Schulen, Krankenhäuser u.s.) durch bessere Kontakte – zu Kunden, zu Lieferanten und innerbetrieblich.

I n t e r e s s e n t e n: Das Buch eignet sich für alle, die viel telefonieren und dies mit weniger Streß und mehr Zufriedenheit tun wollen – Führungskräfte und Mitarbeiter in der Wirtschaft Organisationen der öffentlichen Verwaltung – Selbständige – kundenbezogene Mitarbeiter, die langfristige, gute Beziehungen aufbauen und pflegen möchten – (über-) betriebliche Führungs- und Mitarbeiterseminare.

* * * *Electronics Terminology: A Concise Dictionary. Informatik Rezurch*. Butterworth-Heinemann, Newton, USA, 1996, 76 pp., ISBN 0-7506-9751-2.

Electronics Terminology: A Concise Dictionary consists of two sections, acronyms and glossary, featuring electronics, packaging and production, computer, and semiconductor terms and definitions that are current and straight-to-the-point. Many acronyms and definitions are cross-referenced for complete coverage. Its shirt-pocket size makes it a handy quick-reference source for engineers and technicians on the move.

* * * *Cognitive Processing for Vision & Voice*. Proc. of the Fourth NEC Res. Symp. Edited by T. I s h i g u r o. SIAM Society for Industrial and Applied Mathematics, Philadelphia, USA, 1993, 220 pp., ISBN 0-89871-335-8.

The Fourth NEC Research Symposium was held in Fujiyoshida, Japan, on May 26-27, 1993. The theme, *Cognitive Processing for Vision and Voice*, brought together participants with a variety of scientific backgrounds from universities, institutes, and industries in the United States, Europe, and Japan. Specialists in biological information processing, cognitive psychology, neural networks, vision, voice, semantics, and related disciplines shared ideas and explored future technological possibilities in talks and discussions. The NEC Corporation is proud to have organized this symposium and to publish its proceedings.

Microelectronics technologies have contributed to the growth of the world electronics industry with its enormous volume of VLSI products. Optical technologies have led to very efficient optical fiber communication systems. With these two technologies, both information processing and transmission speeds have been greatly enhanced. However, cognitive processing mechanisms are still unclear. We have yet to succeed in implementing such functions well in computers. Computers cannot yet converse effectively with humans, recognize human faces, or understand natural languages.

Through this series of NEC Research Symposia and their proceedings, the NEC Corporation hopes to make a tangible contribution towards the progress of science and technology, and eventually towards the enhancement of human potential.

FORBES J.R., *Dictionnaire des techniques et technologies modernes. Modern Dictionary of Engineering and Technology.* TEC & DOC LAVOISIER, Cachan, Paris, Vol. **1**, Français-Anglais, 1997, 640 pp., FF 605, GB£ 67, US$ 119; Vol. **2**, Anglais-Français, 1997, 640 p., FF 605, GB£ 67, US$ 119, ISBN 2-7430-018985, 2-7430-0188-7.

Les nouvelles éditions de ces dictionnaires techniques français-anglais et anglais-français comportent maintenant quelque 43 000 entrées; en plus des nombreuses entrées consacrées précédemment à des domaines comme l'informatique, les télécommunications, la robotique, les fibres optiques, les industries alimentaires, les techniques de l'eau la biologie moléculaire et le génie génétique, près de 3 000 nouvelles entrées reflètent dans ces éditions l'importance actuelle de l'informatique, des réseaux et médias, ainsi que de l'écologie et l'environnement.

Elles intéresseront de nombreux industriels, chercheurs, techniciens, traducteurs et interprètes soucieux d'élargir leurs connaissances.

S o m m a i r e. Avant-Propos; Présentation générale et notes explicatives; Abréviations entre parenthèses; Annexes: 1. Éléments chimiques et leurs symboles; 2. Verbes irréguliers courants.

* * *

These general technical dictionaries have now been updated with an additional 3,000 entries which cover developments in areas such as networks, multimedia and the environment. The clear and straightforward layout gives quick and easy access to the 43,000 entries contained in these new and enlarged editions. Translation and spelling differences between British and US usage have been taken into account and frequently used abbreviations are also included.

In short, these are the most complete reference tools dedicated to the evolving technology of the last 20 years or so.

C o n t e n t s. Foreword; General presentation and explanatory notes; Abbreviations in brackets; Appendices: 1. Chemical elements and their symbols; 2. Common irregular verbs.

SKOBELEV O., *Sensordynamik.* Expert Verlag, Renningen, Germany, 1997, 246 S., ISBN 3-8169-1369-5.

Das Werk setzt sich aus drei Bänden zusammen.

Im 1. Band werden dynamische Kennfunktionen von Drucksensoren betrachtet. Der Schwerpunkt der Betrachtung liegt beim druckempfindlichen Element (Membran). Es werden dynamische Modelle, Übergangsfunktionen und Frequenzgänge untersucht. Darüber hinaus werden die Abhängigkeit im Zeit- und Frequenzbereich sowie die dynamischen Abweichungen behandelt. Als Beispiel werden die Konstruktion und die statischen Kennlinien von potentiometrischen Drucksensoren untersucht.

Der 2. Band ist dynamischen Kennfunktionen von Widerstandsthermometern gewidmet. Es werden physikalische Grundlagen und dynamische Modelle des Wärmeaustausches, Übergangsfunktionen, Frequenzgänge und dynamische Abweichungen der Widerstandthermometer beschrieben. Als Beispiele werden die Konstruktionen von Metall- und Halbleiter-Widerstandsthermometern, ihre statischen Kennlinien und Modelle eines stationären Wärmeaustausches untersucht.

Im 3. Band werden dynamische Kennfunktionen der Beschleunigungs-, Schwingungs- und Stoßsensoren untersucht. Im ersten Teil werden Konstruktionsbeispiele des potentiometrischen Beschleunigungssensors beschrieben und seine statischen Kennfunktionen analysiert. Es werden dynamisches Modell, Übergangsfunktionen und Frequenzgänge sowie dynamische Abweichungen des piezoelektrischen Beschleunigungssensors behandelt.

Jeder Band besteht aus zwei Teilen: (1) dem Buch mit der Theorie und praktischen Aufgaben sowie mit Anweisungen für Benutzer; (2) aus einer Diskette mit dem Simulationsprogramm, das die Programmablaufbedingungen für den Aufgabenteil schafft.

Für die Arbeit mit den Programmen ist ein Personalcomputer IBM PC/AT oder ein dazu kompatibler PC mit einem Videoadapter VGA, mit mindestens 512 KByte Arbeitsspeicher, mindestens 1 MByte freier Speicherkapazität auf der Festplatte, dem Betriebssystem MS-DOS 3.30 (oder höher)

und MS WINDOWS 3.1 erforderlich. Das Werk wurde für Studenten und Fachleute mit systemtechnischer Orientierung wie automatisierte Steuerungssysteme, Informationssysteme und Meßsysteme usw. geschrieben.

SHIE QIAN. *Joint Time–Frequency Analysis. Methods and Applications.* Prentice Hall, Hemel Hempstead, England, 1996, 302 pp., ISBN 0-13-254384-2.

Prior to the '90s, joint time–frequency analysis (JTFA) had been continued to academic research because of the complexity of the algorithms and the limitations of computing power. But later progress in the area of JTFA and PC technology have dramatically expanded JTFA applications.

Addressing the area's growing demand for more comprehensive material, *Joint Time–Frequency Analysis. Methods and Applications* offers insight into successful applications and covers both linear and bilinear algorithms. More than a hundred illustrations and an extensive bibliography provide additional support.

Joint Time–Frequency Analysis. Methods and Applications is separated into three parts. Part I reviews classical signal analysis fundamentals for JTFA. Theoretical developments are presented in Part II. Well-known time–frequency algorithms and two proven JTFA algorithms (time–frequency distribution series and adaptive spectrogram) are introduced and their pros and cons are also addressed. Part III discusses three real JTFA applications in the areas of radar image processing, biomedical signal analysis, and economy data analysis contributed by experts in their respective fields. Each chapter begins with a discussion of motivation, progresses to theoretical analysis, and concludes with numerical implementations.

Key topics include: a) Short-Time Fourier Transform (STFT) and Gabor Expansion; b) Wavelets for JTFA; c) Wigner–Ville Distribution and Cohen's Class; d) Adaptive Representation; e) Time-Variant Filtering; f) STFT-, Gabor–Wigner-, and Adaptive Representation-Based Spectrogram.

Also included are two floppy disks containing a limited version of the Joint Time–Frequency Analyzer developed by National Instruments Corporation. Together with the dozen examples found in the book, the reader can quickly learn and experience different JTFA algorithms discussed in this book.

System requirements: Operating systems: Windows 3.1™, Windows 95 and Windows NT™, Minimum hardware specification: IBM-PC or compatible 486, 33 MHz, 8 M RAM, 240 M HD, SVGA monitor.

v. BAECKMANN W. (federführend), *Meßtechnik beim kathodischen Korrosionsschutz.* Expert Verlag, Renningen, Germany, 1992, 226 S., ISBN 3-8169-0889-6.

Korrosionsuntersuchungen in Elektrolyten und im Erdboden sowie die Einrichtung kathodischer Korrosionsschutzanlagen erfordern gründliche elektrochemische und elektrische Messungen. Zur Durchführung dieser Messungen sind Grundkenntnisse der Meßverfahren und praktische Erfahrungen mit den Meßgeräten erforderlich.

Dieser Themenband vermittelt beides. Dem Anfänger erläutert er die spezifischen Merkmale der Korrosionsschutzmessungen; dem Fachmann gibt er mit Hilfe von Formeln, Tabellen und Hinweisen praktische Hilfen für die Lösung seiner Aufgaben.

I n h a l t: Meßtechnische Voraussetzungen für Korrosionsschutz-Untersuchungen – Praxis der Potentialmessung – Bodenwiderstandsmessung und Messungen an Lagerbehältern – Fehlerortung mit Wechselstrom – Messungen an Umhüllungen – Fehlerortung mit Gleichstrom – Wechselstrommessungen – Bestimmungen der Erdausbreitungswiderstände von Anoden – Anhang.

HEILEMANN O. (federführend), *Digitale Übertragungstechnik. PCM-Grundlagen und Meßverfahren.* Expert Verlag, Renningen, Germany, 1992, 261 S., ISBN 3-8169-0768-7.

Aus Gründen der Wirtschaftlichkeit bestand schon immer der Wunsch, über einen einzigen Nachrichtenweg mehr als nur eine Nachricht zu übertragen. Eine Möglichkeit zur Mehrfachausnutzung eines Übertragungswegs ist die Verschachtelung der Nachricht im Zeitmultiplex. Bai dieser Methode wird das Signal nicht kontinuierlich, sondern in Form von zeitlich aufeinanderfolgenden Proben übertrage Diese Proben können in bestimmten zeitlichen Abständen genommen werden,

ohne daß die übertragende Information verfälscht wird. In den Pausen zwischen der Probenentnahme aus einem Signal können Proben von anderen Nachrichten eingefügt und übertragen werden. Werden die Abtastproben in binäre Codenwörter umgewandelt, so spricht man von Pulscodemodulation.

In diesem Themenband werden Kenntnisse über das Verfahren der Pulscodenmodulation über die Systemtechnik und die notwendigen Meßaufgaben vermittelt. Es sind besonders solche Interessenten angesprochen, die private Übertragungsnetze betreiben und die sich in dieses Gebiet schnell einleben müssen. Der Stoff ist für Betriebs- und Wartungspersonal gleichermaßen geeignet wie für Mitarbeiter aus Produktion und Prüfung nachrichtentechnischer Einrichtungen.

ORSZÁGOS MŰSZAKI INFORMÁCIÓS KÖZPONT ÉS KÖNYVTÁR 1983

Data apariţiei: august 1998, Comanda: 167
Coli tipar: 9,5, Tiraj: 275 exemplare

UNIVERSITATEA TEHNICĂ „GH. ASACHI" IAŞI
TIPOGRAFIA

Str. Lascăr Catargi Nr. 38

ISSN 0258-9109